University of Crete – School of Medicine, Graduate Program in Bioinformatics
Institute of Molecular Biology and Biotechnology, Foundation for Research and Technology

Computational Neuroscience Modeling of Adult Neurogenesis in Dentate Gyrus and its Impact in Pattern Separation

Maria Karatsoli, MSc student

Graduate Thesis Committee

Dr. Panayiota Poirazi

Prof. Domna Karagogeos

Prof. Christophoros Nikolaou

Heraklion, January 2020

ABSTRACT

Hippocampus is engaged in memory processes, like episodic and spatial memory. Hippocampal Dentate Gyrus (DG) is one of the two regions where adult neurogenesis occurs in mammals, and has been suggested to underlie pattern separation, i.e., the ability to formulate distinct memories of similar episodes. Principal neurons of the DG, granule cells (GCs), are considered to perform pattern separation through sparsifying and orthogonalizing their inputs. We investigate the role of newborn GCs in pattern separation using a simple computational, yet, biophysically relevant, spiking neural network. The DG network consists of 2,000 GCs (1,800 developmentally-born GCs (dbGCs >8 weeks-old), 100 mature adult-born (mab) GCs (6-8 weeks-old) and 100 immature (iab) GCs (4 weeks-old)), 100 GABAergic basket cells, 80 glutamatergic mossy cells, and 40 HIPP interneurons. Each neuronal type is simulated as a point neuron, using the adaptive exponential integrate-and-fire (AdEx) model. GCs are simulated as multicompartmental point neurons, consisting of a somatic compartment connected with 12- (dbGCs) or 3-dendrites (mabGCs and iabGCs). Five different networks were used: two control networks A,B (1900 dbGCs, 50 mabGCs, 50 iabGCs and 1800 dbGCs, 100 mabGCs, 100 iabGCs for networks A,B respectively), a network C with equal percentages of each GC subpopulation (33.3%), one network D with 50% dbGCs, 25% mabGCs and 25% iabGCs and a network E without adult neurogenesis (2000 dbGCs). Moreover, we simulated two additional networks; network B without abGC-BC synapses that lead to over-excitation of abGC population (network F) and network B without abGC-MC synapses (network G) that did not lead to over-excitation. Study's results showed that GC activity was highest in the network with the highest percentage of abGCs (66% abGCs) populations (mean ± std: 3.39 ± 0.67), followed by the 50-50% network (2.97 ± 0.61), which was in turn higher than the control networks (1.38 ± 0.41 & 1.57 ± 0.38 for networks A,B respectively). Complete lack of adult neurogenesis resulted in a network with the lowest GC population activity. These simulations indicate that as the population of abGCs grows, while keeping the total GC population the same, the excitability of the DG network increases. This is because abGCs are more active than the overall GC population, irrespectively of the network's composition. Another set of simulations examined DG network's capacity of performing pattern separation in the above networks for EC Layer II inputs that shared a degree of similarity (60%, 70%, 80% or 90%). The results indicated that the f_1 scores of output patterns were decreased as the pattern separation task became more and more difficult and that conclusion was valid for DG networks C,D,E. Hence, we deduced that the presence of abGCs seems to aim pattern separation efficiency for easy tasks ($f_{1(input)}$ = 0.4, 0.3) but does not contribute significantly for more complex tasks ($f_{1(input)}$ = 0.2, 0.1). Networks F,G exhibit pattern separation but not better than control network B.

ΠΕΡΙΛΗΨΗ

Ο ιππόκαμπος εμπλέκεται σε μνημονικές διαδικασίες, όπως είναι η επεισοδική και η χωρική μνήμη. Η οδοντωτή έλικα (dentate gyrus - DG) στον ιππόκαμπο αποτελεί μία από τις δύο περιοχές όπου η ενήλικη νευρογένεση συμβαίνει στα θηλαστικά, και έχει προταθεί ότι εξυπηρετεί την λειτουργία του διαχωρισμού μοτίβων, δηλαδή της ικανότητας σχηματισμού διακριτών μνημών από παρόμοια επεισόδια. Ο κύριος κυτταρικός πληθυσμός της οδοντωτής έλικας είναι τα κοκκιώδη κύτταρα (granule cells - GCs), τα οποία θεωρούνται ότι επιτελούν τον διαχωρισμό των μοτίβων καθιστώντας πιο αραιά και ορθογώνια τα σήματα εισόδου που λαμβάνουν. Διερευνούμε τον ρόλο των ενήλικα γεννημένων GCs (abGCs) στην διαδικασία του διαχωρισμού μοτίβων χρησιμοποιώντας ένα απλό υπολογιστικό, ωστόσο βιοφυσικά σχετικό, νευρικό δίκτυο ενεργών κυττάρων. Το δίκτυο DG αποτελείται από 2000 GCs (1,800 εμβρυϊκής προέλευσης κοκκιώδη κύτταρα (dbGCs > 8 εβδομάδων), 100 ώριμα ενήλικα γεννημένα κοκκιώδη κύτταρα (mabGCs 6-8 εβδομάδων) and 100 ανώριμα ενήλικα γεννημένα κύτταρα (iabGCs 4 εβδομάδων), 100 GABAεργικά καλαθοειδή κύτταρα (basket cells - BCs), 80 γλουταματεργικά βρυώδη κύτταρα (mossy cells - MCs), and 40 HIPP ενδιάμεσους νευρώνες. Κάθε νευρικός τύπος προσομοιώνεται ως ένας νευρώνας-σημείο (point neuron) χρησιμοποιώντας το νευρικό μοντέλο adaptive exponential integrate-and-fire model (AdEx). Τα κοκκιώδη κύτταρα προσομοιώνονται ως διαμερισματοποιημένοι νευρώνες-σημεία, αποτελούμενοι από το σωμα που συνδέεται με 12- (dbGCs) ή 3-δενδρίτες (iabGCs και mabGCs). Πέντε διαφορετικές συστάσεις νευρικών δικτύων χρησιμοποιήθηκαν: δύο δίκτυα ελέγχου A,B (1900 dbGCs, 50 mabGCs, 50 iabGCs και 1800 dbGCs, 100 mabGCs, 100 iabGCs για τα δίκτυα A,B αντίστοιχα) , ένα δίκτυο C με ίσα ποσοστά από τους τρεις υποπληθυσμούς GCs (33.3%), ένα δίκτυο D με 50% dbGCs, 25% mabGCs και 25% iabGCs και ένα δίκτυο E χωρίς ενήλικη νευρογένεση (2000 dbGCs). Επιπρόσθετα, προσομοιώσαμε δύο επιπλέον δίκτυα˙ το δικτυο B χωρίς συνάψεις abGC-BC που οδήγησε σε υπερ-ενεργοποίηση των abGCs (δίκτυο F) και το δίκτυο B χωρίς συνάψεις abGCs-MCs το οποίο δεν οδήγησε σε υπερ-ενεργοποίηση του πληθυσμού των GCs. Τα αποτελέσματα της μελέτης έδειξαν ότι η δραστηριότητα των GCs ήταν υψηλότερη στο δίκτυο με το υψηλότερο ποσοστό abGCs (66% abGCs) (μ.ό. ± τ.α: 3.39 ± 0.67), ακολοθούμενη από το δίκτυο με το ποσοστό 50%-50% σε dbGCs και abGCs (2.97 ± 0.61), η οποία δραστηριότητα ήταν κατά συνέπεια υψηλότερη από ό,τι στα δίκτυα ελέγχου A,B (1.38 ± 0.41 & 1.57 ± 0.38 για τα δίκτυα A,B αντίστοιχα). Η απουσία ενήλικης νευρογένεσης στο δίκτυο E οδήγησε στα χαμηλότερα επίπεδα δραστηριότητας για τον πληθυσμό των GCs στο σύνολό τους. Οι προσομοιώσεις αυτές υποδεικνύουν ότι καθώς ο πληθυσμός των abGCs αυξάνει, ενώ ο ολικός πληθυσμός των GCs διατηρείται σταθερός, η δραστηριότητα του DG δικτύου αυξάνεται επίσης. Αυτό συμβαίνει επειδή τα abGCs είναι πιο δραστικά από τα ήδη υπάρχοντα dbGCs ανεξάρτητα από την σύσταση του δικτύου DG. Άλλες προσομοιώσεις εξέτασαν την ικανότητα του δικτύου DG να πραγματοποιεί διαχωρισμό μοτίβων στα πραπάνω δίκτυα για σήματα εισόδου προερχόμενα από το στρώμα II του ενδορινικού φλοιού. Τα σήματα αυτά μοιράζονται ένα βαθμό ομοιότητας (60%, 70%, 80% ή 90%). Τα αποτελέσματα έδειξαν ότι τα f_1 σκορ των σημάτων εξόδου μειώνονταν καθώς οι δοκιμασίες διαχωρισμού μοτίβων αυξάνονταν σε δυσκολία και αυτό το συμπέρασμα ήταν έγκυρο για κάθε ένα από τα δίκτυα C,D και E. Συνεπώς, συμπεραίνουμε ότι η παρουσία των abGCs φαίνεται να διευκολύνει τον διαχωρισμό μοτίβων για εύκολες δοκιμασίες ($f_{1(input)}$ = 0.4, 0.3) ενώ στην περίπτωση δύκολων μοτίβων ($f_{1(input)}$ = 0.2, 0.1) , η παρουσία των abGCs δεν φαίνεται να συνεισφέρει

σημαντικά. Τα δίκτυα F,G εκτελούν διαχωρισμό μοτίβων αλλά όχι καλύτερα από το δίκτυο ελέγχου B.

dedicated to my father Gerasimos,

Acknowledgments

Back in June 2017, when I became accepted to the Graduate Program of Bioinformatics in the University of Crete, I was really enthusiastic about this new beginning. My entrance into this graduate program brought me a step closer to obtain all the necessary skills in order to pursue a new start in my immature scientific career in the field of computational neuroscience. I would like to express my sincere gratitude to Dr. Panayiota Poirazi for the confidence and the support that she provided me as well as her insightful and critical observations that inspired me to complete my graduate thesis.

At this point, I would also like to thank the other member of my graduate thesis committee: Prof. Dr. Christoforos Nikolaou for the beautiful collaboration that we had during the graduate courses “Introduction in R” and “Algorihms in Boinformatics” as well as for his acceptance to be member of my thesis committee. Moreover, I would like to thank Prof. Dr. Karagogeos for her participation into my thesis committe.

During my graduate thesis, I was cooperated closely with post-doctoral researcher Spyridon Chavlis, who aided me to manage to accomplish my targets and I would like to thank him for his time and help. Moreover, I appreciate the help that the other colleagues in the laboratory provided me with many different ways.

My graduate thesis and my graduate studies, will not become reality if I haven’t the moral and financial support from my family; my mother Konstantinia, that always were eager to hear my anxieties and encourage me to continue, my sister Nefeli-Vasiliki for making me always laughing and be calm and my father Gerasimos who was always boosting my self-confidence and devoted time to hear my plans. This graduate thesis is especially dedicated to my father Gerasimos, who didn’t managed to see my thesis completed but until his last moments was the supportive and gentle father that I will always remember with love.

Abbreviations

ab: adult-born
abGC(s): adult-born Granule Cell(s)
AD: Alzheimer's Disease
AP(s): Action Potential(s)
BC(s): Basket Cell(s)
BrdU: BromodeoxyUridine
db: developmentally-born
dbGC(s): developmentally-born Granule Cell(s)
DG: Dentate Gyrus
EC: Entorhinal Cortex
EE: Enriched Environment
EPSC: Excitatory Post-Synaptic Current
EPSP: Excitatory Post-Synaptic Potential
GC(s): Granule Cell(s)
GCL: Granule Cell Layer
GFP: Green Fluorescent Protein
HIPP: Hilar Perforant Path-associated cells
IML: Inner Molecular Layer
IN(s): Interneuron(s)
IPSC: Inhibitory Post-Synaptic Current
IPSP: Inhibitory Post-Synaptic Potential
KS: Kolmogorov-Smirnov
LEC: Lateral Entorhinal Cortex
LPP: Lateral Perforant Path
LTP: Long Term Potentiation
MC(s): Mossy Cell(s)
MEC: Medial Entorhinal Cortex
MF(s): Mossy Fiber(s)
ML: Molecular Layer
MML: Medial Molecular Layer
MPP: Medial Perforant Path
MWM: Morris Water Maze
NPC(s): Neural Progenitor Cell(s)
NSC(s): Neural Stem Cell(s)
OB: Olfactory Bulb
OML: Outer Molecular Layer
PP: Perforant Path
RMS: Rostral Migratory Stream
SGZ: Sub-Granular Zone
SVZ: Sub-Ventricular Zone

List of Figures

Figure 55: Bar-plots with error bars for activity of immature abGC populations in different networks.

Figure 56: Bar-plots with error bars for activity of total GC population in different networks.

Figure 57: Input/output population distances (f_1) for different DG network composition (Experiment 1).

Figure 58: Input/output population distances (f1) for different DG network composition (Experiment 2)

Figure 59: Input/output population distances (f_1) comparing control network B with different DG network compositions

List of tables

Table 23: Activity in the Network D.

Table 24: Activity of GC population in Network E.

Table 25: Activity of GC population in Network F

Table 26: Activity of GC population in Network G.

Table 27: Activity of dbGC population for the different network compositions.

Table 28: Activity of mature abGC population for the different network compositions.

Table 29: Activity of immature abGC population for the different network compositions.

Table 30: Activity of GC population in different Network simulations.

Table 31: Derived statistics after Kolmogorov-Smirnov test examining the activity levels between control network A and network C.

Table 32: Derived statistics after Kolmogorov-Smirnov test examining the activity levels between control network B and network C.

Table 33: Derived statistics after Kolmogorov-Smirnov test examining the activity levels between control network B and network D.

Table 34: Derived statistics after Kolmogorov-Smirnov test examining the activity levels between control network A and network E.

Table 35: Derived statistics after Kolmogorov-Smirnov test examining the activity levels between control network B and network E.

Table 36: Derived statistics after Kolmogorov-Smirnov test examining the activity levels between control network A and network F.

Table 37: Derived statistics after Kolmogorov-Smirnov test examining the activity levels between control network B and network F.

Table 38: Derived statistics after Kolmogorov-Smirnov test examining the activity levels between control network A and network G.

Table 39: Derived statistics after Kolmogorov-Smirnov test examining the activity levels between control network B and network G.

Table 40: Hamming distance and f_1 score for the different cases of the pairs of external EC incoming inputs to the DG network.

Table 41: Mean and standard deviation of f1 scores for output patterns (Experiment 1).

Table 42: D-statistic and p-value after the implementation of Kolmogorov-Smirnov test examining the f_1 scores of output patterns between network A and network C (Experiment 1).

Table 43: D-statistic and p-value after the implementation of Kolmogorov-Smirnov test examining the f_1 scores of output patterns between network B and network C (Experiment 1).

Table 44: D-statistic and p-value after the implementation of Kolmogorov-Smirnov test examining the f_l scores of output patterns between network A and network D (Experiment 1).

Table 45: D-statistic and p-value after the implementation of Kolmogorov-Smirnov test examining the f_l scores of output patterns between network B and network D (Experiment 1).

Table 46: D-statistic and p-value after the implementation of Kolmogorov-Smirnov test examining the f_l scores of output patterns between network A and network E (Experiment 1).

Table 47: D-statistic and p-value after the implementation of Kolmogorov-Smirnov test examining the f_l scores of output patterns between network B and network E (Experiment 1).

Table 48: D-statistic and p-value after the implementation of Kolmogorov-Smirnov test examining the f_l scores of output patterns between network A and network F (Experiment 1).

Table 49: D-statistic and p-value after the implementation of Kolmogorov-Smirnov test examining the f_l scores of output patterns between network B and network F (Experiment 1).

Table 50: D-statistic and p-value after the implementation of Kolmogorov-Smirnov test examining the f_l scores of output patterns between network A and network G (Experiment 1).

Table 51: D-statistic and p-value after the implementation of Kolmogorov-Smirnov test examining the f_l scores of output patterns between network B and network G (Experiment 1).

Table of Contents

1. INTRODUCTION

1.1 Hippocampus

Hippocampus, is a paired structure with mirror-imaged halves in the left and right hemisphere in the temporal lobe of the brain, being crucial for functions like episodic (***Scoville and Milner 1957***) and spatial (***Squire 1992, Scovile and Milner 1957, Burgess et al., 2002, Squire et al., 2004, O'Keefe and Dostrovsky 1971, Hafting et al., 2005***) memory formation, storage and consolidation (***Squire et al., 2004***). Hippocampus, is a heterogeneous structure with gradually segregated functional differences along its dorsoventral axis (***Kjelstrup et al., 2008, Thompson et al., 2008, Fanselow and Dong 2010, Strange et al., 2014***). Experimental studies in rodents, using lesions in different hippocampal subregions along the dorsoventral axis and optogenetic manipulations, revealed the aforementioned heterogeneity. More specifically, lesions of the dorsal hippocampus impaired cognition and spatial learning while optogenetic inhibition of granule neurons of this area deteriorated contextual memory encoding (***Kheirbek et al., 2013***). On the other hand, lesions of the ventral hippocampus affect emotional behavior, social interactions (***Felix-Ortiz and Tye 2014***), and stress-resilience (***Hughes 1965, Stevens and Cowey 1973, Henke 1990, Moser et al., 1993***). Also, optogenetic activation of granule neurons in the rodent ventral hippocampus resulted in amelioration of the anxiety-like behavior (***Kheirbek et al., 2013***).

Although, the dorsal and ventral hippocampus in rodents corresponds to the posterior and anterior hippocampus in humans, respectively. The aforementioned effects continue to exist in humans. In particular, taxi drivers who are demanded to exhibit a large capacity for processing of spatial and contextual information usually have got larger volume of posterior hippocampus (***Maguire et al., 2000***), whereas unmedicated patients with depression have a smaller volume of anterior hippocampus (***Boldrini et al., 2013***).

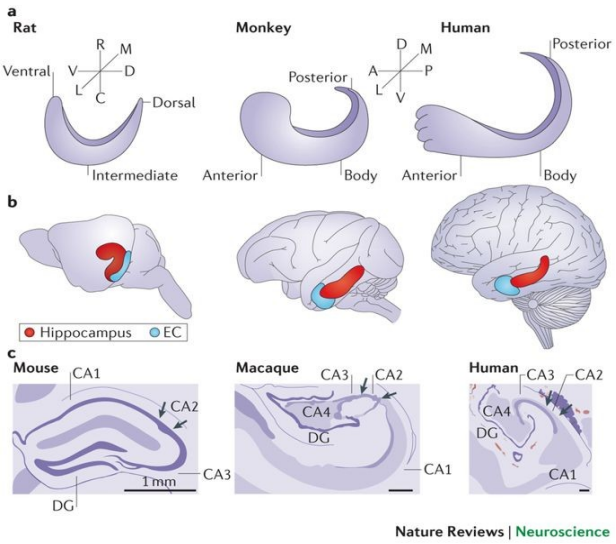

Figure 1: Comparison of hippocampal anatomy across different species. **a)** Schematic representations of the hippocampal long axis in rats (left), macaque monkeys (middle) and humans (right). The longitudinal axis is described as ventrodorsal in rodents and as anteroposterior in primates. **b)** The full long axis of the hippocampus (red) can be seen in brains of rats (left), monkeys (middle) and humans (right), with the entorhinal cortex shown in blue. **c)** Drawings of Nissl cross-sections of mouse (left), macaque (middle), and

human hippocampi (right). A, anterior; C, caudal; D, dorsal; DG, dentate gyrus; L, lateral; M, medial; P, posterior; R, rostral; V, ventral (***Adopted by Strange et al., 2014***)

Hippocampal formation is comprised of dentate gyrus (DG), hippocampus (*Cornus Ammonis - CA* regions), subiculum, presubiculum, parasubiculum (***O'Mara 2005***) as well as entorhinal cortex (EC) (***Coras et al., 2014***). Recently, has been identified also a new area/subdivision for CA region, named the CA4 region (***Coras et al., 2014***).

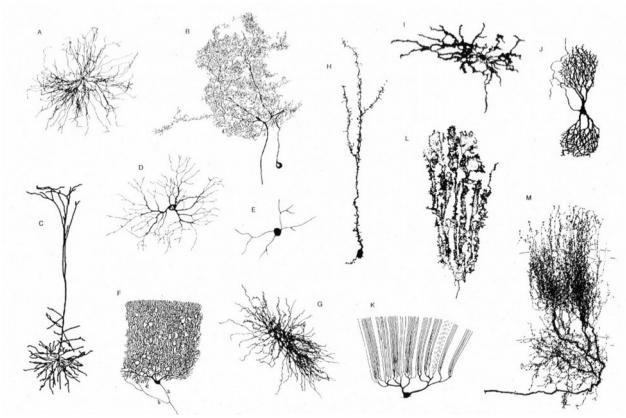

Figure 2: Cellular diversity in the hippocampus. In hippocampal area can be found many morphological diverse neurons. The differences may be about the shape of the soma, the dendritic tree (basal, apical or both), the number and shape of dendritic spines, the dendritic length etc. (***Adopted by Dendrites, Oxford University Press 2015; Modified from Mel, B.W. Neural Computation, 1994***).

In the hippocampal cortical region there are excitatory glutamatergic principal neurons (pyramidal cells in CA1, CA2, CA3 hippocampal regions, while granule cells (GCs) & mossy cells (MCs) in DG) and inhibitory GABAergic interneurons (INs). Principal hippocampal neurons are connected to each other through glutamatergic synapses, formulating the hippocampal trisynaptic circuit (***Andersen et al., 1971***).

Interestingly, the hippocampus interacts with other brain structures related with the control of emotions, thus hippocampus is also pivotal for emotional behavior (***Sahay & Hen 2007***). Hippocampus possess a noteworthy role not only in acquisition of new memories, but also in retrieval of old ones as well. Hence, hippocampus using a partial amount of information (the so-called cues), manage to reactivate the full representation of already stored memories, a function termed as pattern completion which was mainly attributed to synaptic transmission and plasticity of the recurrent network of CA3 hippocampal area (***Marr 1971, McNaughton and Morris 1987, O'Reilly and McClelland 1994, Treves and Rolls 1994, Hasselmo et al., 1995***).

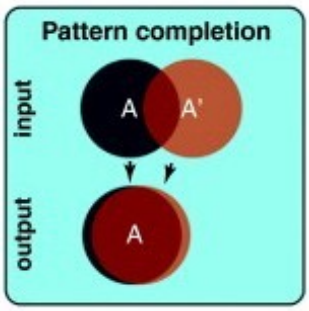

Figure 3: Pattern completion process. Schematic conceptual representation of the pattern completion function of the hippocampus. Pattern completion can be thought as making overlapping representations (A and A') even more overlapping. (***Adapted by Yassa & Stark 2011***)

Along many years of scientific research, several possible roles have been attributed to hippocampus, highlighting the importance of information processing into the classic trisynaptic loop. Among them, a vital hippocampal function is the so-called pattern separation which has been attributed to DG hippocampal structure. Pattern separation is the ability of adult hippocampus to formulate distinct memories of similar episodes. Especially, pattern separation was attributed to synaptic transmission and plasticity in the feed-forward network of EC → DG → CA3. The way through which this is accomplished, is via the formulation of distinctive representations of the temporal and spatial characteristics that identify each specific event. Thus, in this feed-forward circuit takes place segregation both in time and space for initially overlapping EC memory engrams (***Marr 1971, McNaughton and Morris 1987, O'Reilly and McClelland 1994, Treves and Rolls 1994, Leutgeb et al., 2007, Bakker et al., 2008***).

Figure 4: Pattern separation process in the DG. **A-B)** Different versions of the same objects given as sensory inputs to the brain. It is supposed that DG is responsible for permitting us to recognize the different versions of the same object. (***Adopted from Bakker et al., 2008***) **C)** A schematic representation of input/output transfer function in DG. In this conceptual representation, pattern separation process is the transformation of similar, overlapping representations (A and A') into more distinct ones (***Adopted by Yassa and Stark 2011***).

To put in a nutshell, it is widely hypothesized that pattern separation is accomplished via two ways. A first approach, considers GC neuronal population as the mechanism of orthogonalization of inputs, through sparsity, i.e the firing of a small percentage of GCs for a given environment/stimulus (***Jung and McNaughton, 1993, Leutgeb et al., 2007***). Particularly, 2 -5% of the GC population is active in a typical exploration of a given environment according to the

experiments (*Chawla et al., 2005, Ramirez-Amaya et al., 2006, Tashiro et al., 2007*). Thus, the sparse spiking of GCs is supposed to contribute to the orthogonalization of correlated input patterns. The second proposed mechanism of pattern separation, includes the recruitment of different populations of hippocampal place cells, imposed by strong inputs from the GC axons during memory encoding, which act as "detonators". These renowned "place cells", which fire only at specific locations remaining silent in other places (*O'Koffe and Dostrovsky 1971*) have the tendency to "remap" after the exposure to multiple uncorrelated representations, even if minor changes have happened in them (*Muller and Kubie 1987, Bostock et al., 1991, Markus et al., 1995*). The "remapping" that is mediated by place cells, could be considered as a type of pattern separation, because slight discrepancies in inputs are modified into less similar representations.
The attribute of pattern separation to DG is not only a theoretical idea, but also a valid experimentally tested proposed function. Lesions of the DG in rodents resulted in impaired performance in pattern separation tasks (*Gilbert et al., 2001, Hunsaker and Kesner 2008*). The same effect was induced also after deletion of NMDARs in GCs of mice (*McHugh et al., 2007*). Interestingly, another key feature of DG, adult neurogenesis, is experimentally implicated in spatial pattern separation (*Clelland et al., 2009, Creer et al., 2010*). This ability of the DG to perform spatial pattern separation, has been regarded as a critical function of the hippocampus, facilitating the creation of foundations for the contextual memory (*Lee and Kesner 2004*), a fundamental aspect that permits animals' survival, facilitating them to recognize discrepancies among extremely similar contexts.

1.2 Dentate gyrus

Anatomically, DG is a cortical structure into the hippocampal area (*Amaral and Lavenex 2007*) with a regular organization of its principal cell layers and a laminar distribution (*Amaral et al. 2007*). The basic trilaminar structural organization of the DG is well conserved in all examined species while there are not observed crucial phylogenetic modifications (*Amaral et al. 2007*). The principal neuronal population of the DG is comprised by the GCs, highly polarized cells with a particular orientation of their cone-shaped dendritic tree towards the three levels (inner, medial, outer) of molecular layer (ML), while their oval-shaped cell body is located in the granule cell layer (GCL). The axons of granule neurons (mossy fibers - MFs) are found at the polymorphic layer also known as hilus, and recently termed as CA4. In the hilus, is located a subclass of GCs named ectopic GCs (*Scharfman et al., 2007*). Also, in the IML are found the semilunar GCs (*Larimer et al., 2010, Williams et al., 2007*).

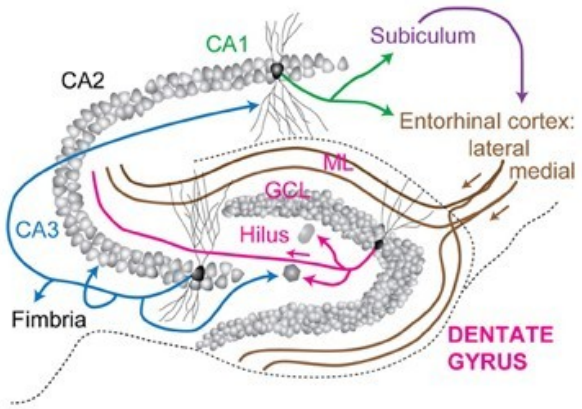

Figure 5: A schematic representation of the rat hippocampal circuit. The colorful arrows represent the excitatory axonal projections from representative principal cells within each layer to their downstream targets. An example is the projections from the DG cells that target the excitatory hilar mossy cells and the inhibitory interneurons as well as CA3 pyramidal neurons and INs (***Adapted by Piatti et al., 2013***).

Importantly, DG is one of the two confirmed brain regions in mammals where adult neurogenesis takes place (***Zhao et al., 2008***) with the integration of newly generated neurons into the functional established DG network (***van Praag et al., 2002, Toni et al., 2008, Jessberger and Kempermann 2003***).

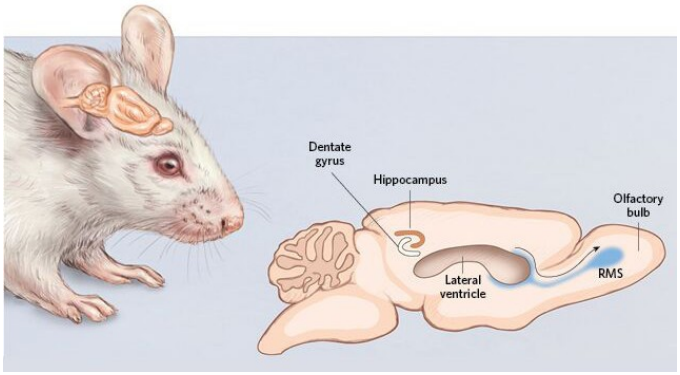

Figure 6: Neurogenic niches in the mammalian brain. In mammals, adult neurogenesis take place in two different sites; olfactory bulb and hippocampal dentate gyrus. The neurogenic niche in olfactory bulb is the rostral migratory stream, while in dentate gyrus is the subgranular zone (***Adapted by © Laurie O'Keefe. inset illustrations based on L. Varela-Nallar, N.C. Inestrosa, (2013) Front Cell Neurosci, 7:100, 2013. doi: 10.3389/fncel.2013.00100***).

A special characteristic of the DG is that it receives mainly unidirectional connections, with the EC providing the major external input via the perforant path (PP). DG, is primarily innervated by glutamatergic synaptic inputs from the lateral entorhinal cortex (LEC) via the lateral perforant path (LPP) and from the medial entorhinal cortex (MEC) via the medial perforant path (MPP). Especially, the LPP inputs carry non-spatial, contextual information while the MPP inputs carries mainly spatial information (***Luna et al., 2019***). Thus, DG is the first relay station where information from the EC Layer II is processed until it conveys to CA3 subregion (***Amaral et al., 2007, Treves et al., 2008***). EC main excitatory/glutamatergic inputs to DG - via fibers known as PP- lead to the first step of information processing that ends up to the production of episodic memories (***Amaral et al., 2007***). EC Layer II inputs are the major afferents to the outer molecular layer (OML) and medial molecular layer (MML) of the DG (***Amaral et al., 2007, Steward et al., 1976, Witter 2007***). The main afferent inputs of inner molecular layer (IML) are the axons of MCs (***Ribak et al., 1985,***

Scharfman & Myers 2012, Buckmaster et al., 1996). DG output ends up to CA3 hippocampal region and is derived by GC axons, the MFs (*Scharfman 2016*).
GC dendrites significantly contribute in the processing of the PP input through the dendritic integration procedure (*Krueppel et al., 2011*). Hence, in the outer two thirds of the ML, dendrites of GCs receive inputs from the EC via PP, while dendrites in the IML, receive associational/commissural inputs onto their proximal dendrites (*Krueppel et al., 2011*).

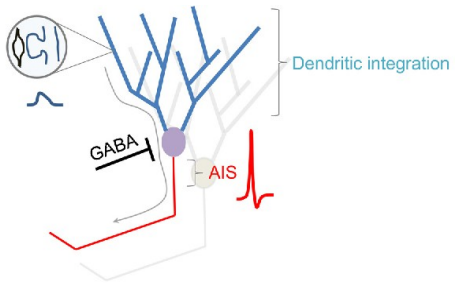

Figure 7: Dendritic integration in the GCs. Neuronal output is not only influenced by the synaptic excitatory drive that a given neuron receives, but also by GABAergic inhibition and the intrinsic properties of the cell. These three aforementioned levels of regulation, control plastic properties of GCs when acting all together (*Adapted by Lopez-Rojas and Kreutz 2016*).

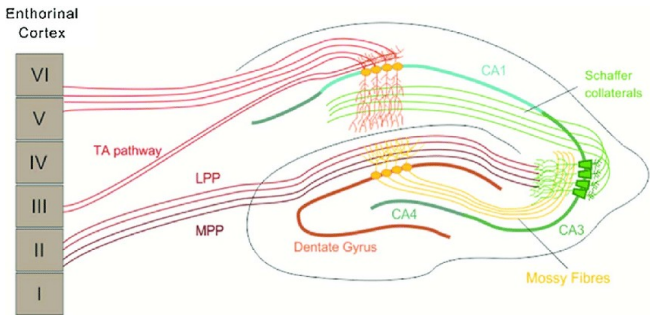

Figure 8: A schematic representation of the hippocampal circuit. The dentate gyrus (DG) receives the majority of its inputs from the Layer II of the Entorhinal Cortex (EC) through perforant pathway (PP) afferents. More specifically, it receives inputs from the Medial EC (MEC) via Medial PP (MPP) and inputs from the Lateral EC (LEC) via Lateral Perforant Pathway (LPP). The axons of the granule neurons project towards the pyramidal cells of CA3 hippocampal subregion. These axonal projections are the mossy fibers (MFs). The projections of the CA3 pyramidal neurons from the Schaffer collaterals, establish synapses with the dendrites of the CA1 pyramidal cells. Finally, the CA1 pyramidal neurons close the loop, completing the trisynaptic hippocampal circuit projecting its fibres to the deep layers of the EC. Moreover, CA1 pyramidal cells receive direct inputs from Layer III of the EC through the temporoammonic pathway (TA). CA3 also accepts direct inputs from EC Layer II. (*Adopted by Pinar et al., 2017*)

1.3 Major cell types in dentate gyrus

1.3.1 Granule cells (GCs)

GCs of DG consist its main excitatory neuronal population (*Amaral et al. 2007*). GCs have a characteristic morphology that does not resemble the classic morphology of pyramidal neurons in hippocampal area. More specifically, they have got an elliptical-shaped cell body (length ~10.0 μm and width ~18.0 μm) (*Claiborne et al. 1990*), while their dendritic tree is coned-shaped with spiny apical dendrites, i.e GCs are highly polarized. These dendritic processes are very thin and extend

throughout the ML (***Amaral et al. 2007***). As the dendrites diverge from the IML, they become thinner leading to smaller diameters as well as rendering their electrophysiological characterization very challenging (***Amaral et al. 2007***).

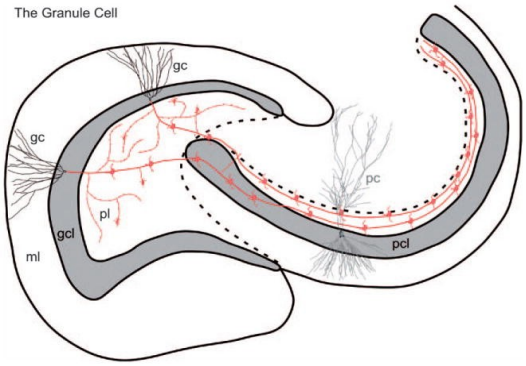

Figure 9: A typical dentate granule cell. In the illustration is also incorporated the axonal arbor of the granule cell. A collateral plexus gives rise to multiple (~200) typical synapses on cells located within the polymorphic cell layer (pcl). The majority of these synapses are onto the dendrites of inhibitory interneurons. Also, some of the large mossy fiber synapses are distributed in the polymorphic layer. Many of these terminate to the proximal dendrites of excitatory mossy cells. The mossy fibers axons ultimately enter the CA3 subregion and they terminate with mossy fiber expansions on a small number (~15-20) of CA3 pyramidal cells (***Adopted by Amaral et al., 2007***).

Granule dendritic tree has a larger total dendritic length in suprapyramidal blade (~3500 μm) in comparison with infrapyramidal blade (~2800 μm) while the density of dendritic spines is 1.6 spines/μm and 1.3 spines/μm at supra- and infra-pyramidal blade, respectively (***Desmond and Levy, 1985***). Summing up, there are ~5600 supra-pyramidal and ~3640 infra-pyramidal spines. Taking into consideration that dendritic spines are the major sites where excitatory synapses are located, the aforementioned spine numbers are potential indicators for the number of excitatory synapses that GCs receive from all other sources (***Amaral et al. 2007***). In rats, GCs have only apical dendrites, however, in humans and monkeys have been identified DG GCs with basal dendrites as well (***Seress and Mrzljak, 1987***).

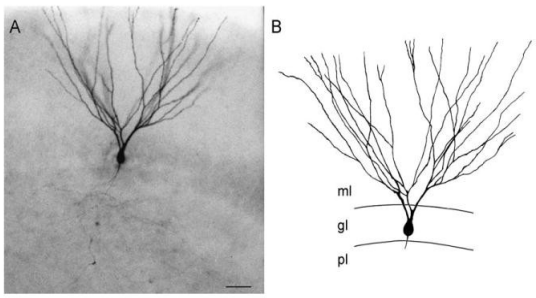

Figure 10: Photomicrograph of a typical dentate granule cell. In the Figure A, we see a photomicrograph and in the picture B a prototypical granule cell that has filled with Lucifer yellow in a hippocampal slice. The dendritic processes arise mainly from the apical surface of the cell body, and the axon emerges from the basal surface. The spiny dendrites extend into the molecular layer (ml) until the hippocampal fissure, and the axon collateralizes within the polymorphic layer (pl) (***Adopted by Amaral et al., 2007***).

The dbGCs in DG consist 90-95% of the GC population (***Schlessinger et al., 1975, Altman and Bayer 1990***). This type of GCs are produced early during development and they do not surpass

further divisions. The remaining 5-10% of GC population consist the newly generated abGCs that are derived from NPCs in the SGZ of the DG (***Altman and Das 1965, Eriksson et al., 1998, Gould et al., 1999, Imayoshi et al., 2008***). Spine density and dendritic complexity of these abGCs, augments and bears resemblance with dbGCs as development continues (***Crain et al., 1973***).
The low firing rates of GCs in combination with their sparse connectivity with CA3 pyramidal cells (***Amaral et al. 1990***), favor and support the capability of GCs to perform pattern separation, making GCs suitable candidates of pattern separation ability.

1.3.2 Mossy Cells

Mossy cells (MCs) constitutes a measurable amount of neurons in the hippocampal DG region located only in the hilus (***Amaral et al., 2007, Scharfman & Myers 2012, Amaral 1978***). They are part of a complex circuit as they innervate both the GCs and the INs located in the DG. This finding is really interesting because MCs excite GCs through glutamatergic synapses and also inhibit them indirectly through the excitation of local INs (***Scharfman 2016***). Interestingly, the net effect of MC excitation is the inhibition of GCs activity aiding pattern separation in the DG (***Jinde et al., 2012, Danielson et al., 2017***).

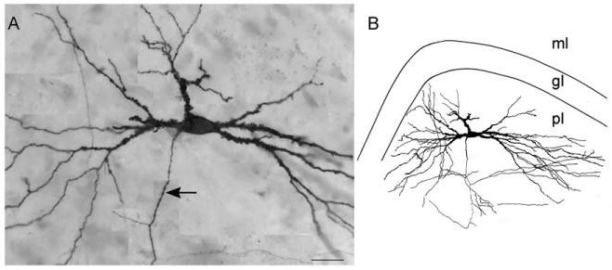

Figure 11. Typical mossy cell representation. A montage of several focal planes (A), and a drawing of a typical mossy cell with its thorny excrescence and its dendritic tree (B). The thorny excrescences are proximal to the soma while the dendrites extend throughout nearly the entire polymorphic region, but few enter either the granule cell or molecular layers. (***Adopted by Amaral et al., 2007***).

MCs own their name to Amaral (***Amaral et al., 1978***), who studied them and other cell types that are located in the hilus (polymorphic layer) using the classic Golgi method. He named them mossy due to their 'mossy' appearance, i.e the presence of thorny exerceness on proximal dendrites (***Scharfman 2016***), i.e very large and complex spines (***Amaral et al., 2007***) which are not present on interneurons or GCs (***Ribak et al., 1985, Amaral 1978, Frotscher et al., 1991***). MCs have a large cell body (~25-35 μm) with a triangular or multipolar shape (***Amaral et al., 2007***). This cell body consists the starting point from which three or more thick dendrites are heading towards the hilus after traveling a long distance. These main thick dendrites, bifurcate once or twice, creating new dendritic branches extended into the ML (***Ribak et al., 1985, Scharfman & Myers 2012, Amaral 1978, Frotscher et al., 1991, Scharfman 1991, Blackstad 2016***).

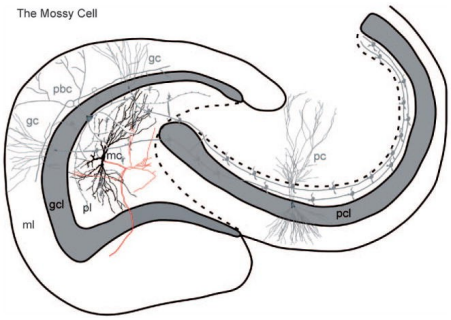

Figure 12: The mossy cell. A drawing of a typical mossy cell (mc) in the polymorphic cell layer (pcl). The axon of the mossy cell develops a plexus within the polymorphic layer, and also an ipsilateral projection to the inner molecular layer, known as associational pathway. The main axon also projects contralaterally to the inner molecular layer, forming the commissural pathway (***Adopted by Amaral et al., 2007***).

1.3.3 HIPP Cells

HIPP cells are a considerable population of INs in the DG, with their cell body located in the hilus (***Scharfman 2016***). They receive input from EC Layer II and project to the DG at the distal dendrites (***Freund & Buzsaki 1996, Halasy & Somogyi 1993, Han et al., 1993***).

1.3.4 Basket cells

Basket cells (BCs) of DG are another type of GABAergic parvalbumin-expressing interneurons that target the perisomatic area of GCs (***Kraushaar and Jonas 2000***).

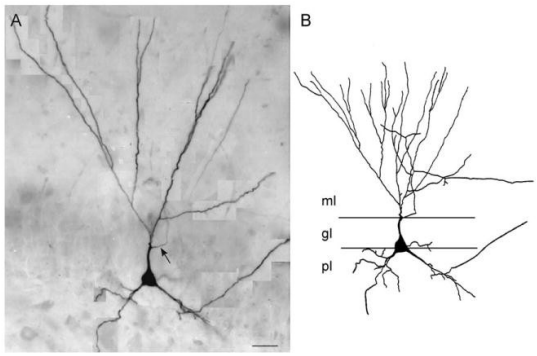

Figure 13: Basket cell (BC) and its dendritic distribution into distinct layers. A prototypical pyramidal BC is shown after intracellular injection of neurobiotin. In (A) we observe a montage that was created after the visualization of the cell and in the (B) a line drawing of a typical BC (***Adopted by Amaral et al., 2007***).

Their name is attributed due to the fact that they formulate a plexus around the cell body of GCs like a basket. BCs are cell types resistant to seizures because they are tolerant to excitotoxic factors that affect other types of INs in DG, like HIPP cells (***Sloviter 1987, Sloviter 1989, Schwarzer et al., 1995***).

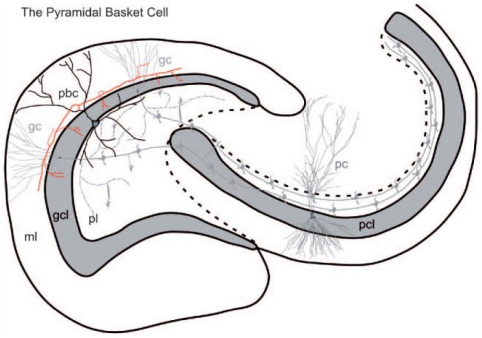

Figure 14: A typical basket cell. The cell body of the basket cell is located at the interface between the granule cell layer (gcl) and the polymorphic cell layer (pcl). The axons of the basket cell emerges from the apical dendrite. Collaterals of this axon form a curtain of terminals that synapse with the granule cell bodies (***Adopted by Amaral et al., 2007***).

1.4 A historical preview of adult neurogenesis

The concept of adult neurogenesis is a highly controversial issue that concerns the scientific community till nowadays, while its existence in the human brain has both supporters and opponents. In 1928, the father of modern neuroscience, Santiago Ramón y Cajal wrote:

"*Once development has ended, the founts of growth and regeneration dried up irrevocably. In the adult centers the nerve paths are something fixed, ended and immutable. Everything must die, nothing may be regenerated.*"

However, this point of view was challenged when Altman and Das in 1965, reported for the first time that they discovered autoradiographic and histological evidence of postnatal neurogenesis (***Altman & Das, 1965***). Nevertheless, it was not earlier until the middle 1990s, that was started to become widely accepted the fact that new neurons are produced and are incorporated in the adult brain (***Gross 2000, Kaplan 2001***).

The first insights into human adult neurogenesis, came with the scientific paper of Eriksson P.S. (***Eriksson et al. 1998***) shedding light into the investigation of this procedure in human adult hippocampus, especially in the DG.

A considerable number of following studies supported these findings, leading today in a well-established scientific literature and research that supports adult neurogenesis as a fact in mammals, and even in humans (***Eriksson et al. 1998, Bergmann et al. 2015, Spalding et al. 2013, Boldrini et al. 2018***). Adult neurogenesis was identified early in many brain regions in songbirds (***Nottebohm 2002***), in other bird species as well as in reptiles, fish (***Zupanc 2001***) and a wide range of vertebrates (***Cayre et al., 2001***). However, adult neurogenesis in mammals, seems to be restricted in two specific brain regions, including the DG in the hippocampus and the olfactory bulb (OB) (***Ming and Song 2011***).

In humans particularly, adult neurogenesis has been detected only in DG, making it unlikely to take place in the OB (***Aimone et al., 2016***). Some other more controversial studies, have been reported neurogenesis in neocortex (***Cameron et al. 2008, Gould 2007, Could et al. 1999***) and hypothalamus (***Kokoeva et al. 2005***) but these results are not well-accepted from scientific community (***Rakic 2002***) due to the lack of a solid amount of quantitative datasets in order to perform comprehensive

comparisons (*Snyder 2019*). More specifically, the claim about adult neurogenesis in the neocortex was rejected after the application of a radiocarbon dating method that was implemented in neurons derived from postmortem brains of people that were exposed to ionizing radiation during the atomic bomb testing in the 1960s (*Spalding et al. 2013*). Nevertheless, this technique revealed consistent rates of neurogenesis in human hippocampus even into the ninth decade of their lives.

Overall, adult neurogenesis is evident in mammals and in a large variety of species from rodents (*Jessberger and Gage 2014, Snyder et al., 2009*) to monkeys (*Gould et al., 1998, 1999*).

While in vertebrates, like fish and reptiles which share a more primitive nervous system - adult neurogenesis seems prevalent in many brain regions, in primates, with more advanced and complicated nervous systems, adult neurogenesis is more restricted. This observation substantiate the existence of ample evolutionary pressures that attenuated neurogenesis in other brain areas and resulted in the OB and DG, two relatively detached structures, where an evolutionary gain-of function existed (*Aimone et al., 2016*).

A variety of experimental techniques paved the way towards the dissolving of skeptical thoughts about the existence of adult neurogenesis. First of all, scientists developed immunohistological techniques for the labeling of dividing cells with nucleotide analogues (for example, bromodeoxyuridine-BrdU) as well as protein markers specific to neurons (for example, NeuN) or genetic markers (*Kempermann et al. 2015*). The combination of the aforementioned techniques accompanied with confocal imaging techniques, identified adult-born neurons with great consistency and precision (*Luzzati et al., 2011*). Furthermore, it was observed that the incorporation of adult-born neurons it was affected by behavioral parameters, like physical exercise (*van Praag et al. 1999*), enriched environments (*Kempermann et al. 1997*), age (*Katsimpardi and Lledo 2018*), learning (*Gould et al. 1999*) or stress conditions (*Schoenfeld and Gould 2012, Levone et al., 2015, Mirescu and Gould 2006*). Interestingly, hippocampal neurogenesis is also increased in pathological conditions like hypoxia (*Zhu et al. 2005, Varela-Nallar et al. 2014*), ischemia (*Liu et al. 1998, Jin et al. 2001*), seizures (*Parent et al. 1997, Scharfman et al. 2000*) and traumatic brain injury (*Dash et al. 2001, Chirumamilla et al. 2002, Villasana et al. 2014, Villasana et al. 2015*). The addition of adult-born neurons in hippocampal DG is of crucial importance for memory and learning (*Shors et al. 2001, Dupret et al. 2008, Sahay et al. 2011*). The integration of newborn neurons after adult neurogenesis in hippocampus in pathological situations like the ones previously referred, might compensate for functional deficits and dysfunction contributing to cognitive recovery (*Villasana et al. 2015*).

Adult neurogenesis offers new perspectives and possibilities for structural plasticity while providing at the same time regenerative capacities in adult mammalian brain (*Kempermann & Gage 1999, Fuchs & Gould 2000, Temple & Alvarez-Buylla 1999, Doetsch & Hen 2005, Ming & Song 2005, van Praag et al. 2002, Carleton et al 2003, Schmidt-Hieber et al 2004*).

Recent studies, using advanced and improved protocols for the identification and visualization of abGCs in human brain (*Moreno-Jiménez 2019*), have shed light on the issue of adult neurogenesis in DG region of the hippocampus. An important study provided evidence for continued neurogenesis in adulthood at high rates, suggesting its important role in human behavior (*Spalding et al., 2013*). In particular, they calculated that approximately 700 abGCs are added each day in the hippocampal circuit of middle-aged adults (*Spalding et al., 2013*).

Nevertheless, till nowadays, human DG adult neurogenesis raises conflicting results with a recent study failing to detect newborn neurons beyond adolescent (***Sorrells et al. 2018***) while at the same time period, another published study pinpointed the presence of adult hippocampal neurogenesis in humans even throughout aging (***Boldrini et al., 2018***). Human adult neurogenesis in the hippocampus is a promising area of research in which scientists are pursuing to get deeper insights into its contribution in mechanisms of learning and memory and its role under pathological conditions. A recent study in humans, substantiate the latter interest with the comparison of adult neurogenesis levels both on controls and Alzheimer diseased cases (***Moreno-Jiménez et al., 2019***).

1.5 The importance of studying adult neurogenesis

There is an increasing number of animal studies that supports the causal role of adult neurogenesis in a variety of hippocampus-dependent functions. The addition of newborn neurons into the preexisting DG network of developmentally-born (db) GCs adds flexibility in learning and adaptation in behavior, augmenting the plasticity of the system and contributing to the confrontation of cognitive and emotional challenges (***Anacker et al., 2017, Cameron et al., 2015, Opendak et al., 2015, Snyder 2019***).

Neurogenesis in the adult brain and neurogenesis in neonatal brain, seems to present differences, indicating the discrepancies between these two environments. The study of neurogenesis in hippocampal DG is a model in order to investigate how the microenvironment of this neurogenic niche affect the neural stem cell (NSC) fate in adult or neonatal brain. Experimental studies using hippocampal neural progenitor cells (NPCs), show that *in vitro* conditions could determine the phenotype of newborn neurons (***Song et al., 2002, Deiseroth et al., 2004, Shen et al., 2004***). The study of adult neurogenesis could provide deeper insights into the understanding of the incorporation of NSCs in the adult healthy and diseased brain.

1.6 Neurogenic niches in the mammalian brain

In the mammalian adult brain, there are two identified regions where adult neurogenesis takes place. These regions are the subventricular zone (SVZ) of the lateral ventricle in the OB and the subgranular zone (SGZ) in the DG (***Ming & Song 2011***). In these two regions, NSCs give rise to NPCs which in turn, differentiate into neurons or glia (***Gage 2000***). Newborn neurons identified in the SVZ of the OB migrate through the rostral migratory stream (RMS) and become GCs and periglomerular neurons of the OB. However, adult neurogenesis in human OB has not been detected (***Aimone et al., 2016***). Neurons born in the SGZ of the DG, migrate towards the granule cell layer (GCL) giving rise to adult-born GCs (abGCs) while they manage to be fully and functionally integrated into the hippocampal circuit (***van Praag et al., 2002, Toni et al., 2008***).

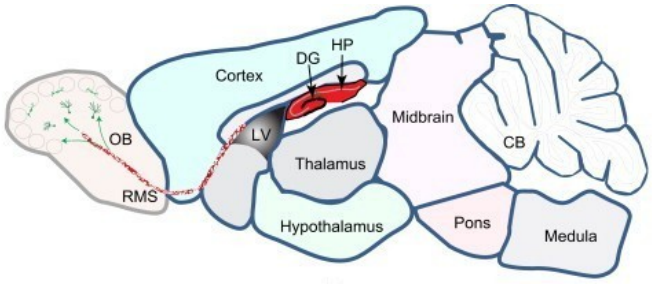

Figure 15: A saggital section view of an adult rodent brain. The two regions that adult neurogenesis takes place are highlighted with red color (dentate gyrus (DG) in the hippocampal (HP) formation & olfactory bulb (OB) with its neurogenic niche; rostral migratory stream (RMS) (***Adapted by Ming & Song 2011***).

Indeed, OB and DG are two regions that are relatively detached from each other while they do not share enough similarities. Concretely, OB is a primary sensory region, reliable for processing of incoming raw olfactory inputs, while the DG is a deep brain structure, with a trilaminar organization, without having immediate vicinity with incoming sensory inputs.

NSCs - in OB neurogenic niche of SVZ - being adjacent to the lateral wall of the lateral ventricle, and NSCs - in neurogenic niche of SGZ - in the hippocampus, are characterized as glia cells since they consist a subpopulation of astrocytes (***Doetsch 2003***).These newborn neurons are derived by progenitors cells and are produced everyday. Only a small percentage of them finally manage to survive and be fully incorporated in a functional way in the hippocampal circuit (***Ming & Song 2011***).

There is experimental evidence which support the statement that SVZ of the OB and SGZ of the DG are “neurogenic niches”. Thus, transplantation of NPCs from the SVZ of the OB into ectopic regions of the adult brain, has as a result to appear the phenomenon of gliogenesis, according to which NPCs gave rise to oligodendrocytes and astrocytes (***Seidenfaden et al., 2006***). On the other hand, transplantation of NPCs from a non-neurogenic region, like the spinal cord, to a neurogenic region, like the DG, has as a result to give rise to neurons (***Shihabuddin et al., 2000***). The aforementioned experimental results, reinforce the hypothesis that the local microenvironment in neurogenic niches promotes adult neurogenesis, which takes place specifically in these two regions.

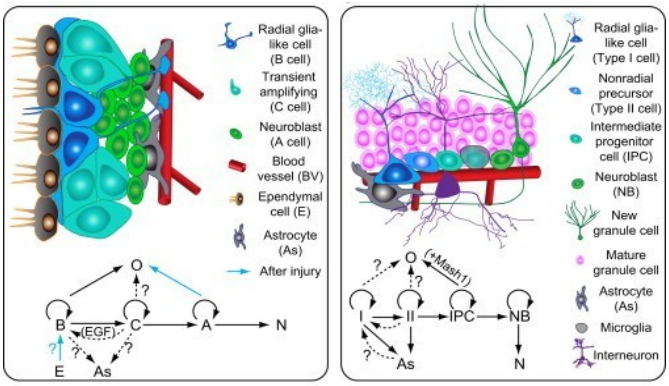

Figure 16: Neurogenic niches of olfactory bulb and dentate gyrus with their cellular populations. Schematic illustration of the neurogenic niches in the olfactory bulb (left) and in the dentate gyrus (right) with a model of potential lineage relationship under basal (solid arrows, left & right) and injury conditions (blue arrows left) (***Adapted by Ming & Song 2011***).

The development of abGCs in DG, recapitulates the embryonic development of developmentally/perinatally born granule neurons, which means that they follow an outside-in-layering pattern of development, with the dbGCs to be located in the outer GCL and the abGCs located in the inner or middle GCL (***Mathews et al. 2010, Kempermann et al. 2015***). However, the time period that is needed for newborn neurons to be fully mature in the adult hippocampus is longer than the respective time period for perinatally-born granule neurons (***Overstreet-Wadiche et al., 2006***). Studies in rodents and primates imply a pattern for the addition of DG neurons along ventral to dorsal axis, supra-pyramidal to infra-pyramidal and superficial to deep gradients (***Schlessinger et al., 1975, Rakic and Nowakowski 1981***).

1.7 The Stages of Maturation in Adult-Born Neurons

Adult neurogenesis in the DG starts with the proliferation of NPCs in the SGZ (***Deng et al., 2010***). During this proliferation period, the vast majority of NPCs differentiate into the primary neuronal population of DG, the GCs, while a minority of NPCs give rise to glia (***Cameron et al., 1993***). During adult neurogenesis, only a small fraction of adult-born generated neurons manage to survive, surpassing the barriers, and be incorporated into the hippocampal circuit, whereas the vast majority of adult-born neurons undergo apoptosis (***Biebl et al., 2000, Dayer et al., 2003, Sierra et al., 2010***). Newborn GCs become fully mature after a time period that endures approximately two months (~8 weeks). The endurance of maturation period is species-dependent (***Snyder et al., 2009***). During maturation time period, newborn GCs abide a protracted period of morphological and physiological maturation (***Zhao et al., 2006***). Fully mature abGCs, are almost indistinguishable from dbGCs. However, the maturation process of abGCs takes longer time to be completed (***Zhao et al., 2006, Overstreet-Wadiche et al., 2006***) compared with the perinatally born GCs, implying possible differences in the environment of neurogenic niches between adult and neonatal hippocampus.

- **1 week after birth of newborn granule neurons in the adult DG**

In the course of the 1st week after their birth, abGCs have managed to be committed to the neuronal lineage, thus they surpass the initial differentiation and migration towards the inner GCL of DG without having synaptically integrated in the network (***Deng et al., 2010***). It is during this time period that they undergo tonical activation mediated by GABA in the neurogenic niche (***Zhao et al., 2006, Esposito et al., 2005, Ge et al., 2006***). Newborn neurons <1 week after their generation extend their axonal projections, known as MFs, through the hilus, towards the CA3 and CA2 hippocampal environments (***Llorens-Martín et al., 2015, Zhao et al., 2006***).

- **2nd week after birth of newborn neurons in the adult DG**

During the 2nd week after their birth, newborn GCs begin to obtain more neuronal characteristics. These include the first appearance of polarized processes, with dendrites oriented and elongated towards the ML, MFs (the axons of GCs), directing and stretching to the hilus and CA3 subregion (***Zhao et al., 2006***), as well as the formation of the dendritic spines (***Zhao et al., 2006***). These very young abGCs are characterized by very high input resistance and altered firing activity compared with dbGCs (***Esposito et al., 2005***). Moreover, a characteristic of particular interest during this time period, is the absence of glutamatergic inputs in young abGCs. This could be explained by the nonexistence of dendritic spines in the ML (***Zhao et al., 2006, Esposito et al., 2005***), which are the sites where the excitatory synapse formation take place. On the contrary, during this time period are

present GABAergic synaptic inputs which provoke depolarization due to the presence Na^+-K^+-$2Cl^-$ co-transporter (NKCC1 chloride importer) (***Represa and Ben-Ari, 2005***). These GABAergic inputs, are presumably derived by local INs leading to responses with slow synaptic kinetics (rise and decay time) (***Esposito et al., 2005, Ge et al., 2006, Overstreet-Wadiche et al., 2005, Markwardt et al., 2009***). This initial depolarizing effect of GABAergic synaptic inputs in newborn granule neurons before excitatory synaptogenesis, seems to possess a trophic role aiding in their survival and maturation (***Represa and Ben-Ari, 2005, Ge et al., 2007***). $GABA_A$-receptor mediated depolarization promotes the following activation of NMDA receptors having as a result the unsilencing of the initial glutamatergic synapses on developing neurons (***Leinekugel et al., 1997, Wang and Kriegstein 2008***). Hence, during the first 2 weeks, immature granule neurons lack of glutamatergic inputs and their activity is limited to intrinsic hippocampal activity only.

- **3rd week after birth of newborn neurons in the adult DG**

The 3rd week after the birth of the newborn granule neurons in the adult DG signals the formation of afferent and efferent connections of newborn GCs with the existing neuronal network. What is more, ~16 days after birth, newborn GCs begin to form the first dendritic spines, the structures in which will take place the creation of excitatory synapses. By the 16th day, dendritic spines start to create synapses with afferent axons fibers of the EC Layer II (***Zhao et al., 2006, Toni et al., 2007***). This local synaptic activity facilitates the integration of newborn GCs into the existing neuronal network (***Toni et al., 2007***). Quantitative studies indicate that it is during the 3rd - 4th week that spine density reaches its peak.

Another important change that takes place during this time period, is the conversion of GABAergic synaptic inputs from excitatory (depolarizing action) to inhibitory (hyperpolarizing action). In addition, glutamatergic synaptic inputs start to appear (***Esposito et al., 2005, Ge et al., 2006***). NMDA-receptor (NMDAR) is implicated in synaptic plasticity linked with neuronal development, which seems to be high between 2-3 weeks after birth of newborn GCs (***Bliss & Collingridge 1993***). During this time period, the survival of newborn granule neurons is highly dependent on NMDAR-mediated cell-autonomous activity (***Esposito et al., 2005, Ge et al., 2006, Tashiro et al., 2006***). The electrophysiological characteristics are still indicative of immature abGCs including high input resistance and high resting membrane potentials (***Esposito et al., 2005***), which in turn explains the low threshold for the induction of long-term potentiation (LTP) and the high excitability observed in abGCs (2-3 weeks old).

Newborn neurons from 1-3 weeks old post-mitotic could be committed to the neuronal fate if they confront EE, learning tasks or electrical stimulation (***Kee et al., 2007, Tashiro et al., 2007, Kitamura et al., 2010, Anderson et al., 2010***), which proves the importance of this time period for the survival of newly-generated GCs. Experimental studies in abGCs during this time period, have highlighted the importance of GABAergic depolarization and the presence of NMDA receptors (***Tashiro et al., 2006***) in order to promote newborn neurons survival.

It is during ~2-3 weeks post-mitosis that newborn neurons start to create synapses with the excitatory population of pyramidal neurons in CA3 and CA2 hippocampal subregions (***Gu et al., 2012, Llorens-Martín et al., 2015, Toni et al., 2008***), as well as with hilar MCs (***Toni et al., 2008***).

- **4th-6th week after birth of newborn neurons in the adult DG**

The 4th week after the birth of DG abGCs, initiates the phase where immature abGCs exhibit strong LTP, which is indicated by the lower threshold for the induction of LTP and higher LTP amplitude in

comparison with mature GCs (***Ge et al., 2007***). That temporal subpopulation of immature abGCs have got high intrinsic excitability, mediated by NMDAR subunit NR2B (***Ge et al., 2007***). At the age of 4-weeks old, abGCs have been fully and functionally integrated into the trisynaptic hippocampal circuit. As far as their morphology is concerned, dendritic length, dendritic spines and axonal buttons of this neuronal population continues to surpass structural modifications (***Zhao et al., 2006, Toni et al., 2007, Toni et al., 2008***).

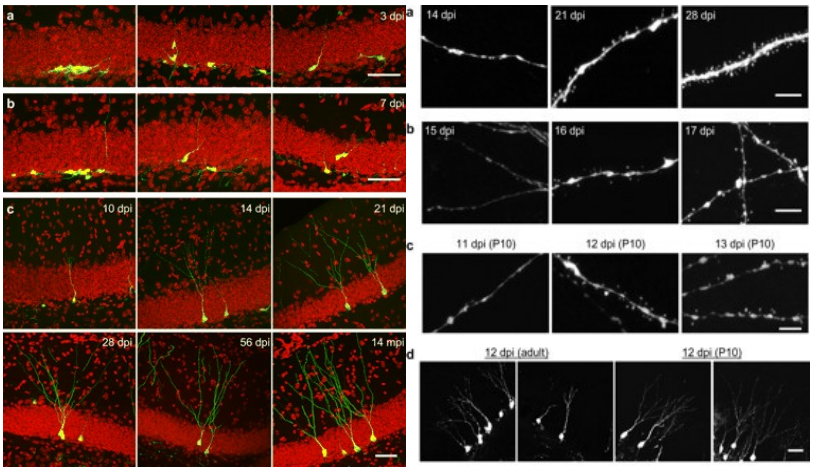

Figure 17: Maturation stages of adult-born granule cells. **Left:** Experimental data of the morphological development of adult-born granule neurons in the adult brain of mouse. Dividing cells of 7- to 10-week-old C57BL//6 mice were labeled with GFP through retrovirus-mediated gene transduction (***Adopted by Zhao et al., 2006***). **Right:** Spinogenesis in newborn granule neurons in dentate gyrus of adult brain in mice. Examples (a-d) of dendritic segments from adult mouse brains taken at different days after virus injection (***Adopted by Zhao et al., 2006***).

During adult neurogenesis in the DG, immature neurons start to extend their apical dendrites towards ML by ~1 week after differentiation of NPCs of SGZ in immature abGCs. First, dendritic spines make their appearance at ~16 days post division (16 d.p.d.), while spine density is augmented considerably between ~21 d.p.d. and ~28 d.p.d. (between ~3-4 weeks-old immature abGCs) (***Zhao et al., 2016***). This time period, especially after 4 weeks from the cell birth of new neurons, is of crucial importance for the processes of memory and learning in the adult hippocampus, while it is speculated that the neuronal population of this age contributes with a special role in the function of adult DG (***Tashiro et al., 2007,Nakashiba et al., 2012***). The augmentation of the number of dendritic spines seems to reach a stable point/plateau at ~56 days post division. It is the first period of maturation of abGCs, between 1-2 months, that are of special importance for the plastic and dynamic character of spines, which is also regulated by network activity (***Zhao et al., 2006***).
MFs manage to reach CA3 region even without the formation of the first dendritic spines (***Zhao et al., 2006***). Already, at 10 days post division, thin axon fibers are present in the hilus, elongating more and more until they will reach the CA3 region (***Zhao et al., 2006***).
Taking into consideration the differences that GCs of DG present according to the time period in which we study them, it is well-based to make the assumption that they potentially have also different roles in different time periods of their maturation (***Schmidt-Hieber et al., 2004, Espósito et al., 2005, Nakashiba et al., 2012, Ge et al., 2006, Overstreet-Wadiche et al., 2006, Piatti et al., 2006***).

1.8 Possible roles of adult-born granule neurons in hippocampal-based behaviors

Hippocampus different parts along the dorsoventral axis are implicated also in different functions. Hence, the dorsal hippocampal area is more implicated in spatial navigation, learning and memory processes while the ventral hippocampal area is more important for stress and anxiety regulation (***Fanselow and Dong 2010, Kheirbek et al., 2013***). The addition and incorporation of newborn adult neurons in the DG, takes place along the dorsoventral axis of this hippocampal structure. As a result, it is logically based to assume that this newly added population of neurons may be implicated in more hippocampal functions (***Cope and Gould 2019***). The adoption of experimental techniques such as knockdown studies, elimination of adult-born neuronal population, x-ray irradiation, pharmacological or transgenic techniques in cooperation with computational models could potentially provide secure results (***Cope and Gould 2019***).

Because of their special morphological and electrophysiological characteristics - that were mentioned in the previous section - abGCs are considered as unique contributors to hippocampal function (***Kempermann et al., 2004, Aimone et al., 2006, Treves et al., 2008***).

There is a plethora of studies indicating the special contribution of abGCs in hippocampal-dependent behaviors. During the birth of newborn neurons in the DG, the majority of these cells does not manage to survive and be incorporated in the hippocampal circuit. This massive cell death can be rescued by deletion of pro-apoptotic protein Bax (***Sun et al., 2004, Kim et al., 2009***) or conditional deletion in Nestin-expressing progenitors leading to elevated numbers of abGCs (***Sahay et al., 2011, Ikrar et al., 2013***). The aforementioned experiments permit neuroscientists to understand the contribution of adult-born neurons in hippocampal based behaviors. Furthermore, abGCs are considered as independent encoding units that encode discrete spatial and temporal information affecting the function of dbGCs (***Anacker and Hen 2017***).The possible contribution of abGCs in hippocampal processing of information was indicated by experimental studies in which low or absent levels of neurogenesis has as a result impaired performance in the accomplishment of hippocampal-dependent learning tasks (***Abrous et al., 2005, Doetsch & Hen 2005, Leuner et al., 2006, Dupret et al., 2008, Imayoshi et al., 2008***) or hippocampus-dependent memory function (***Winocur et al., 2006***).

It has been recognized that learning procedure recruits abGCs (***Gould et al., 1999, Leuner et al., 2004,***). Namely, experiments in rodents have highlighted the importance of adult neurogenesis in hippocampal based learning tasks, like temporal based associations or spatial contextual navigation (***Drapeau et al., 2003, Dupret et al., 2007, Shors et al., 2001, Shors et al., 2002***). Morris water maze (MWM) is a common experimental technique used to study the spatial memory. Studies that have used c-Fos and Arc as indicators for neuronal activation, have pinpointed the possible implication of young GCs in spatial information processing and memory formation, proposing that this temporal category of GCs is recruited preferentially into specific neuronal circuits (***Kee et al., 2007, Ramirez-Amaya et al., 2006, Tashiro et al., 2007***). In these procedures there is a bidirectional process; adult neurogenesis is needed for the accomplishment of these trials but also, these trials promote adult neurogenesis. On the contrary, other studies have indicated that adult neurogenesis is not required for the accomplishment of non-hippocampal based learning tasks (***Döbrössy et al.,***

2003). Thus adult-born neurons contribute significantly in hippocampal-based learning and memory process.

During the critical period, abGCs could be recruited during spatial learning, fear memory retrieval and anxiogenic conditions (***Tashiro et al., 2006, Kirby et al., 2012, Schoenfeld et al., 2013, Stone et al., 2011, Kee et al., 2007***). In experiments with the location of the rodent/mice into novel and/or enriched environment, adult neurogenesis was increased, implying a possible role of abGCs to novelty encoding (***Kempermann et al., 1997, Kempermann et al., 1998, van Praag et al., 1999***). Thus, abGC incorporation into the adult DG facilitates the encoding of new information without affecting former memories (***Aimone et al., 2009, Appleby et al., 2009, Appleby et al., 2011***). Moreover, as it was underlined both by computational and electrophysiological studies, abGCs during this critical period may support the temporal information encoding (***Aimone et al., 2006, Rangel et al., 2014***). Studies that made use of the expression levels of immediate early genes in order to formulate a complete image of neuronal activity, found out that the contribution of abGCs is focused on spatial processing and memory formation, two procedures during which they are active (***Ramirez-Amaya et al., 2006, Kee et al., 2007, Tashiro et al., 2007***). Hence, adult-born neurons exert a crucial role in novelty encoding, temporal information coding and spatial memory formation.

It is noteworthy to be referred that this adult type of plasticity is different from the developmental plasticity, with adult neurogenesis being a mechanism with dual role. Hence, adult neurogenesis not only replace the neuronal population that is lost due to normal aging, but also provides an ongoing developmental process during which abGCs are added in the mature neuronal population, augmenting the plasticity and the storage capacity of DG, using the appropriate responses to environment (e.g. enriched environment *vs* stressful environment) (***Galvan and Jin 2007***).

The specific contribution that abGCs have in pattern separation process was investigated with experiments in mice. In one set of experiments, the reduction of abGCs in mice has as a result impaired performance in pattern separation (***Clelland et al., 2009, Scobie et al., 2009, Tronel et al., 2012***). In another set of experiments in mice, the reverse procedure was followed, with augmentation of abGCs leading to the improvement of pattern separation capability (***Creer et al., 2010, Sahay et al., 2011***). However, neither of the aforementioned studies made a temporal distinction in adult-born granule neuronal populations while we are aware that mature and immature abGCs have special intrinsic properties depending on the maturation stage that they are. Thus, the parameter of time could be a possible indicator of different functional contribution of abGCs in the hippocampal trisynaptic circuit. Experimental study in transgenic mice lines has proposed the contribution of immature abGCs (~3-4 weeks after their birth) in pattern separation, while the dbGCs and mature abGCs seems to affect more consistently the pattern completion (***Nakashiba et al., 2012***). Experimental data from behavioral studies and computational models, support the notion that the principal role of adult neurogenesis is to ameliorate pattern separation (***Deng, Aimone and Gage 2010***). The ablation of adult neurogenesis in the DG could have potential defects in the process of contextual pattern separation. Experimental research, using special transgenic mice lines where adult neurogenesis was ablated (***Dupret et al., 2008, Revest et al., 2009***), has revealed this effect (***Frankland et al., 1998, McHugh et al., 2007***) even when the ablation of adult neurogenesis was induced after extensive training (***Tronel et al., 2012***). Conclusively, abGCs are implicated in

spatial memory (*Dupret et al., 2008, Imayoshi et al., 2008, Zhang et al., 2008, Deng et al., 2009*) and spatial pattern separation (*Clelland et al., 2009, Creer et al., 2010*).
There is considerable evidence of the involvement of adult neurogenesis in pathological conditions related to mental health (*Snyder 2019, Toda et al., 2018, Yun et al., 2016*), like depression (*Miller et al., 2015*), schizophrenia (*Yun et al., 2016*), anxiety (*Miller et al., 2015*), chronic stress, addiction (*Mandyam et al., 2012*), epilepsy (*Jessberger & Parent 2015, Rotheneichner et al. 2013, Cho et al., 2014, Danzer 2012, Danzer 2019*) and age-related disorders like the memory fading due to aging or dementia (including Alzheimer's Disease (AD)) (*Moreno-Jiménez et al., 2019, Lazarov & Marr 2010, Scopa et al., 2019*).
A model of adult neurogenesis in the hippocampus based on biologically plausible hippocampal circuits (*Weisz & Argibay, 2009*), supports that the capacity of hippocampal network for new information storage is elevated through neurogenesis, as well as boosting the process of forgetting old memories. What is more, Weisz and Argibay (*Weisz & Argibay 2012*), indicated a new working hypothesis, highlighting the mechanism of forgetting as a possible and realistic role to be attributed to adult neurogenesis. More specifically, they recognize that newborn neurons added in the network, endow the network with mechanisms like pattern separation of events distinct in time, pattern integration of temporarily close events, and in the creation of a mechanism of interference through the retrieval of old memories relating adult neurogenesis with forgetting (*Weisz & Argibay 2012*).
Computational studies have suggested the necessity of adult neurogenesis for the avoidance of interference of memories and the existence of cognitive flexibility (*Appleby et al., 2009, Appleby et al., 2011, Wiskott et al., 2006, Rubin et al., 2014, McClelland et al., 1995, Hvosief-Eide & Oomen 2016*).

1.9 Regulators of adult hippocampal neurogenesis

One of the most important factors that regulate adult neurogenesis in the hippocampus, is the hippocampal-dependent learning (*Gould et al., 1999*). Experimental studies have pinpointed that hippocampus-dependent learning, and not hippocampal-independent tasks, promotes the survival and the elevation of numbers of abGCs at ~1-week of age (*Gould et al., 1999, Epp et al., 2007, Leuner et al., 2004, Leuner et al., 2006*). Nevertheless, the hippocampal-associated learning affects only abGCs at the age of 1-week and older - meaning that they have already been committed to the neuronal lineage - and not NPCs of the SGZ (*Gould et al., 1999*). Similarly, the experiment using the MWM, promotes the survival and proliferation of abGCs of ~1-week old but not younger, in which is induced apoptosis (*Dupret et al., 2007*).
The existence of EE aids adult neurogenesis, promoting the survival of immature abGCs (*Kempermann et al,. 1997*). Furthermore, EE facilitates hippocampal-dependent learning and memory in paradigms like MWM or object recognition tests (*Kempermann et al., 1997, Bruel-Jungerman et al., 2005*). Notably, however, the EE affects immature abGCs that are < 3-weeks-old and not older, implying that the effect of EE is limited only in certain phases of maturation period, thus, it is dependent on the age of abGCs (*Tashiro et al., 2007*).
Moreover, other studies report that physical exercise not only acts beneficial for the physical health of trainees, but also contributes to the improvement of cognition and other brain functions (*Hillman et al., 2008, van Praag 2009*). Especially, voluntary running enhances adult neurogenesis not only in young but also in old animals (*van Praag et al. 1999, van Praag et al. 2005*).

1.10 Dendrites of granule neurons

Dendrites of GCs in DG possess some special characteristics as far as their morphology and integrative properties are concerned, consisting them different from dendrites of other hippocampal neurons such as the dendrites of pyramidal neurons in CA1 and CA3 hippocampal regions.

A special dendritic structure of GCs are the dendritic spines, small bulbous protrusions where takes place the formation of synapses. The glutamatergic, excitatory inputs arrive at dendritic spines of abGCs. The first dendritic spines, make their appearance in newborn neurons ~16 days after neuronal birth. The spine density follows an augmented period which reaches its peak at ~4-weeks after neuronal birth and continues to augment with lower rate the following weeks until the immature abGCs reach their full maturation at ~8 weeks-old (***Zhao et al., 2006***). During this time period NMDARs play a crucial role in spinogenegis.

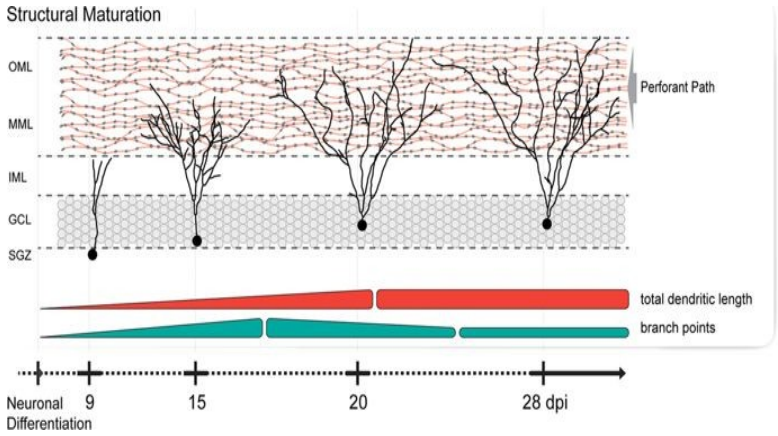

Figure 18: Temporal progression of adult-born granule neurons structural maturation. As it is clear from the graph, during the second week of development, the abGCs exhibit a phase of dynamic dendritic extension and retraction, branching and restructuring their dendritic arbor with a high net increase in both total dendritic length and branch points. During the third week after their birth, newborn neurons display elaborate dendritic tree while reaching at a maximum level of dendritic complexity. During this time frame, the restructuring dynamics are less pronounced. Lastly, between the third and fourth week, pronounced dendritic pruning is observed as the number of branches decreases. It is at the forth week after their birth that abGCs reach at a structural stabilization phase with only minor refinements of their dendritic arbor (***Adapted by Radic et al., 2017***).

The role of NMDARs after their birth, seems to be dual during GC development in adult DG. The first role is related with the promotion of the formation of dendritic spines and survival of abGCs. The second role that NMDARs perform is related with the spines magnification and the recruitment of AMPARs after the spine formation (***Mu et al. 2015***).

Also, $GABA_B$ seems to possess a possible role in GCs because is capable of adjusting the afferents from PP in the course of high-frequency stimulation (***Wang & Wojtowicz 1997***).

Dendrites of GCs branch generously in the inner third of the ML proximal to the soma, and continuously give rise to thin (small-caliber) dendrites that reach the outer and middle ML. GC dendrites of the outer two thirds of the ML receive and integrate the inputs from EC while dendrites of the inner third of the ML accept associational/commissural inputs (***Krueppel et al., 2011***). The dendritic tree of a DG GC is of characteristic shape, formulating a cone-shaped arbor (***Amaral et al., 2007***) with the major part of excitatory synapses to take place in the dendritic spines of the OML and MML. The voltage transfer of inputs, as well as their dendritic integration in these sites, is highly connected with active and passive properties of GC dendrites (***Krueppel et al., 2011***).

According to experimental study of dual somatodendritic records, it was shown that GC dendrites contribute to attenuation of synaptic input in dendritic spines of GCs, while they also process different spatiotemporal input patterns in a linear manner with a gain (***Krueppel et al., 2011***). However, a recent experimental study indicates the existence of dendritic spikes in GCs (***Kim et al., 2018***)**.**

Two key features that determine the dendritic integration are the morphological and passive properties of dendritic arbor, as well as the expression of voltage-gated ion channels. The presence of voltage-gated conductance can supply single dendritic branches with active properties as well as moderate excitatory postsynaptic potential (EPSP) propagation (***London and Häusser 2005***).

In dendrites of GCs, the presence of Na^+ voltage-gated channels seems to affect the dendritic propagation of evoked action potential (***Jefferys 1979***) however, this affection is weaker in comparison with that in pyramidal cell dendrites, a fact that is also reflected in the low tendency for generation of regenerative depolarization in GC dendrites. GC dendrites display a frequency-dependent voltage attenuation, exhibiting a considerably stiff attenuation as frequency augments (***Krueppel et al., 2011***). According to an experimental and computational study (***Krueppel et al., 2011***), GC dendrites exhibit linear integration with a variable gain in contrast with pyramidal cells CA1 which exhibit nonlinear integration. Hence, GC dendrites are characterized as linear integrators and strong attenuators.

A computational model (***Chavlis et al., 2017***) suggests that dendrites of DG GCs provide these particular neurons with high efficacy to perform pattern separation while their pruning (atrophy like in pathological situations), leads to deficiencies in this ability, thus GC dendrites contribute to pattern separation through controlling sparsity.

Moreover, the motility of dendritic spines reach its peak between time period of 1 to 2 months (4-8 weeks) after birth of abGCs while decreases afterwards (***Ge et al., 2007***).

1.10.1 Different dendritic effects of developmentally-born in comparison with adult-born granule neurons

Dendritic processes, consisting the places where synapse formation happens, arise a special interest for research. Dendritic spines are the major candidates for synaptic formation leading to the facilitation of neuronal communication and transfer of information (***Martina et al., 2003***).

From their birth until their full maturation, granule neurons undergo a period of extensive morphological and electrophysiological alterations which typically endure for 2 months (8-weeks). It has been noticed that during development, the length of dendrites augments while their input resistance decreases. Hence, we conclude that dbGCs have more elaborate dendritic trees, more elongated dendrites and lower input resistance, comparatively with abGCs. These newborn GCs have less complex dendritic trees, got thinner and shorter dendrites, thus indicating higher input resistance in comparison with dbGCs. The aforementioned differences, urge us to examine the relationship between dendritic morphology, passive electrical properties and EPSP waveform.

The accomplishment of neuronal communication is a complex process and the intricacy for the actualization of synaptic integration is controlled by a plethora of parameters like neuronal soma, dendritic complexity, axonal morphology, ion channel expression and distribution in neuronal membranes. The whole procedure becomes more complicated with the addition of time parameter

concerning how active properties of neurons, like action potential firing, are controlled (***Nicoll et al., 1993, Libersat and Duch 2004, Gulledge et al., 2005***).
The EPSP waveform is shaped by the membrane properties of the axons, somata and dendrites. What is more, EPSP time course is regulated in a noteworthy degree by the depolarizing EPSC and the intrinsic membrane properties.
The sprouting of GC dendritic tree during development contributes to the lower input resistance of dbGCs and the smaller membrane time constant , resulting in faster EPSPs.

1.10.2 Differences in dendritic morphology of dentate gyrus granule neurons according to their developmental phase

The dbGCs of DG in comparison with abGCs have not only differences in active and passive properties, but also in their dendritic morphology and structure e.g the number of dendritic spines, the total dendritic length, the elaboration of dendritic trees.
The architectural configuration of dendrites possess a paramount contribution in the integration and processing of inputs (***Lefebvre et al., 2015***). As a result, the presence of dendrites in our model is of crucial importance because it permits us to take into consideration their contribution in information processing. Additionally, the dendritic differences reflect the developmental effect on computational functions that DG GCs perform. It was revealed that neurons that possess more elaborate dendritic branches are preferentially recruited during spatial navigation (***Diamantaki et al., 2016***).

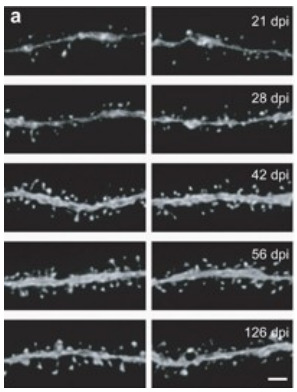

Figure 19: Maturation of granule neurons born in the adult brain of mouse. We can observe the dendritic spine analysis from newborn neurons at 21, 28, 42, 56 and 126 days after viral injection (***Adapted by Zhao et al., 2006***).

1.11 Why do we choose to model adult-born granule neurons separately?

In our network model, we decided to incorporate not only the numerically privileged population of dbGCs, but also the two distinct populations of abGCs.
Although it was widely reported that abGCs as they mature (especially at 8-weeks after their birth) become more and more indistinguishable from dbGCs, they possess some unique properties that supply them with noteworthy behavioral functions. Novel experimental evidence reveals that these special properties of adult-born neurons are widely conserved beyond the traditionally defined critical period of 4-6 weeks old (***Snyder, 2019***).

Particularly, studies in rodents have revealed slower maturation of neurons born in the adult DG. While their development recapitulates embryonic development of dbGCs, the duration of the whole process in much longer (***Overstreet-Wadiche et al., 2006***). Moreover, newborn neurons augment their dendritic spine number and the number of formulated synapses and elongate their dendrites with a retardation in comparison with the same process in dbGCs (***Trinchero et al., 2017***).
Additional indications include studies with experience-dependent modification of newborn neurons in the adult DG. EE or running lead to an elaborate dendritic tree and an increment of dendritic spine density for newborn abGCs ~1-weeks after their birth (***Tronel et al., 2010***). Also, enhanced structural plasticity is noticed in abGCs of 2-4 months old while their removal impaired learning (***Lemaire et al., 2012***).

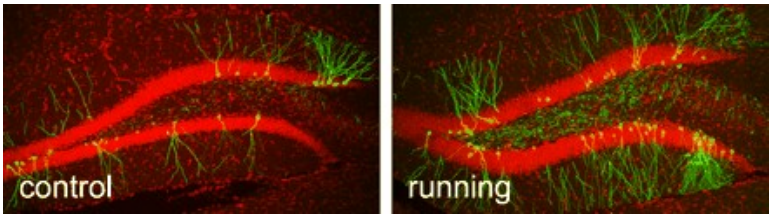

Figure 20: Dentate granule neurons in control and running conditions. Imaging of mature granule neurons after GFP labeling in control and voluntary running mice at 56 dpi. It is obvious that voluntary running promotes maturation of adult-born granule neurons (***Adopted by Zhao et al., 2006***).

1.11.1 Special characteristics of immature abGCs

The period of maturation of newborn GCs in the adult DG could be characterized as a critical time period between 2-6 weeks after their birth. A series of key studies in rodents, especially mice, has revealed the special characteristics of immature abGCs during the aforementioned time period.
Newborn GCs are not fully developed and they undergo a short temporal period until they reach their full maturation. During this special time period, these neurons exhibit distinctive intrinsic and synaptic properties which differ from the respective properties when they are indistinguishable from old GCs. These discrepancies may be responsible for the underlying contribution of neurogenesis to memory encoding (***Schmidt-Hieber et al., 2004, Ge et al., 2007, Aimone et al., 2011, Marín-Burgin et al., 2012, Dieni et al., 2013, Brunner et al., 2014, Dieni et al., 2016***).
More specifically, immature abGCs exhibit enhanced excitability and plasticity from ~ 2 weeks to 5 months after their birth (***Wang et al., 2000, Snyder et al., 2001, van Praag et al., 2002, Ambrogini et al., 2004, Schmidt-Hieber et al., 2004, Espósito et al., 2005, Ramirez-Amaya 2005, Song et al., 2005, Ge et al., 2006, Overstreet-Wadiche et al., 2006***). Also, immature GCs exert a special role in dbGCs as their augmentation decreases EPSCs and spine density in mature neurons (***Adlaf et al., 2017***). What is more, except membrane properties, and connectivity, immature abGCs also present differences that concern their morphology in comparison with dbGCs (***Espósito et al., 2005, Ge et al., 2006, Overstreet-Wadiche et al., 2006, Piatti et al., 2006, Zhao et al., 2006***).
During the maturation period of immature abGCs, it is noted that they present enhanced plasticity (***Schmidt-Hieber et al., 2004, Ge et al., 2007***). Except their high input resistance, abGCs are characterized by increased tendency for the appearance of long term potentiation (LTP) due to the Layer II EC inputs via the PP (***Wang et al., 2000, Schmidt-Hieber et al., 2004, Ge et al., 2007***).
Accumulating evidence from experimental and behavioral studies reinforces the claim that immature abGCs of ~4-weeks old contribute in a special way to the DG function through their

unique properties. For example, behavioral studies of eye-blink conditioning and long-term MWM retrieval have pinpointed that the reduction in the numbers of ≤4-weeks old immature abGCs drive in impaired performance in the above behavioral tasks (***Shors et al., 2001, Snyder et al., 2005***). It should be noted that this observation is valid only for neuronal population of GCs at the age of ≤4-weeks old but not for older granule neurons.

The existence of a critical period in maturation of abGCs also specifies the existence of two crucial characteristics, absent from mature GCs. The first one is their elevated synaptic plasticity (***Wang et al., 2000, Snyder et al., 2001, Schmidt-Hieber et al., 2004, Ge et al., 2007***), while the second one is about their input-dependent survival, mediated by NMDA-receptor involvement (***Tashiro et al., 2006***).

The existence of this critical time period, places the parameter of time as a crucial determinant of DG function. It was proposed (***Aimone et al. 2006***) that these newborn GCs may possess a key role in the formation of temporal associations in memory. This proposal, taking into consideration the dynamic nature of the temporal constitution of DG GC population, suggests that there are temporal clusters of long-term episodic memories within the gradual changing of hippocampal DG. We should note that the duration of the critical period in the development of abGCs, concerns experimental findings in mice. If we attempt scaling up this critical period in humans according to their lifespan, then this critical period of enhanced plasticity and morphological dynamic nature could last for at least a decade.

At this point it should be noted that mature abGCs that are ~6-weeks old after their birth, ordinarily are characterized as indistinguishable from dbGCs (>8-weeks old). However, there is increasing evidence about their unique properties that extend the 4-6 weeks, also known as critical period of abGCs.

To summarize, during the critical period 4-6 weeks of age for abGCs, the special characteristics of young granule neurons that distinguish them from the dbGCs are the following:

- Distinct electrophysiological properties
- High intrinsic excitability (***Espósito et al., 2005, Ambrogini et al., 2004, Overstreet-Wadiche et al., 2005, Wang et al., 2000, Schmidt-Hieber et al., 2004, Couillard-Despres et al., 2006***)
- Weak glutamatergic inputs from Layer II of EC are able to elicit action potentials
- High input resistance
    - Young adult-born neurons display high input resistance due to a low density of membrane K^+ channels during early development
- Lack of GABAergic inhibition
    - Due to the high input resistance and lack of GABAergic inhibition, abGCs have a tendency to be hyperexcitable as well as exhibit lower activation threshold in comparison with dbGCs
- For some time period, abGCs exhibit excitatory instead of inhibitory response to the GABA neurotransmitter (***Chancey et al., 2013***), a characteristic which partially explains why these neuronal population is more excitable than mature granule neurons, which are strongly inhibited (***Amaral et al., 2007, Pelkey et al., 2017***)
- Firing behavior of high efficacy

- Enhanced LTP (*Ge et al., 2007*) and plasticity, mediated by NR2B-containing NMDA receptors (*Tannenholz et al., 2016, Ge et al., 2007, Toni et al., 2016*)
- Increased LTP amplitude (*Ge et al., 2007*)
- Decreased LTP induction threshold (*Ge et al., 2007, Schmidt-Hieber et al., 2004*)
- Lower threshold for LTP of their cortical inputs (from EC Layer II) which is attributed to the presence of T-type Ca^{+2} channels, NR2B-containing NMDA receptors and reduced GABAergic inhibition (*Wang et al., 2000, Snyder et al., 2001, Schmidt-Hieber et al., 2004, Ge et al., 2007*).
- Developmentally regulated synaptic expression of NR2B subtypes which possess also an instructive role in the enhanced plasticity (*Ge et al., 2007*).
- Shorter dendritic tree
- Thinner dendritic processes
- Immediate-early gene studies that are indicators of cellular activity imply higher responsiveness of newborn GCs to new environments (*H. Makino, A.Tashiro and F.H.G., Soc. Neurosci. Abstr. 141.3, 2005*)
- Demonstrate a special effect in hippocampal-based behaviors (*Denny et al., 2012*)

1.11.2 GABAergic Synapses at abGCs of dentate gyrus

The major inhibitory neurotransmitter in the adult brain is GABA, which exerts its fast action through activation of Cl^- ions $GABA_A$-receptors (*Bartos et al., 2007, Ben-Ari 2002, Owens & Kriegstein 2002, Delpire 2000, Payne et al., 2003*). Experimental evidence show that during the procedure of maturation of abGCs, GABAergic action is altered from depolarizing to hyperpolarizing (*Ge et al., 2006, Sun et al., 2009, Ming and Song 2011*). GABA reversal potential (E_{GABA}) changes during development of granule cells from -40 mV to -70 mV (*Chiang et al., 2012*). This decline in GABA reversal potential (E_{GABA}) during maturation could be explained by the higher intracellular concentration of Cl^- in newborn neurons in the adult brain. Moreover, $GABA_A$ conductance in dbGCs will remain 'shunting' when it occurs during action potential generation (*Chiang et al., 2012*).

Inhibitory INs into the DG, primarily release GABA, which in turn, activates ionotropic $GABA_A$Rs or metabotropic $GABA_B$Rs. In dbGCs, there are Cl^- channels that hyperpolarize them. In abGCs, $GABA_A$R-mediated currents are depolarizing due to a reverse Cl^- gradient.

For the dbGCs, GABA is the main inhibitory neurotransmitter, however, for immature abGCs and NPCs, GABA acts as a trophic factor via Cl^- mediated depolarization. In newborn granule neurons, the expression of Na^+-K^+-$2Cl^-$ cotransporter 1 (NKCC1, a Cl^- importer) is high while K^+-Cl^- cotransporter 2 (KCC2, a Cl^- exporter) is low, leading to high intracellular Cl^- concentration (*Chiang et al., 2012*).

Experimental evidence supports that newborn granule neurons in the adult brain firstly accept tonic activation mediated by GABA before the appearance of phasic/synaptic activation (*Ge et al., 2006*), afterwards they accept GABA-mediated synaptic inputs and in the end excitatory glutamate-mediated synaptic inputs following the same integration process in the adult brain as in neonates developmental procedure (*Ben-Ari 2002, Owens & Kriegstein 2002, Wang et al., 2005, Overstreet-Wadiche et al., 2005, Wang et al., 2003, Tozuka et al., 2005*).

GABAergic INs in the DG, manage to control the neuronal activity via inhibition, through the release of the neurotransmitter GABA (***Freund and Buzsáki 1996, McBain and Fisahn 2001, Klausberger and Somogyi 2008***). GABAergic INs may act through two ways: either targeting the soma of the principal neuron or its dendrites. Perisomatic targeting interneurons in the DG, like BCs, control the spike initiation of principal type of neurons in the DG – granule neurons - via axonal innervations onto perisomatic areas of GCs (***Cobb et al. 1995, Miles et al. 1996***), while dendritic targeting INs like HIPP cells, regulate dendritic, electrical and biochemical signaling and synaptic plasticity through innervating dendrites of GCs (***Miles et al. 1996, Leão et al. 2012, Chiu et al. 2013***).

1.11.3 AMPA/NMDA Synapses at abGCs

It was shown that abGCs express functional AMPA and NMDA receptors (***Schmidt-Salzmann and Bischofbrger 2014***). Initially, the density of AMPA receptors in immature neurons that have started to accept excitatory synaptic inputs is small (***Schmidt-Salzmann and Bischofbrger 2014***). Nevertheless, AMPA receptor density is increased until the granule neuron reach its full maturation (***Schmidt-Salzmann et al., 2014***). NMDA receptors' kinetics and density, do not appear noteworthy differences between dbGCs and abGCs having as a result an enhanced NMDA/AMPA receptor density ratio (***Schmidt-Salzmann et al., 2014***). Iontophoretic application of glutamate into abGCs revealed an enhanced dendritic NMDA/AMPA ratio.
The formation of new glutamatergic synapses in abGCs is very important for their future survival and maturation (***Tashiro et al., 2006, Tronel et al., 2010***) as well as for the information processing in the hippocampus (***Kee et al., 2007, Cleeland et al., 2009, Sahay et al., 2011, Nakashiba et al., 2012, Gu et al., 2012***). Immature abGCs express functional NMDA receptors even before the synapse formation (***Tashiro et al., 2006***). Expression density and gating properties of extra-synaptic NMDA-receptors are not significantly different between mature and immature GCs (***Schmidt-Salzmann et al., 2014***).

1.12 Posing the main target of this study

To reinstate the main target of this study, reasonably, we pose the question: **what's the role of newborn adult granule neurons in the hippocampus function and hippocampus-related behaviors?**
Nonetheless, there is more evidence from computational and experimental behavioral studies for the role of adult neurogenesis in learning and memory (***Deng et al., 2010, van Praag et al., 2002, van Praag et al., 1999, Gould et al., 1999***). There is increased evidence that DG contributes to spatial and episodic memory serving as a pattern separator (***Leutgeb et al., 2007, Nakashiba et al., 2008, Bakker et al., 2008***).

2. MATERIALS & METHODS

2.1 Modeling the neuronal populations of the network

The principal neuronal population of DG Network – i.e GCs - were modeled in their three different maturation stages (dbGCs, mature abGCs, immature abGCs) as simplified neurons (***Izhikevich 2003, Burkitt 2006***) without internal geometry, i.e. as "point neurons" with various number of compartments. Specifically, the GC populations were simulated as multicompartmental neurons with soma and dendrites (12 dendrites → 21 dendritic compartments for dbGCs and 3 dendrites → 9 dendritic compartments for abGCs) in order to investigate the contribution of dendrites in pattern separation. As far as the remaining neuronal populations of MCs, BCs and HIPP cells are concerned, they were simulated as simple somatic compartments without dendritic processes.

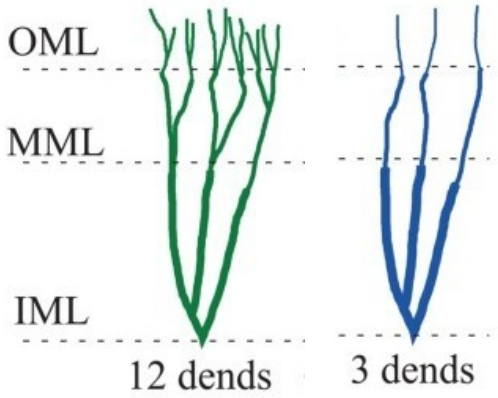

Figure 21: Morphology of the modeled granule neurons. The dentate gyrus is divided into three distinct layers; the molecular, the granular and the polymorphic layer (hilus). The GC dendrites extend in the molecular layer, which is further divided into the inner, medial and outer molecular layer. In our multicompartmental neuronal model, we discretized the dendritic compartments both of dbGCs and abGCs accordingly. In the left side (green) we can see the multicompartmental dbGC which is comprised of 12 dendrites and 21 dendritic compartments, while in the right (blue) we can see a modeled abGC which is comprised of 3 dendrites and 9 dendritic compartments (***Adapted by Chavlis et al., 2017***).

For the modeling of GCs in the DG computational network, we took into consideration experimental findings about the morphology of their dendritic and somatic compartments (***Claiborne et al. 1990***). Whenever, it was necessary, we adjusted them in order to simulate the intrinsic properties of GCs during their different developmental stages in an efficient manner by matching the experimental evidence.

In the following table, are summarized the morphological characteristics of GC populations in the DG network.

SOMA	**dbGCs**	**Mature abGCs**	**Immature abGCs**	**Source***
Length (μm)	18.0	15.0	12.0	*Amaral et al., 2007*
Diameter (μm)	14.0	12.0	10.0	*Amaral et al. 2007*
DENDRITES	**Length – Diameter (μm)**	**Length-Diameter (μm)**	**Length-Diameter (μm)**	

Distal	215 – 0.90	180 – 0.90	110 – 0.65	*Schmidt-Hieber et al., 2004*
Medial	215 – 1.0	180 – 1.10	110 - 0.85	*Krueppel et al., 2011*
Proximal	215 – 1.50	180 – 1.30	110 - 1.25	*Schmidt-Hieber et al., 2004*
No. segments	21	9	9	
No. branches	3	3	3	
No. tips	12	3	3	

Table 1: Morphological characteristics of modeled granule cells. A summary of the morphological characteristics of somatic and dendritic compartments of granule cells at different developmental stages. When it is necessary, the experimental findings for morphological characteristics were adjusted in order to reproduce better their intrinsic properties.
* The anatomical data for dbGCs, mature and immature abGCs may deviate in some cases but this is justified by the simplicity of our implemented model.

2.1.1 Modeling BCs, MCs, and HIPP Cells

In the neuronal populations of MCs, BCs and HIPP cells the implemented model was the Adaptive Exponential Integrate-and-Fire (AdEx) model (***Brette & Gerstner 2005***). In the following section we describe the AdEx model with further details. BCs, MCs and HIPP cells were modeled as simple point neurons without dendritic compartments. The table below summarizes the model parameters for the populations of BCs, MCs and HIPP cells.

Model Parameters	Basket Cells	Mossy Cells	HIPP Cells
E_L (mV)	-52.0	-64.0	-59.0
g_L (nS)	18.054	4.53	1.930
C (nF)	0.1793	0.621	0.0584
V_r (mV)	-45.0	-49.0	-56
V_T (mV)	-39.0	-42.0	-50
ΔT (mV)	2	2	2
a (nS)	0.1	2	0.82
τ_w (ms)	100	180	93
b (nS)	0.0205	0.0829	0.015

Table 2: Parameters of Adaptive-Exponential Integrate-and-Fire (AdEx) model for basket, mossy and HIPP cells.

2.1.2 Modeling GC Principal Neuronal Population

In the network of our computational model, we included three different neuronal populations of granule neurons according to their maturation stage that coexist each time that we study DG network. These were dbGCs (>8 weeks-old), mature abGCs (~8 weeks-old) and immature abGCs (~4 weeks-old).
The main incentive that motivated us to simulate GCs as multicompartmental neurons was our target to unravel how their dendritic processes may contribute to the pattern separation function according to different maturation stages or for different network compositions. Hence, we included not only the soma but also dendritic compartments (12 for the dbGCs and 3 for the mature and immature abGCs). At this stage, we should mention that the dendritic morphology for GCs was

based on anatomical data extracted from bibliography (***Claiborne et al. 1990***). The AdEx model was implemented only in the somatic compartment of the GC population, while in their dendritic compartments was implemented the Leaky Integrate-and-Fire (LIF) model. The spike mechanism was active only in the soma and absent in the dendritic compartments. Current bibliography support the inexistence of dendritic spikes in GCs (***Krueppel et al., 2011***) except a recently published study (***Kim et al. 2018***).

We are aware of the division of DG into three distinct layers: the molecular, granular, and polymorphic/hilus (***Amaral et al., 2007***). The dendritic processes of GCs are extending into the molecular layer, which is further divided into IML, MML and OML from bottom to top. Following this architectural structure, we discretized the dendritic compartments accordingly. Based on anatomical data we are aware that the dbGCs possess 10-15 dendrites, so we included 12 dendrites (21 dendritic compartments) in the modeled dbGC in our network. As far as the abGCs are concerned, we are aware that they have got thinner and shorter dendritic processes, so we included 3 dendrites (9 dendritic compartments) for the abGCs. In that way we could investigate if the dendritic processes and the maturation stage of DG's main neuronal population, affect pattern separation function and the activity of the DG network. Taking also into account the existence of dendritic spines in the GC dendrites (***Aradi & Holmes 1999***), we increased the dendritic capacitance of dendritic compartments in comparison with that of the somatic in order to account for the increased surface area in the biological neurons. In the table below, are presented the parameters of the AdEx model that we utilized in order to reproduce the intrinsic properties of GC populations during different developmental stages.

AdEx Parameters	dbGCs	Mature abGCs	Immature abGCs
	Soma - Dendrites	Soma - Dendrites	Soma - Dendrites
E_L (mV)	-80.6, -75.6	-71.7, -66.7	-63.0, -58.0
g_L (S/cm^2)	35 x 10^{-4} - 35 x 10^{-4}	7 x 10^{-4} - 4 x 10^{-4}	6 x 10^{-4} - 3 x 10^{-4}
C (μF/cm^2)	1.5 - 2.5	1.0 - 2.5	1.0 - 2.5
V_r (mV)	-59.8	-57.7	-57.7
V_T (mV)	-45.0	-49.0	-40.0
ΔT (mV)	2	2	2
a (nS)	1.0	1.0	0.85
τ_w (ms)	25	28	30
b (nS)	0.1	0.0805	0.0805

Table 3: AdEx parameters for GCs at three distinct maturation stages. A summary of AdEx model parameters for GC populations in the DG network. In parentheses are denoted the units for each parameters they were indicated in the Brian Simulator 1.4.4.

2.2 Adaptive Exponential Integrate and Fire Model (AdEx)

Adaptive Exponential Integrate-and-Fire-Model (AdEx) is a two dimensional Integrate-and-Fire model which combines an exponential spike mechanism with an adaptation equation (***Brette & Gerstner 2005***). This model is a simplified phenomenological neuron model of the integrate-and-fire category that give the advantage of fewer parameters that need to be set. AdEx model is based on the exponential integrate-and-fire model, (***Fourcaud et al. 2003***) and the two-variable model of Izhikevich (***Izhikevich, 2003***).

The AdEx model is described by the two following differential equations:

$$C\frac{dV}{dt} = -g_L(V - E_L) + g_L\Delta_T \exp(\frac{V - V_T}{\Delta_T}) - w + I \quad (1)$$

$$\tau_w \frac{dw}{dt} = a(V - E_L) - w \quad (2)$$

At spike time:

$$at \quad t = t^f \quad reset \quad V \rightarrow V_r \qquad at \quad t = t^f \quad reset \quad w \rightarrow w + b$$

In the following table, are summarized the parameters of the AdEx Model:

Parameters
C (membrane capacitance)
$\mathbf{g_L}$ (leak conductance)
$\mathbf{E_L}$ (leak reversal potential)
$\mathbf{V_T}$ (spike threshold)
$\mathbf{\Delta_T}$ (slope factor)
$\mathbf{\tau_w}$ (adaptation time constant)
a (subthreshold adaptation)
b (spike-triggered adaptation)

Table 4: A summary of the parameters of the AdEx Model

2.2.1 Physiological interpretation of the AdEx model

The (1) differential equation for the voltage expresses the conservation of the currents across the membrane. Capacitative current ($\frac{C \cdot dV}{dt}$) ought to be balanced by the injected current (I) and the negative of the membrane current. The membrane current is represented with three terms:

1. The leak current ($g_L \cdot (V - E_L)$), which is linear with the voltage and increases with the distance from the resting potential E_L,
2. The exponential term ($g_L \cdot \Delta_T \exp(\frac{V - V_T}{\Delta_T})$) which describes the voltage dependent activation of the Na^+ channel if we assume that the activation is instantaneous
3. The adaptation current w

The (2) differential equation for the variable w, describes the evolution of the adaptation current with time constant τ_w. This equation includes spike-triggered adaptation through the reset condition $w \rightarrow w + b$ as well as a linear coupling of the second variable, w, with the voltage via the parameter a.

2.3 Validation of intrinsic properties

In order to build up a robust, reliable and trustworthy computational model that will reflect the electrophysiological, passive and active properties of granule neurons of DG as reliably as possible, we implemented a set of validation tests. In this way, we tested our model against experimental data. The validation procedure was implemented for three distinct temporal categories of granule neurons. The first category is about immature abGCs that are 4-weeks old (4-weeks after their birth in the adult DG). In previous section, we are referred to the special characteristics of this category of abGCs, and why we decided to study and incorporate them distinctly in the model. The second category, includes the mature abGCs, that are 8-weeks old (8 weeks after their birth in the adult DG). The third category includes the dbGCs (perinatally born or old GCs > 8-weeks old). In this part, we should note that electrophysiological properties, as far as the abGCs are concerned, were less available in current scientific bibliography due to the difficulties that abGCs present in their experimental manipulation. These cells have small diameter, thin dendritic processes, thus, there is a considerable obstacle to obtain electrophysiological measurements from them, such as dual patch clamp somatodendritic recordings. In circumstances like the aforementioned, that we have not got at our disposal exact experimental values, we inferred them based on experiments that described the electrophysiological behavior of these cells in comparison with dbGCs.

The model which was implemented in somatic compartments of the aforementioned three categories of neurons, was the AdEx model which was described more detailed in the previous section. In dendritic compartments of the three categories of granule neurons, it was implemented a simple LIF model. The major advantage of AdEx usage, is that it can capture the spiking properties of neurons while a small set of parameters is needed to be tuned.

The first validation test that was implemented, concerned input resistance (R_{in}) and sag ratio. In order to accomplish that, we implemented in the soma negative square current pulse for 1-s (1000 ms) and then we used the formula: $R_{in} = \Delta V_m / I_{injected}$, where ΔV_m is the membrane response to current stimulation. More specifically, $\Delta V_m = V_2 - V_1$ where V_1 the membrane potential at $t_1 = 198$ ms (a short time before we start applying square current pulse) and V_2 the membrane potential at $t_2 =$ 1998 ms (a short time before we stop applying square current pulse).

Applying the same protocol as in R_{in} validation experiment, in order to validate the sag ratio, we used the formula: sag ratio = $\Delta V_m / \Delta V_{max}$, where ΔV_m is the membrane response to negative square current pulse and ΔV_{max} is the membrane difference $\Delta V_{min} - V_1$ where V_1 the membrane potential at $t_1 = 198$ ms (a short time before we start applying square current pulse) and ΔV_{min} the minimum membrane potential during membrane stimulation with current injection.

In the figures below we present the derived diagrams after implementing negative square pulse in the soma of the GCs at three different developmental stages in order to reproduce the experimentally derived value of R_{in}. The table summarizes the intrinsic property R_{in} as it was derived by experimentalists and as it was reproduced by our model.

R_{in}	Model	Experiment
dbGCs	239	224 ± 7 (*Mongiat et al., 2009*)
Mature abGCs	324	322 ± 38.9 (*Gu et al., 2012*)
Immature abGCs	537	519 ± 30 (*Mongiat et al., 2009*)

Table 5: Summary of intrinsic property R_{in} for the three developmental stages of granule neurons. We present the values for R_{in} as they were calculated after the implementation of experimental protocols and as they were reproduced by our model.

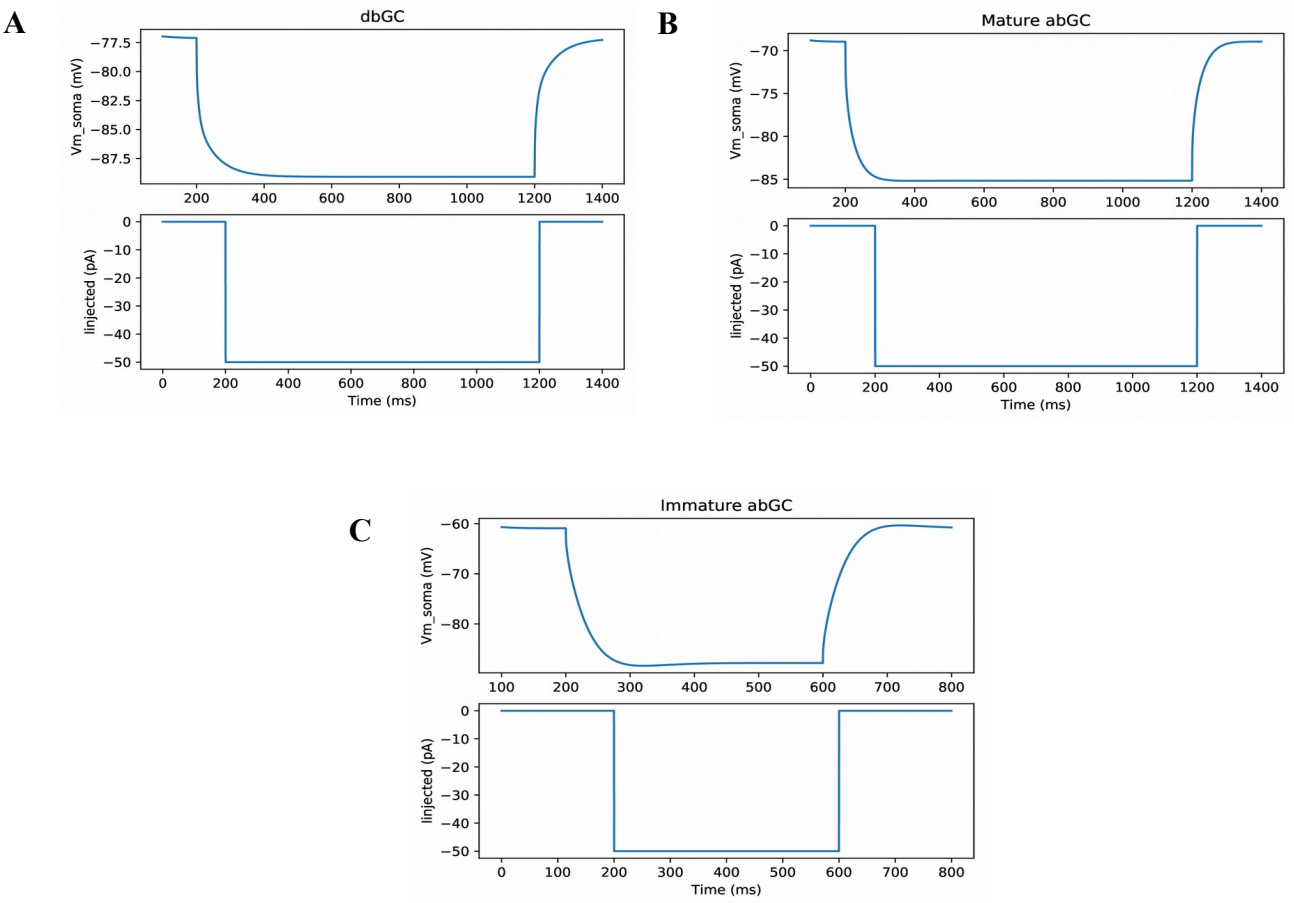

Figure 22: Reproducing the experimentally derived R_{in} with computational modeling. A) Voltage trace and current trace for a modeled developmentally-born granule cell after current injection of -50 pA in the soma for 1-s, B) Voltage trace and current trace for a modeled mature adult-born granule cell after current injection of -50 pA in the soma for 1-s, C) Voltage trace and current trace for a modeled immature adult-born granule cell after current injection of -50 pA in the soma for 1-s.

The same protocol was implemented in order to reproduce also the sag ratio of granule neurons at the three different developmental stages. Sag ratio is defined as the ratio between the exponentially extrapolated voltage to the steady-state voltage. The table below summarizes the experimentally derived sag ratio and the values reproduced by our model.

sag ratio	Model	Experiment
dbGC	1.0	1.0 ± 0.2 (*Kowalski et al., 2016*)
Mature abGC	0.999	*no data available*
Immature abGC	0.979	*no data available*

Table 6: Summary of the intrinsic property sag ratio for three developmental stages of granule neurons. In the table are presented the experimentally derived values after electrophysiological experiments and the reproduced values from the model. In cases where experimental data were not available (mature and immature adult-born granule cells) we attempted to be in accordance with known experimental data for the developmentally-born neuronal population.

In a second set of experiments, we applied sub-threshold positive square current pulse for 1-s (1000 ms) at the soma of granule neuron in order to validate the membrane time constant (τ_m). For the calculation of membrane time constant, we calculated the time needed for membrane potential to reach 63% of the voltage at steady state (during the rising phase), or alternatively, the time needed for membrane potential to reach 37% of the voltage at steady state (during the decay phase).
In the following table are summarized the experimental derived τ_m of the membrane for granule neurons at three developmental stages as well as the reproduced values by our model after performing the tests that were described before.

τ_m (ms)	Model	Experimental
dbGCs	14.8	16 ± 1 (*Kowalski et al., 2016*)
Mature abGCs	16.5	26.9 (*Brunner et al., 2014*)
Immature abGCs	24.7	27 ± 2 (*Nakashiba et al., 2012*)

Table 7: Summary of the τ_m of membrane for three different developmental stages of granule neurons. We pose the experimentally calculated τ_m as well as the reproduced value from the model.

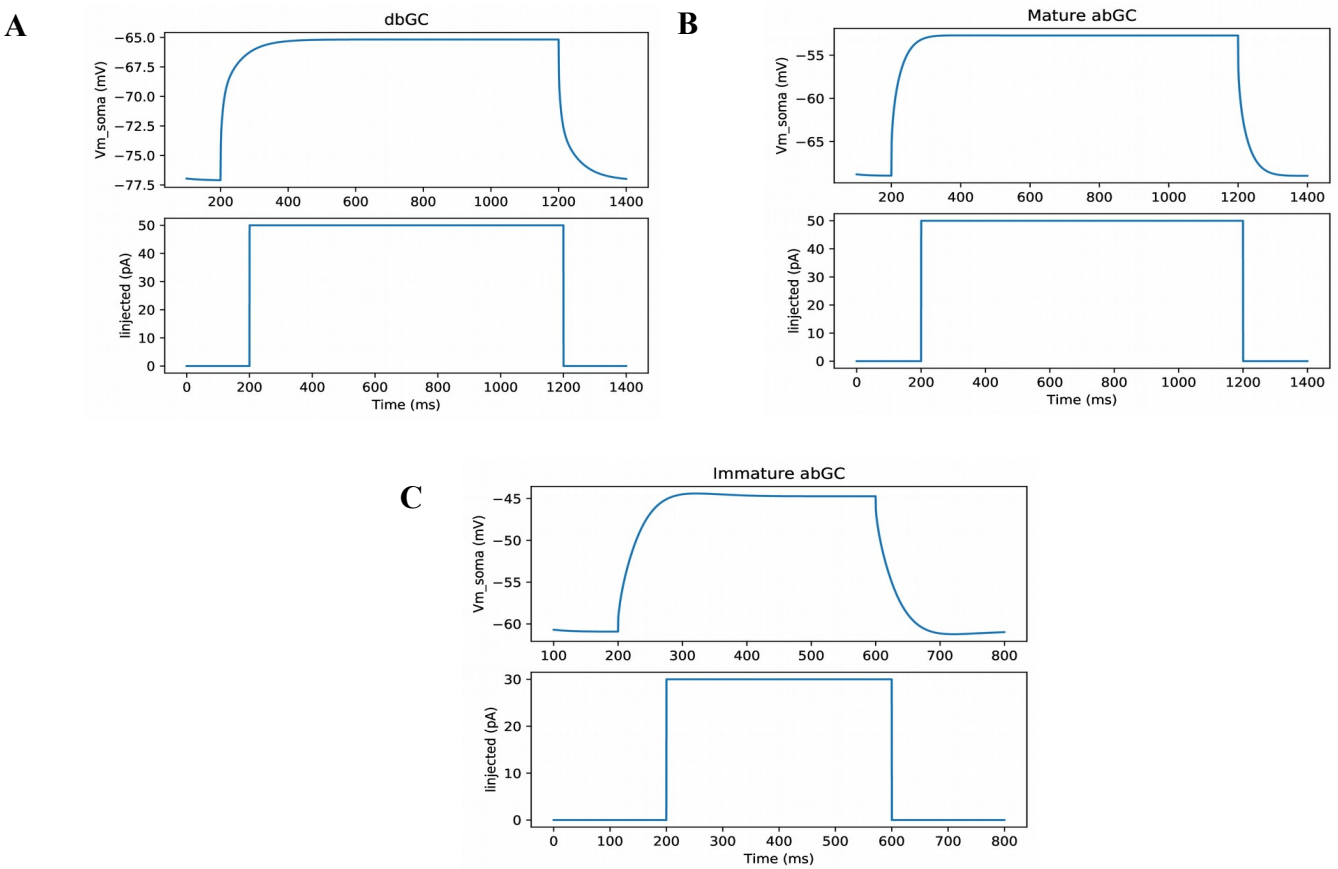

Figure 23: Reproducing the experimentally derived τ_m with computational modeling. A) Voltage trace and current trace for a modeled developmentally-born granule cell after current injection of +50 pA in the soma for 1-s, B) Voltage trace and current trace

for a modeled mature adult-born granule cell after current injection of +50 pA in the soma for 1-s, C) Voltage trace and current trace for a modeled immature adult-born granule cell after current injection of +30 pA in the soma for 1-s

In another set of experiments, we tried to validate the rheobase, i.e. the minimum current injected in the soma of the neuron in order to be emitted at least one spike. To find out this, we applied positive square current pulse in the soma of granule neuron for 1-s (1000 ms), with small current step in order to discover the minimum required current for the triggering of a spike or spikes. The table below summarizes the experimentally as well as the model reproduced rheobase, while the figures illustrate the computationally implemented protocols as they were described before.

Rheobase	Model	Experiment
dbGCs	134	135 ± 11 (*Kowalski et al., 2016*)
Mature abGCs	61	84.5 ± 5.1 (*Laplagne et al., 2007*)
Immature abGCs	38	33 ± 6.6 (*Vivar et al., 2012*)

Table 8: Summary of rheobase for the three developmental stages of granule neurons. We present the values for rheobase as they were calculated after the implementation of experimental protocols and as they were reproduced by our model.

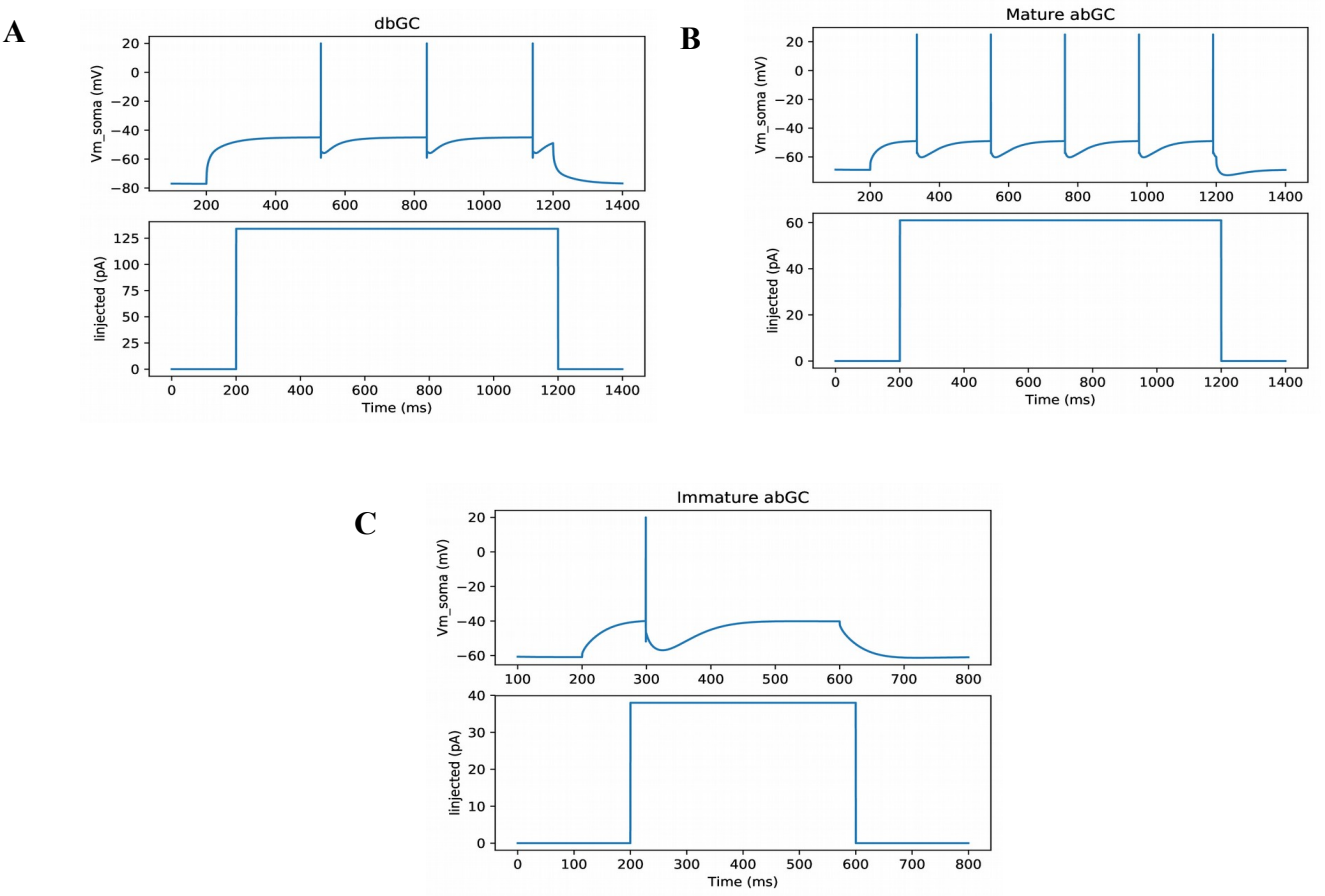

Figure 24: Reproducing the experimentally derived rheobase with computational modeling. A) Voltage trace and current trace for a modeled developmentally-born granule cell after current injection of +134 pA (rheobase) in the soma for 1-s, B) Voltage trace and current trace for a modeled mature adult-born granule cell after current injection of +61 pA in the soma for 1-s, C) Voltage trace and current trace for a modeled immature adult-born granule cell after current injection of +38 pA in the soma for 400 ms

Moreover, we tried to capture the firing behavior of modeled neurons, through the creation of I-f and I-V curves. We have at our disposal I-f and I-V curves from experimental protocols in dbGCs (old GCs), but restricted data from immature abGCs and mature abGCs.

The following plots, depict the current–frequency (I-f curve) and current-voltage (I-V curve) relationship for a modeled immature abGC. The applied protocol included the somatic current injection of a range of currents, from negative to positive currents (-50 pA to +240 pA). The application of somatic current stimulation was step-wise (11 pA) for a total stimulation period of 1-s. We should note that in the I-V curve the slope give us the calculated from the model input resistance (R_{in}) which is in close proximity with the experimentally derived R_{in}. Indeed, for the immature abGC that is highly excitable with high R_{in}, the slope in I-V curve is indicative.

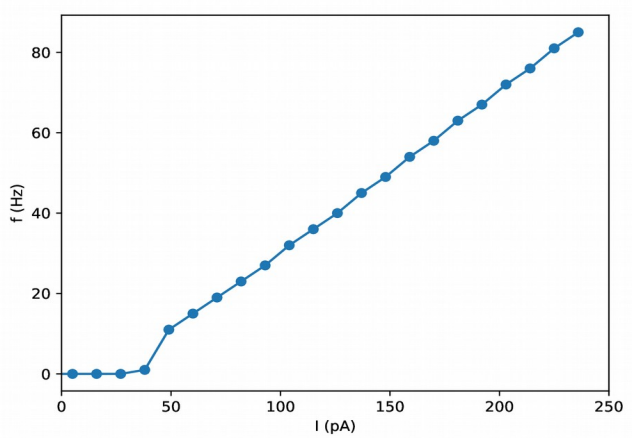

Figure 25: Current-frequency (I-f) relationship for the immature abGC model. y-axis represents the firing rate of each neuron in Hz, while x-axis shows the somatic current injections in pA. I-f curve with corresponding frequency (Hz) to current injections of -50 to +240 pA with 11 pA step-size for a total soma current stimulation of 1-s.

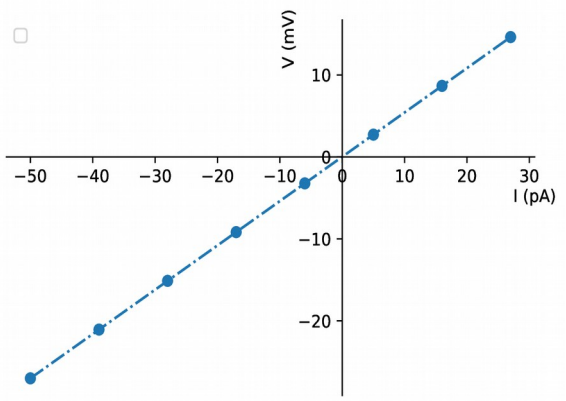

Figure 26: Current-Voltage (I-V) curves for the immature abGC model. Voltage responses to current injections of -50 pA to rheobase with 11 pA step-wise for a total soma current stimulation of 1-s.

Our model could reproduce in a consistent way experimentally derived plots of voltage traces.

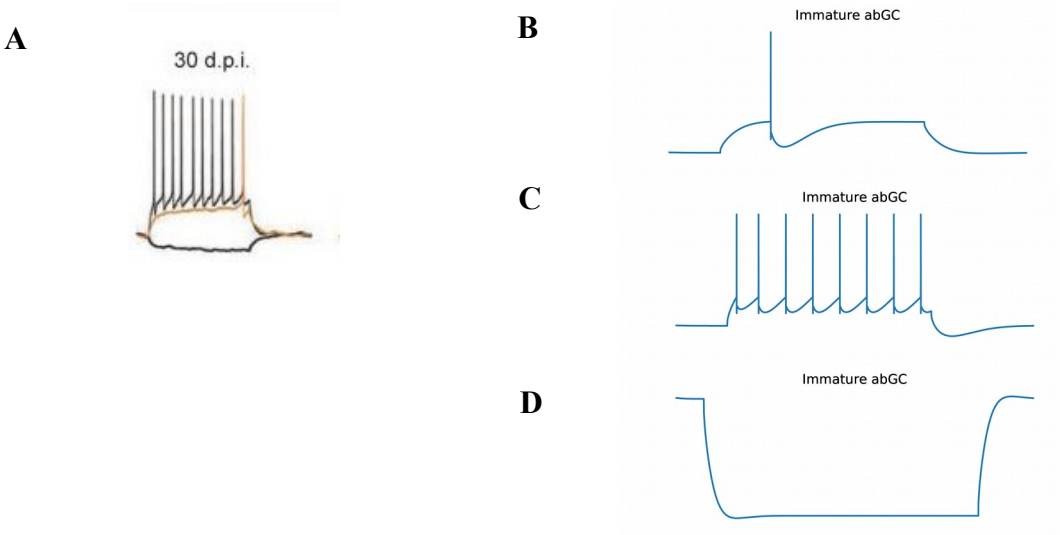

Figure 27: Traces representative of membrane potentials in response to current injections, for immature abGCs at 30 d.p.i (A, ***Adapted by Vivar et al., 2012***). Depolarizing steps were delivered at threshold (B) and twice threshold current (C). Also, a negative square current pulse (-50 pA) was applied (D).

In the table below, are summarized the intrinsic properties for immature abGCs as were calculated from experiments and as were reproduced by our model. As we can see, they are in close proximity.

Immature abGCs	Model	Experiment	Source
R_{in} (MΩ)	537	519 ± 30 (n=68)	*Mongiat et al., 2009*
sag ratio	0.979	---	---
τ_m (ms)	24.7	27 ± 2 (n=29)	*Nakashiba et al., 2012*
Rheobase (pA)	38	33 ± 6.6 (n=3)	*Vivar et al., 2012*
Max firing freq (Hz)	87*	52	*Brunner et al., 2014*

Table 9: Intrinsic properties of immature abGCs. A summary of the intrinsic properties of immature abGCs (~ 4-weeks old) as were extracted from experiments and as were predicted by our model. *: for total simulation of 1-s for current injection at the soma I_{inj} = + 240 pA, ---: no available data from experiments

Similarly, the following plots, depict the current–frequency (I-f curve) and current-voltage (I-V curve) relationship for a modeled mature abGC. The applied protocol included the somatic current injection of a range of currents, from negative to positive currents (-50 pA to +240 pA). The application of somatic current stimulation was step-wise (11 pA) for a total stimulation period of 1-s. We should note that in the I-V curve, the slope could give us the calculated from the model input resistance (R_{in}) which is in close proximity with experimental R_{in}. The mature abGC is less excitable in comparison with the modeled immature abGC and the same is true for the calculated R_{in}, as we can observe from the slope of the I-V curve.

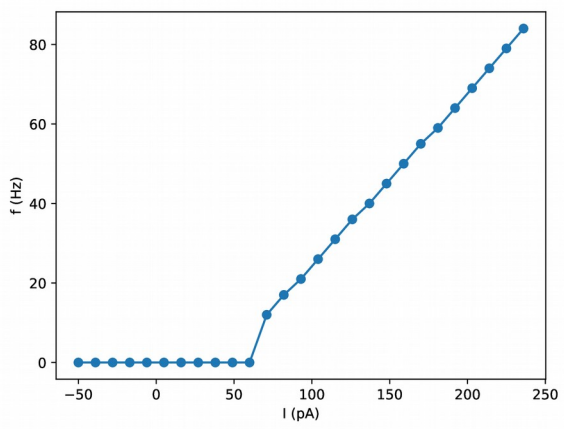

Figure 28: Current-frequency (I-f) relationship for the mature abGC model. y-axis represents the firing rate of each neuron in Hz, while x-axis shows the somatic current injections in pA. I-f curve of mature abGC with corresponding frequency (Hz) to current injections of -50 to +240 pA with 11 pA step-wise for a total soma current stimulation of 1-s.

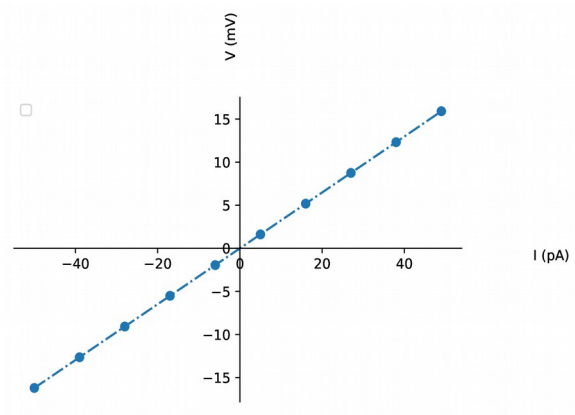

Figure 29: Current-Voltage (I-V) curves for the mature abGC model. Voltage responses to current injections of -50 pA to rheobase with 11 pA step-wise for a total soma current stimulation of 1-s.

In the table below, are summarized the intrinsic properties for mature abGCs as were calculated from experiments and as were reproduced by our model. As we deduce, the properties reproduced by the model are in close proximity with experimental values.

Mature abGCs	Model	Experiment	Source
R_{in} (MΩ)	324	322 ± 38.9 (10-15)	*Gu et al., 2012*
sag ratio	0.999	---	---
τ_m (ms)	16.50	26.9	*Brunner et al., 2014*
Rheobase (pA)	61	84.5 ± 5.1 (n=31)	*Laplagne et al., 2007*
Max firing freq (Hz)	84*	41	*Brunner et al., 2014*

Table 10: Intrinsic properties of mature abGCs. A table summary of the intrinsic properties of mature abGCs as they were extracted from experiments and as they were predicted by our model. Signs explained: *: for total simulation of 400 ms and current injection at the soma I_{inj} = + 250 pA and --- : no available experimental data.

The validation of intrinsic properties for mature abGCs comes in accordance with experimental data as we can conclude from the voltage traces that were observed in experiments and were reproduced by our model.

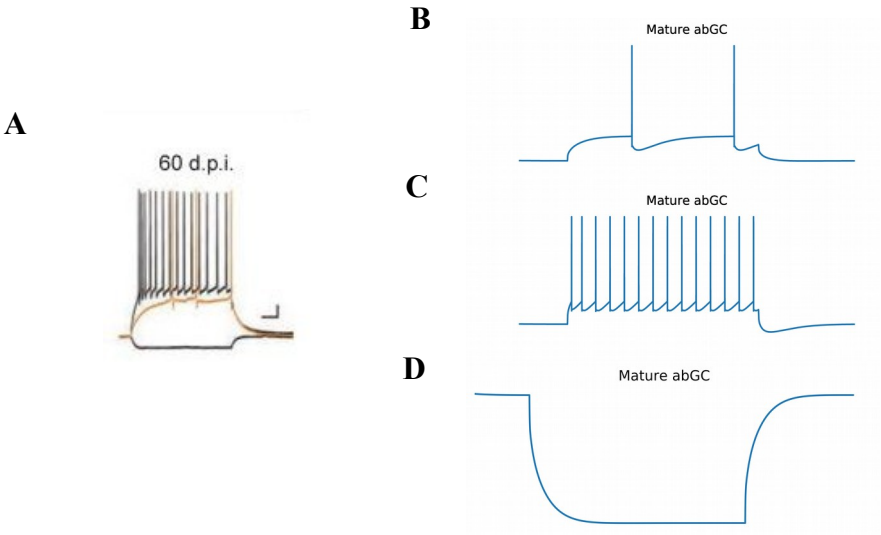

Figure 30: Traces representative of membrane potentials in response to current injections, for mature abGCs at 60 d.p.i (A, ***Adapted by Vivar et al., 2012***). Depolarizing steps were delivered at threshold (B) and twice threshold current (C). Also, a negative square current pulse (-50 pA) was applied (D).

In the table below, are summarized the intrinsic properties for dbGCs as were calculated from experiments and as were reproduced by our model.

dbGCs	Model	Experiment	Source
R_{in} (MΩ)	239	224 ± 7 (n=89)	*Mongiat et al., 2009*
sag ratio	1.0	1.0 ± 0.2 (n=6)	*Kowalski et al., 2016*
τ_m (ms)	14.8	16 ± 1 (n=5)	*Kowalski et al., 2016*
Rheobase (pA)	134	135 ± 11	*Kowalski et al., 2016*
Max firing freq (Hz)	51*	54	*Lübke et al., 1998*

Table 11: Intrinsic properties of dbGCs. A table summary of the intrinsic properties of dbGCs (>8-weeks old) as they were extracted from experiments and as they were predicted by our model. Signs explained: *: for total simulation of 1-s and current injection at the soma I_{inj} = +250 pA , ---: no available experimental data

The following plots, depicts the current–frequency (I-f curve) and current-voltage (I-V curve) relationship for a modeled dbGC (old GC). The applied protocol included the somatic current injection of a range of currents, from negative to positive currents (-50 pA to +240 pA). The application of somatic current stimulation was step-wise (11 pA) for a total stimulation period of 1-s. We should note that in the I-V curve the slope could give us the calculated from the model input resistance (R_{in}) which is in close proximity with the experimentally derived R_{in}. Indeed, for the dbGC that is not highly excitable with lower R_{in} in comparison with modeled abGCs, the slope in I-V curve is smaller.

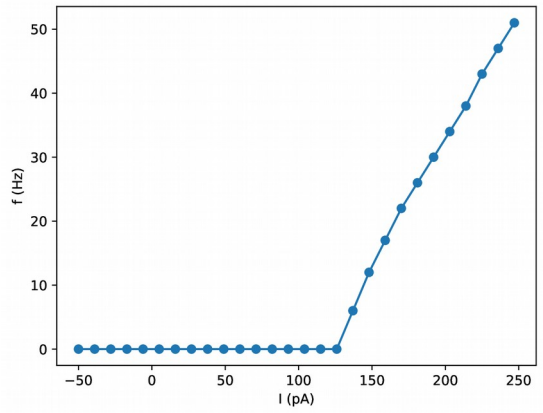

Figure 31: Current-frequency (I-f) relationship for the dbGC model. y-axis represents the firing rate of each neuron in Hz, while x-axis shows the somatic current injections in pA. I-f curve of dbGC for corresponding frequency (Hz) to current injections of -50 to +240 pA with 11-pA step-wise for a total soma current stimulation of 1-s.

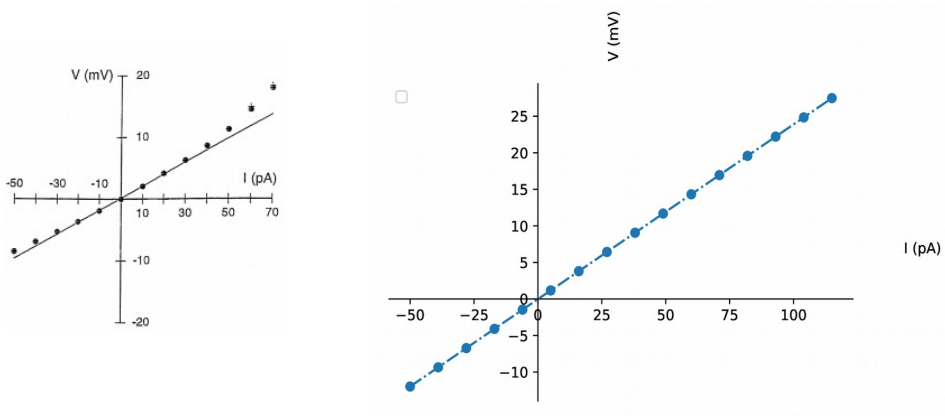

Figure 32: Current-Voltage (I-V) curves for the dbGC model. Voltage responses to current injections of -50 pA to rheobase with 11-pA step-wise for a total soma current stimulation of 1-s. The left insert was adapted by Lübke et al., 1998.

The validation of intrinsic properties for dbGCs comes in accordance with experimental data as we can conclude from the voltage traces that were observed in experiments and were predicted from the model.

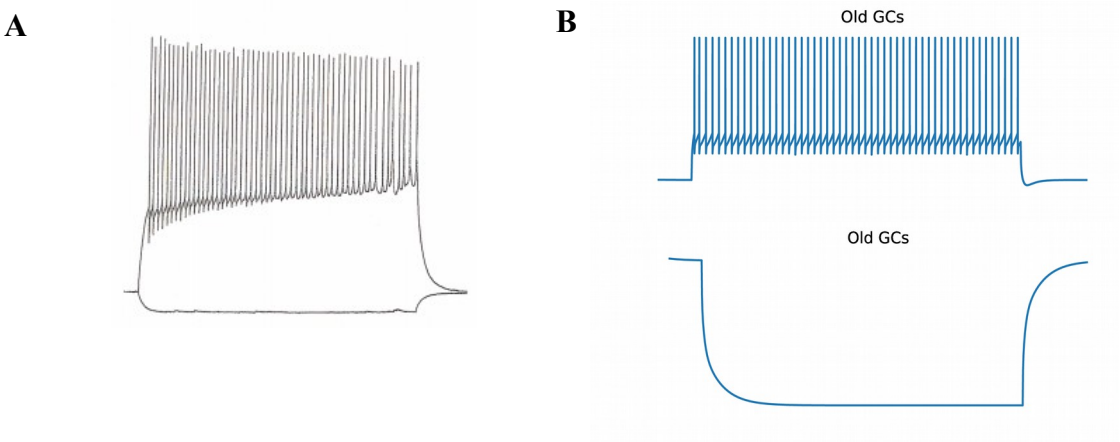

Figure 33: Voltage trace of dbGCs after current injection I_{inj} +250 pA and -50 pA for total current stimulation of the soma for 1-s. The applied protocol was adopted by experimental procedures (A, ***Adapted by Lübke et al., 1998***) and was implemented for validation purposes in the modeled dbGC (B).

For comparative reasons, we pose the following common plot of current-frequency (I-f) relationship for the modeled GCs at three different developmental stages; dbGCs, mature and immature abGCs.

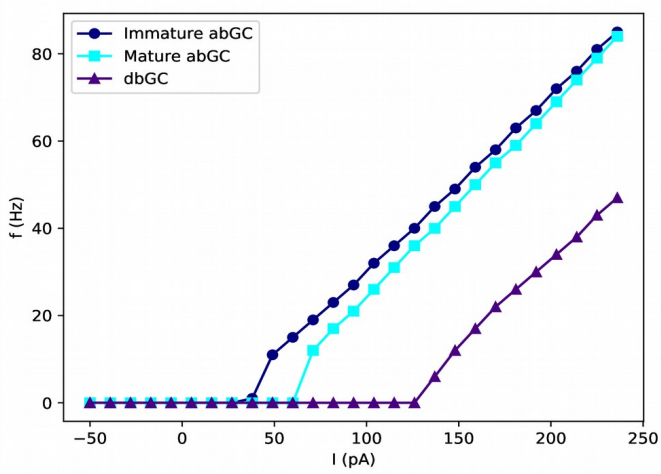

Figure 34: Common plot of current-frequency (I-f) relationship for the dbGC, mature abGC and immature abGC model. y-axis represents the firing rate of each neuron in Hz, while x-axis shows the somatic current injections in pA. The I-f curve is about dbGC, mature and immature abGC for corresponding frequency (Hz) to current injections of -50 to +240 pA with 11-pA step-wise for a total soma current stimulation of 1-s.

As we deduce from the above curves, the modeled dbGC, mature and immature abGC exhibit firing behavior that comes in accordance with experimental data where dbGC is less excitable than the abGCs. Between abGCs, immature abGCs have higher excitability compared with mature abGCs as it is evident form the above diagram.
In the following figure are depicted the firing traces for MCs, BCs and HIPP cells as were taken from a previous DG model of our laboratory (***Chavlis et al. 2017***).

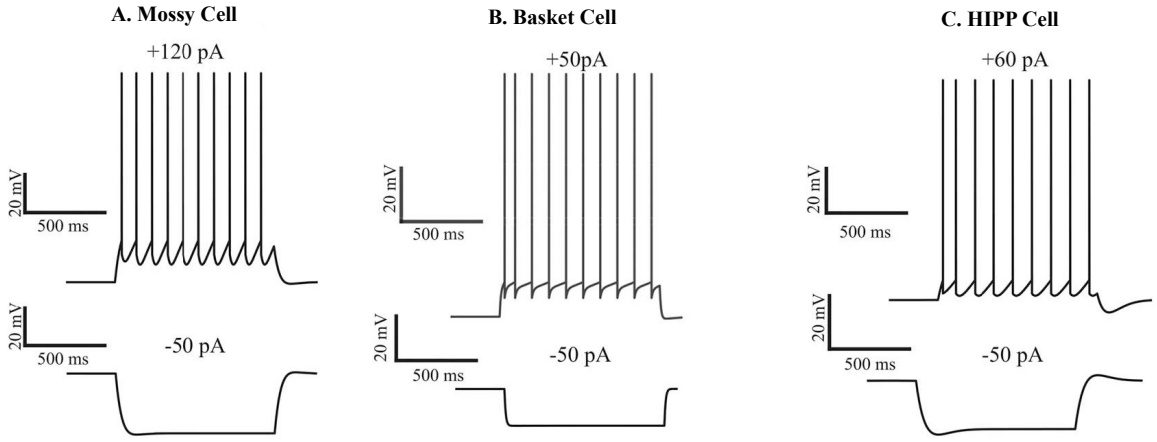

Figure 35: Firing traces of the three model cells in response to current injection (1-s). Note that action potentials are not explicitly modeled in I & F neurons. A: The somatic membrane voltage for the mossy cell (MC) with 1300 pA (top) and 2300 pA (bottom) current injections. B. Same as in A, for the Basket cell (BC), with 1200 pA (top) and 250 pA (bottom) current injections. C. Same as in B, for the HIPP cell, with 1300 pA (top) and 250 pA (bottom) current injections. (***Adopted by Chavlis et al. 2017***).

Taking into consideration that the reproduced by our model experiments were performed in the presence of synaptic activity blockers, the implemented current was injected in the soma of granule neurons for replicating these conditions. We need to clarify that the calculated firing frequency is the maximum because if the injected current in the soma is bigger than the highest implemented, then the neuron did not correspond correctly.
Dendritic spines were incorporated into the models by scaling R_m and C_m of spine-bearing dendrites appropriately. Because spines were implemented in our model by scaling the parameters that depend on membrane surface area, the increase in the membrane surface area was larger in more distal compartments. The relative contribution of individual spines is dependent on the membrane area per unit length and therefore on the diameter of the dendritic shaft.

2.4 Modeling Synapses

In the DG network there are both excitatory (glutamatergic, AMPA & NMDA) synapses and inhibitory (GABAergic) synapses (*see section 1.12.2 and 1.12.3 from Introduction*). Hence, in order to create a biophysical relevant network we included them in our model. As a result, the total synaptic current in our model consists of two components; the excitatory currents (I_{AMPA} & I_{NMDA}) and the inhibitory current (I_{GABA}). For ligand-gated ion channels that mediate synaptic transmission, we could tell that they exhibit an approximately linear current-voltage relationship, such as AMPA and GABA receptors. Therefore, this kind of ligand-gated ion channels could be modeled as an ohmic conductance (g_{syn}) multiplied by the driving force:

$$I_{syn} = g_{syn}(t) \cdot (V_m(t) - E_{syn})$$

where E_{syn} is the reversal potential for AMPA and GABA, respectively.
However, when we want to model NMDA synapses, the approach is a little bit different because in this case the current-voltage relationship cannot be confronted as linear. More specifically, the NMDA receptor-mediated conductance depends on the postsynaptic voltage due to the gate blockage by a positively charged magnesium ion (Mg^{2+}). The fraction of NMDA channels that are not blocked by Mg^{2+} can be fitted by a sigmoidal function (***Jahr & Stevens, 1990***) described by the following formula:

$$s(V) = \frac{1}{1 + \eta \cdot [Mg^{+2}]_o \cdot \exp(-\gamma \cdot V_m)}$$

where, η is the sensitivity of Mg unblock, γ the steepness of Mg unblock, and $[Mg^{2+}]_o$ is the outer magnesium (Mg^{2+}) concentration. The values of η, γ and $[Mg^{2+}]_o$ that were used in the simulations for the NMDA receptors are summarized in the following table:

	η (mM-1)	γ (mV-1)	$[Mg^{2+}]_o$ (mM)
GCs	0.2	0.04	2
MCs	0.28	0.072	1
BCs	0.28	0.072	1
HIPP	0.28	0.072	1

Table 12: The arithmetic values of the parameters that were used for the modeling of the fraction of NMDA channels that are not blocked by Mg^{+2}.

The NMDA synaptic current was calculated by the following equation:

$$I_{syn} = g_{syn}(t) \cdot s(V) \cdot (V_m(t) - E_{syn})$$

For all synaptic currents the ohmic conductance was simulated as a sum of two exponentials terms (***Bartos et al., 2001***). The one term was based on rising while the other was based on the decay phase of the postsynaptic potential. In that way, we have the permission to set the time constants (τ_{decay} and τ_{rise}) independently. This function was simulated as a system of two linear differential equations:

$$g_{syn} = g_{max} \cdot u(t)$$

$$\frac{du}{dt} = \frac{-u}{\tau_{decay}} + h_o \cdot v \cdot (1-u) \qquad \frac{dv}{dt} = \frac{-v}{\tau_{rise}}$$

where τ_{rise} and τ_{decay} are the rise and decay time constants respectively, h_o is a scaling factor and u(t) is the function of two exponentials $u(t) = \exp(-t/\tau_{decay}) - \exp(-t/\tau_{rise})$, which is divided by its maximum amplitude. The scaling factor h_o is set to 1 ms^{-1} for all AMPA and NMDA receptors and all neuronal types in the network. For NMDA receptors, the scaling factor h_o, was set to 0.5 ms^{-1} apart from the NMDA synapses on GCs where it was set to 2 ms^{-1}. Bearing in mind that we did not modeled the axons of neurons, we included in our model a delay between pre- and postsynaptic transmission. Including this delay in the network serves both ways: both for synaptic transmission and axonal conduction delay, while its value depends on presynaptic and postsynaptic neuronal types. The peak conductance (g_{max}), rise (τ_{rise}) and decay (τ_{decay}) time constants, and the delay of various network connections were estimated from experimental data. For the dbGCs, the peak conductance both for AMPA and NMDA was validated against experimental data (***Krueppel et al., 2011***). Experimental findings of this study highlighted that the unitary excitatory postsynaptic potential (uEPSP), i.e. activation of a single synapse, provokes 0.6 mV somatic EPSP, and the peak current ratio of NMDA/AMPA was 1.08. These values were reproduced for the GCs in our computational model.

In the model, we incorporated also background activity in order to simulate the experimental findings of spontaneous activity in DG. Similarly, we used Poisson independent spike trains in order to be reproduced the experimental data for MCs (2-4 Hz spontaneous activity) (***Henze & Buzsáki 2007***) and for BCs (1-2 Hz spontaneous activity) (***Kneisler & Dingledine 1995***). GC population infrequently generates spontaneous activity, even if inhibition is blocked (***Lynch et al 2000***). Hence, we implemented noise inputs, only in order to evoke spontaneous EPSPs (500 noisy inputs of 0.1 Hz spontaneous activity to enhance randomness in the network).

In the following tables we summarize the synaptic parameters for the GCs populations at different maturation stages in the DG network.

Synapses (From/to)	dbGCs	Mature abGCs	Immature abGCs
AMPA (Perforant Path)			
g_{max} (nS)	1.4	1.0	0.55
τ_{rise} (ms)	0.1	0.1	0.1
τ_{decay} (ms)	2.5	2.5	2.5
delay (ms)	3.0	3.0	3.0
NMDA (Perforant Path)			
g_{max} (nS)	0.8711	0.8711	0.8711
τ_{rise} (ms)	0.33	0.33	0.33
τ_{decay} (ms)	50.0	50.0	50.0
delay (ms)	3.0	3.0	3.0

Table 13: Synaptic parameters for AMPA & NMDA synapses from perforant path afferents to GC populations.

Synapses (From/to)	dbGCs	Mature abGCs	Immature abGCs
Mossy Cells			
g_{max} (nS)	0.1066	0.1066	0.1066
τ_{rise} (ms)	0.1	0.1	0.1
τ_{decay} (ms)	2.5	2.5	2.5
delay (ms)	3.0	3.0	3.0
Mossy Cells			
g_{max} (nS)	0.1151	0.1151	0.1151
τ_{rise} (ms)	0.33	0.33	0.33
τ_{decay} (ms)	50.0	50.0	50.0
delay (ms)	3.0	3.0	3.0

Table 14: Synaptic parameters for excitatory mossy cell synapses with GC populations at different maturation stages.

Moreover, in our model we included also inhibitory $GABA_A$ synapses and their synaptic properties are summarized in the following table.

Synapses (From/to)	dbGCs	Mature abGCs	Immature abGCs
$GABA_A$			
Basket Cells			
g_{max} (nS)	14.0	14.0	14.0
τ_{rise} (ms)	0.9	1.80	9.0
τ_{decay} (ms)	6.8	32.8	36.8
delay (ms)	0.85	0.85	0.85
HIPP Cells			
g_{max} (nS)	0.12	0.12	0.12
τ_{rise} (ms)	0.9	9.0	14.0
τ_{decay} (ms)	6.8	80.0	80.0
delay (ms)	1.6	1.6	1.6

Table 15: Synaptic parameters for inhibitory synapses from basket cells or HIPP cells to GC populations at different developmental stages.

Except the main neuronal population of GCs at different maturation stages, we also included in our computational model of the DG network the excitatory population of MC cells and local interneurons like BCs and HIPP cells. Their intrinsic properties were validated based on experimental data that were reproduced by a previous model of our laboratory (***Chavlis et al., 2017***). In the following tables are summarized the synaptic properties for the rest of neuronal populations in the DG network.

Synapses (From/To)	Mossy Cells	Basket Cells	HIPP Cells
AMPA (Perforant Path)			
g_{max} (nS)			0.240
τ_{rise} (ms)			2.0
τ_{decay} (ms)			11.0
Delay (ms)			3.0
Granule Cells			
g_{max} (nS)	0.500	0.210	
τ_{rise} (ms)	0.5	2.5	
τ_{decay} (ms)	6.2	3.5	
Delay (ms)	1.5	0.8	
Mossy Cells			
g_{max} (nS)		0.350	
τ_{rise} (ms)		2.5	
τ_{decay} (ms)		3.5	
Delay (ms)		3.0	
NMDA			
Perforant Path			
g_{max} (nS)			0.276
τ_{rise} (ms)			4.8
τ_{decay} (ms)			110.0
Delay (ms)			3.0
Granule Cells			
g_{max} (nS)	0.525	0.231	
τ_{rise} (ms)	4.0	10.0	
τ_{decay} (ms)	100.0	130.0	
Delay (ms)	1.5	0.8	
Mossy Cells			
g_{max} (nS)		0.385	
τ_{rise} (ms)		10.0	
τ_{decay} (ms)		130.0	
Delay (ms)		3.0	

Table 16: Synaptic parameters for the rest of neuronal populations in the DG network.

2.5 Validation of Synaptic Properties

In a second round of validation procedures, we tried to examine the synaptic properties of GCs. Hence, we created a synaptic mechanism with AMPA and NMDA excitatory (glutamatergic) synapses having one presynaptic neuron while the postsynaptic neuron was the GC (dbGC, mature abGC or immature abGC).

The first experiment, had as its target to find out the current in which the membrane potential stayed stable at -70 mV. In order to accomplish that, we turned off the spike generation mechanism setting the threshold potential high enough while having NMDA channel closed and AMPA open. What is more, we performed another similar experiment, for finding out the current that leads to stable membrane potential of +40 mV. We studied the NMDA receptor-mediated currents while holding the membrane stable at +40 mV in order to overcome voltage-dependent Mg^{+2} block, as it was described in experimental protocols (***Schmidt-Salzmann et al., 2014***). Similarly, in order to accomplish that, we turned off the spike mechanism setting the threshold potential for spiking high enough while having NMDA and AMPA channels open. Through the above described experiments, we managed to derive the g_{AMPA}/g_{NMDA} ratio for the three different categories of granule cells reproducing the experimental data and reproducing the uEPSP (+0.6 mV) (***Krueppel et al., 2011***).

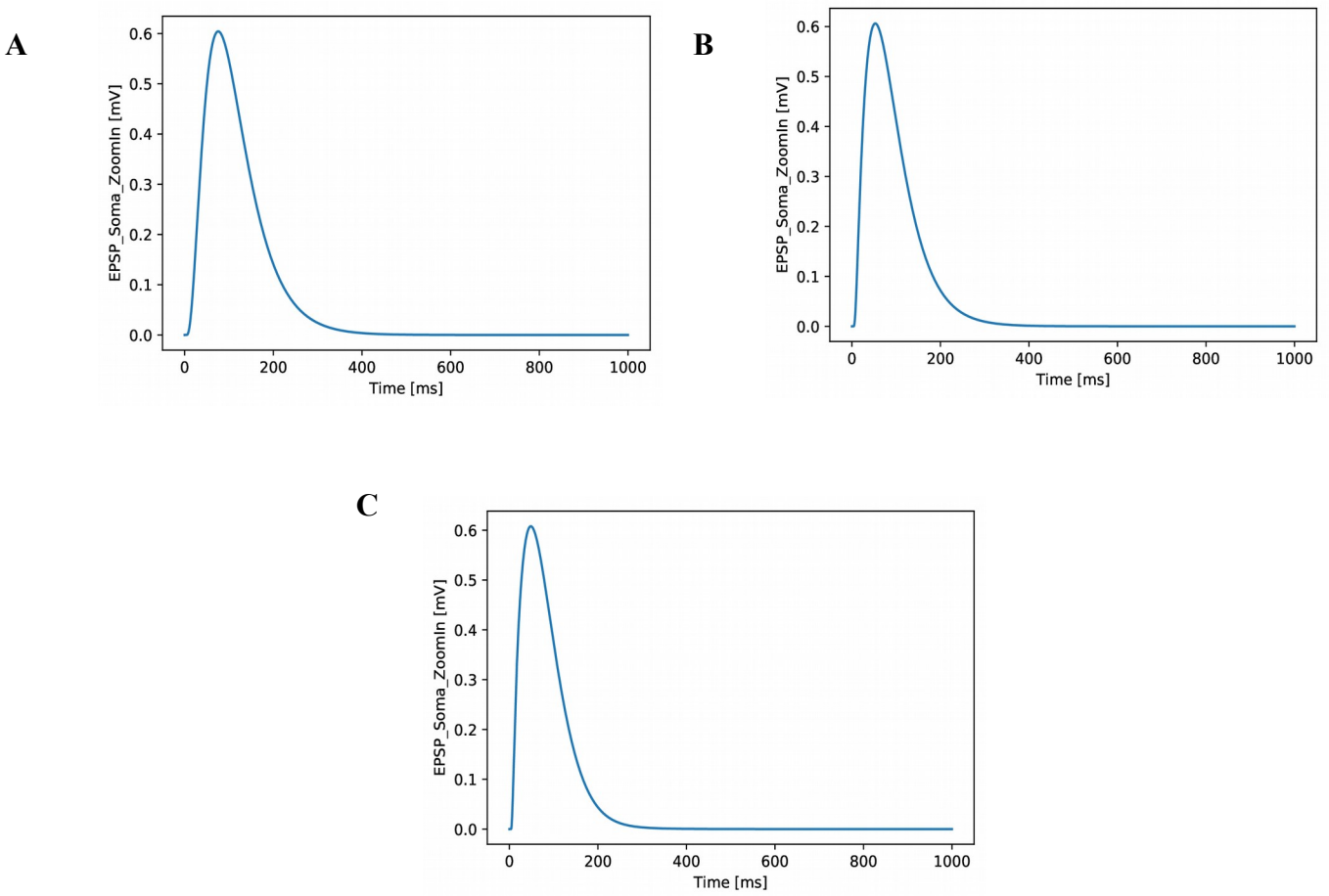

Figure 36: Plots of unitary excitatory post-synaptic potential (uEPSP) for granule neurons at three different developmental stages. After deriving the g_{AMPA}/g_{NMDA} ratio we managed to reproduce the uEPSP for developmentally-born granule neurons which is 0.6 mV (A), mature adult-born granule neurons (B) and immature adult-born granule neurons (C).

2.6 Construction of the network

The implemented model of DG was based on the connectivity characteristics and structure described in (***Myers and Scharfman 2009***) while the main idea and philosophy of this model was especially influenced by a previous computational model built in our laboratory (***Chavlis et al., 2017***). Our DG network consists of the main neuronal population of DG – i.e GCs - in three different maturation stages; dbGCs, mature abGCs and immature abGCs. Also, the model includes the excitatory MCs, and two classes of inhibitory INs which are the BCs and the HIPP cells. We do not include in our model the Hilar Commissural Associational Pathway (HICAP) cells because they are not so well characterized. The simulations were performed using the BRIAN 1.4.4 Simulator written in python (version 2.7) (***Goodman & Brette 2009, Brette & Goodman 2011***) running on a high-performance computing cluster (HPCC) with 312 cores under 64-bit CentOS Linux operating system.

In order to investigate the behavior of adult-born neurons in the DG network and their effect in the ability of DG to perform pattern separation, we incorporated them in our model. The network consisted of 2000 GCs in total with the 5% of the GC population being abGCs (i.e. 1900 dbGCs, 50 mature abGCs and 50 immature abGCs). Alternatively, taking into account recent data that assume a 10% of total GC population to be abGCs, we have a network with 1800 dbGCs, 100 mature abGCs and 100 immature abGCs. In each case, we preserved the total GC population stable, being 2000 GCs. What is more, we integrated in the network the other three major neuronal populations that are met in the DG. Hence, there were also 100 BCs providing feedback inhibition, 80 hilar MCs and 40 HIPP cells providing feedforward inhibition.

The total number of GCs in the network represents 1/500 of the 1 million granule neurons that are located in the rat hippocampus (***West et al., 1991***). This particular selected number of GCs in the network provides us with enough power to explore pattern separation, while conserving the computational efficiency. The abGCs consist the 5%-10% of the total GCs population, so we decided to include 1900 dbGCs, 50 mature and 50 immature abGCs in the first control network (***Drew et al., 2013***). At this time, we should note that we also created a network like the aforementioned, taking although into consideration newer bibliographic data that attribute 10% of abGCs in the network. As a result, in this case we have got 1800 dbGCs, 100 mature abGCs and 100 immature abGCs in the second control network.

Inspired by the lameral organization of DG along its septotemporal axis (***Sloviter and Lømo, 2012***), we divided the 2000 GCs into 100 non-overlapping clusters. The one half of the clusters (50 clusters) was made up by 19 dbGCs and 1 mature abGC and the second half of the clusters was made up by 19 dbGCs and 1 immature abGC. In the case of the network with 1800 dbGCs, 100 mature abGCs and 100 immature abGCs we had in the clusters (100 clusters) with 18 dbGCs, 1 mature abGC and 1 immature abGC.

Apart from the principal excitatory neuronal population of granule neurons, we also incorporated in the network inhibitory INs. The first type is the GABAergic perisomatic targeting BCs while the second type is the hilar interneurons (HIPP cells), that target distal dendritic compartments. As we already mentioned, we have 100 BCs in the network, thus 1 BC per cluster of GCs, in accordance with the form of a “winner-take-all” competition (***Coultrip et al., 1992***). According to this form of competition, all, but the most strongly activated GCs in a cluster, are silenced. Given 100 clusters in

the model, and with one winner within each cluster, approximately 5% of GCs are active for a given stimulus. In this way we compromise and are in agreement with the theoretically and experimentally approximated estimation of 5% activity of GCs for a given stimulus (***Treves et al., 2008, Danielson et al., 2016***).

As far as the hilar neuronal population in the network, we already underlined the presence of 80 MCs and 40 HIPP cells in the network. *In vivo,* the estimated numbers are 30,000 to 50,000 MCs in rats (***West et al., 1991, Buckmaster and Jongen-Rêlo, 1999***) and approximately 12,000 HIPP cells in rats (***Buckmaster and Jongen -Rêlo, 1999***). In our network, the existence of 80 MCs corresponds to 3 - 5 MCs per 100 GCs and the existence of 40 HIPP cells corresponds to < 2 HIPP cells per 100 GCs.

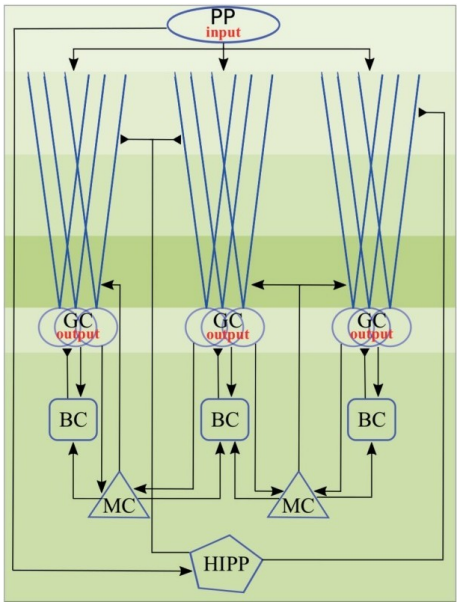

Figure 37: A schematic representation of the DG network model. The different shades of the green color illustrate the trilaminar distribution. PP: perforant path, GC: granule cells, BC: basket cells, MC: mossy cells, HIPP: hilar perforant path-associated cells. The perforant path afferents carry the input to the network from Layer II of the Entorhinal Cortex (EC), and project on both the GCs and HIPP cells. MCs and GCs are connected with each other in a recurrent manner. Also, MCs excite the BCs. BCs target the perisomatic area of GCs inhibiting them while HIPP interneurons target the outer third of the distal dendritic compartments of GCs providing inhibition to GCs. Finally, GCs provide the output of the DG network (***Adopted by Chavlis et al., 2017***).

Input to the network is provided from EC Layer II via PP, thus we simulated 400 afferent inputs derived from independent Poisson spike trains, with 40 Hz frequency in accordance with experimental data (***Hafting et al., 2005***). According to experimental studies, dentate GCs receive input from 10% of the 4,000 EC Layer II afferents that contact a given GC in the rat during a task (***McNaughton et al., 1991***), proposing that a 10% of PPs afferents are active. In agreement with the aforementioned study, 10% of the total entorhinal input is necessary to discharge one GC. So, in our simulation we consider that 10% is the active PP afferents representing a given stimulus. The ratio of GCs to PP afferents is aligned with estimations of about 200,000 EC Layer II cells in the rat (***Amaral et al., 1990***), suggesting a ratio of 20 EC cells per 100 GCs. Implementing the aforementioned, EC-GC connection is sparse, with each GC receiving input from about 2% of EC Layer II neurons. Assuming only 400 input cells; one GC could have only 8 afferents from EC, which in turn would make it impossible for the GC to become active. As a compromise, we used a

randomly determined 20% of EC Layer II cells as input to each GC and additionally, 20% randomly determined EC Layer II cells as input to each HIPP cell; GCs contact each MC with 20% probability; GCs and HIPP cells each feedback to contact a randomly determined 20% of GCs and finally, each MC connects with every BC in the network. Connections are initialized randomly (uniform random distribution) before the start of the simulations and remain fixed across all simulations (no rewiring). The connectivity matrix was the same for all experiments and across all using GC models, apart from the PP → GC, and HIPP → GC synapses due to the difference in GC number of dendrites.

2.6.1 Different network simulations in order to investigate activity and sparsity of the network

In order to unravel the potential role that abGCs may exert in the activity and the sparsity of the DG network, we created six DG networks with different compositions of GC populations.
The different DG networks that we used in the simulations shared the same number of BCs, MCs, and HIPP cells, with the only difference in the composition of the GC neuronal population.
Networks A and B could be considered as the control networks in which the percentage of each GC population comes in accordance with current scientific literature. Hence, the network A is comprised of 2000 GCs in total, 5% of which are abGCs, while Network B is comprised by 2000 GCs in total, 10% of which is comprised of abGCs. The network C has got the same percentage of each GC population (33.3%). In the network D there are 50% dbGCs and 50% abGCs (25% mature abGCs - 25% immature abGCs). The network E is the extreme case where adult neurogenesis is absent (2000 dbGCs). For each of the aforementioned networks, were performed adequate simulations with random initialized inputs from EC Layer II. Moreover, we created two additional networks, the networks F and G which possessed the same number of GCs as the network B (1800 dbGCs, 100 mature abGCs and 100 immature abGCs). Although, the main difference between network B and F was the absence of BC-abGC synapses and for the case of network G, the absence of MC-abGC synapses. Our main motivation was to investigate how the absence of these types of synapses due to dendritic atrophy of abGCs for example, may exert their impact on the activity levels of the DG network. The network compositions for the different simulations are described in the following table:

Network	Old GCs	Mature abGCs	Immature abGCs
A	1900	50	50
B	1800	100	100
C	700	700	700
D	1000	500	500
E	2000	---	---
F	1800	100 (no BC synapses)	100 (no BC synapses)
G	1800	100 (no MC synapses)	100 (no MC synapses)

Table 17: Network composition in GCs. Different DG network compositions for the different simulations that were performed.

The synaptic weights from EC to different GC populations used for the network simulations are summarized in the following table:

Synaptic Weights (EC → GC)	Scaling factor
EC → dbGCs	3.80
EC → Mature abGCs	1.40
EC → Immature abGCs	1.40

Table 18: Synaptic weights parameters. Parameters for the synaptic weights of inputs from EC to different developmental stages of GC populations.

The calculation of activity in the different network compositions was done used the following formula:

$$activity = \frac{N_{active}}{N_{total}} \cdot 100\,\%$$

where N_{active} is the number of neurons from the particular neuronal population (dbGCs, mature abGCs or immature abGCs) divided by the N_{total} which is the total number of neurons from this particular neuronal population in which we are referred in each case. Moreover, we consider as active neurons, each neuron that emits at least one spike.
As far as the calculation of sparsity of different GC populations in the different network compositions are concerned, we used the following formula:

$$sparsity = 1 - activity$$

As sparsity and activity are complement metrics, we have chosen to show only the activity metric.

2.7 Pattern Separation in the DG Network

In the level of a network, we consider that this particular network performs pattern separation when the similarity between two distinct input patterns is higher than the similarity between the corresponding output patterns. During the various simulations that we performed, the input patterns were presented as the activity along the 400 PP afferents. For each input pattern, there are 40 active PP afferents (i.e. 10% input density). For our analysis, in the DG network we consider as active, each GC that emits at least one spike during the presentation of the stimulus (***Myers and Scharfman 2009***), thus the output patterns correspond to the active GCs. In order to quantify the pattern separation efficiency we used both for inputs and outputs the population distance metric f_1 which is calculated by the following formula:

$$f_1 = \frac{HD}{2(1-s)\cdot N}$$

where *s* denotes the sparsity (i.e. the ratio of silent neurons to all neurons as we have calculated it from previous formula of *sparsity*), *N* the number of neurons, and *HD* is the Hamming Distance between two binary patterns (***Hamming 1950***). The Hamming Distance is defined as as the number of positions at which the corresponding values are different. The factor of 2 in the denominator is used to limit our distance measure at one.

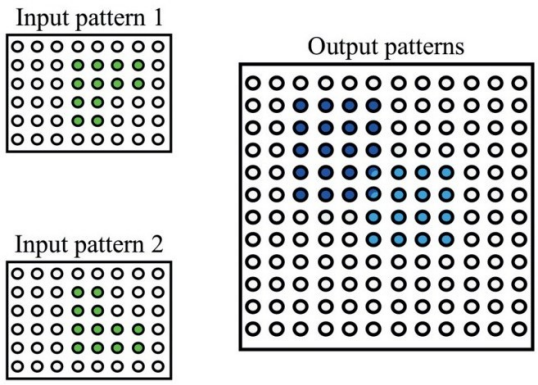

Figure 38: Population-based pattern separation. Schematic representation of pattern separation using population-based coding (metric f_1). When two highly overlapping EC inputs (input 1 and input 2, with identical mean firing rates) arrive in DG, the corresponding outputs are highly dissimilar. At this time point we should pinpoint that the output pattern is sparse because of the low number of GCs that encode any given pattern.

As we already mentioned, our network performs pattern separation if the input distance is smaller than the output distance, i.e. $f_{1(input)} < f_{1(output)}$. Heretofore, we calculated the distance between two binary patterns using only the HD metric. Despite the fact that we constructed the input patterns from PP afferents taking into consideration the input patterns to have the same sparsity (10% are active), the output patterns do not mandatory have the same activity level. Having as our aim to examine the differences among the active neurons of each pattern, we disengage the dependence on sparsity by dividing the HD with the number of neurons that are active in a pattern.

In our network simulations, the output patterns are vectors, each vector with length equal to 2000 and 2-5% active neurons, which in turn correspond to 40-100 neurons. The total number of active neurons lies in the range of 40-200. To describe it more detailed, in case of HD equal to 20, the old metric, i.e., without taking into account the activity (or sparsity) gives a distance equal to 0.01 whereas the f_1 metric ranges from 0.10 to 0.25, depending on the percentage of active GC neurons. Hence, using the f_1 metric ("population-based"), we are taking into consideration the differences only between active neurons. In that way, we succeed to make the metric more robust across different levels of sparsity.

We constructed four groups of input pattern pairs, with different degrees of similarity and we calculated the input and the corresponding output population distances for each group independently. First, we constructed a variety of input patterns with input density 10% (i.e. 40 active neurons) and consequently, four additional input patterns were build with 40 active neurons, 8, 16, 24 and 32 of which are common between patterns, which in turn corresponds to $f_{1(input)} = 0.4$, 0.3, 0.2 and 0.1. The reasoning behind this approach is to examine highly overlapping patterns ($f_{1(input)} = 0.1, 0.2$), as well as less similar ones ($f_{1(input)} = 0.3, 0.4$).

The table below summarizes the main characteristics of the overlapping incoming inputs that we introduce in the DG network. These incoming inputs are derived by the EC Layer II.

EC Layer II Inputs		
Overlap	Hamming Distance	f_1 score
0.9 (90%)	8	0.4
0.8 (80%)	16	0.3
0.7 (70%)	24	0.2
0.6 (60%)	32	0.1

Table 19: Population-based f_1 metric. A summary of the f_1 metric with the respective values for Hamming distance between input patterns and the overlap.

2.8 Statistical Tests

After performing an adequate amount of simulations for each DG network composition, we derived the activity levels for for each GC population. The obtained statistics concerned the mean and standard deviation of activity levels. The main target was to unravel if the activity levels of each GC population, as well as of total GC population, was affected in a statistically significant way by the different DG network compositions. Instead of the classic statistic approach of student t-test, we used the Kolmogorov-Smirnov test which is a little bit more complicated in comparison with student t-test and permits us to detect patterns that student t-test cannot detect. KS test could be used to examine whether two samples are significantly different. The D-statistic is the absolute maximum distance (supremum) between the cumulative distribution functions of the two samples. The closer the number is to zero, the more likely it is that the two samples were drawn from the same distribution.

Our null hypothesis is that the activity levels between control network A (or B) and network C, D, E, F or G were not different in a statistical significant way and were drawn from the same distribution. The significance level that we chose was a = 0.05. For every case where p-value < a, we rejected the null hypothesis and we concluded that the difference in activity levels between control network and the chosen tested network was statistically significant.

Moreover, for the examination of pattern separation function, we derived as result the f_1 scores about the output patterns of the examined DG network. Also, we have as our aim to find out if the pattern separation function is affected by DG network composition, thus we examined if the mean f_1 score between control network A (or B) and DG network of different compositions was statistically significant different. Again, the used statistic test was the KS test. The null hypothesis was that the f_1 score of output patterns between control network A (or B) and network C,D or E were not different in a statistically important way so they were drawn from the same distribution. The level of significance was set a = 0.05 and each time that p-value < a the null hypothesis was rejected. Then, we deduced that the difference in f_1 scores of output patterns was statistically significant.

3. RESULTS

3.1 Neuronal populations in the DG and their models

As we already mentioned, the DG network model is comprised of 2000 GCs (1900 or 1800 dbGCs, 50 or 100 mature abGCs, 50 or 100 immature abGCs for Networks A, B respectively) that represent the three different developmental stages of GCs in the DG. Moreover, in the network there are 80 excitatory MCs, 100 of the inhibitory INs BCs, as well as 40 of the inhibitory interneurons HIPP cells.

For the modeling of MCs, BCs and HIPP cells we used the AdEx model. The GCs were modeled as multicompartmental neuron models comprised of soma and dendrites (12 dendrites → dbGCs, 3 dendrites → abGCs). For the soma was used the AdEx model, while for the dendritic compartments was used the leaky integrate & fire model without spike mechanism. For the morphology of dendritic and somatic compartments, we were based loosely on anatomical data. All computational neuron models were validated against experimental data with respect to their activity and basic electrophysiological properties (***Lübke et al. 1998, Bartos et al. 2001, Krueppel et al. 2011***). Overall, the electrophysiological properties of the computationally modeled neurons included in the DG network, are in fair alignment with experimental findings. At this time point, we should note that the spiking profiles of GCs were not taken into consideration for the estimation of pattern separation in the DG network. A GC model neuron was considered active even if it produced a single spike. Hence, we chose to fit average values rather than temporal profiles of the model neurons.

3.2 The DG Network Model

After performing an adequate amount of simulations for each control Network A or B, we managed to reproduce the active properties for all neuronal types in the control Networks and we observed that mature abGCs are less excitable than immature abGCs, while BCs and HIPP cells emit a large number of action potentials exhibiting a fast-spiking behavior.

Indicatively, the following diagrams represent the firing behavior of dbGCs (old GCs), mature and immature abGC model after the arrival of EC Layer II inputs for the control Network B (90% dbGCs – 10% abGCs).

A

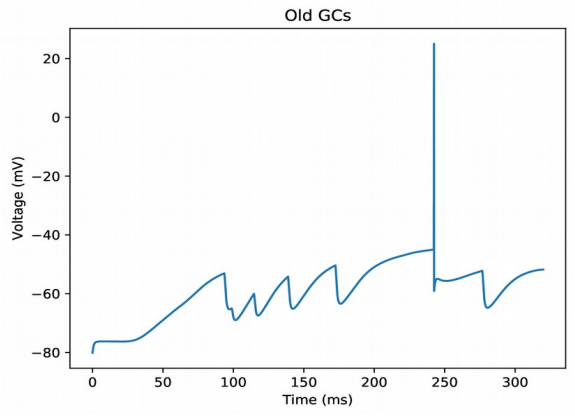

B

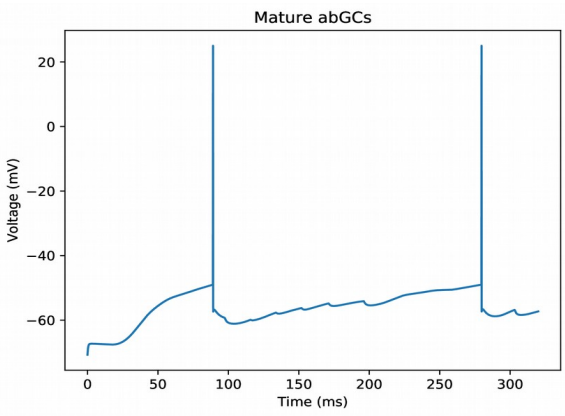

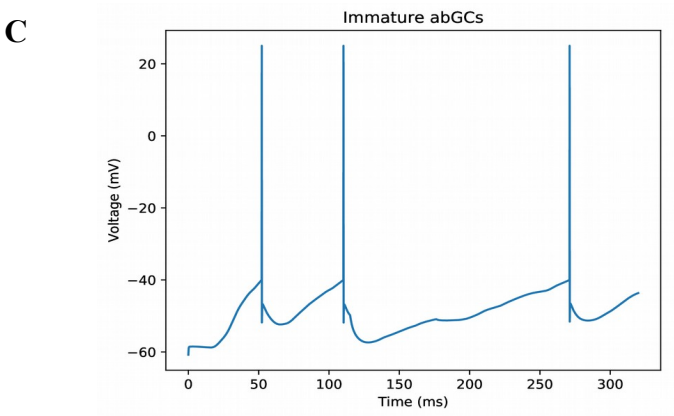

Figure 39: Firing traces of developmentally-born (old GCs), mature and immature abGC model cells in response to EC inputs (300 ms). Note that APs are not explicitly modeled in I & F neurons. A) The somatic membrane voltage of one dbGC model in response to EC inputs B) The somatic membrane voltage of one mature abGC model in response to EC inputs. C) The somatic membrane voltage of one immature abGC model in response to EC inputs.

Moreover, the BC and HIPP cell model in the control Network B exhibit a firing behavior that comes in accordance with the experimental findings that support the fast-spiking character that these types of cell exhibit. MCs also exhibited a spiking profile consistent with experiments.

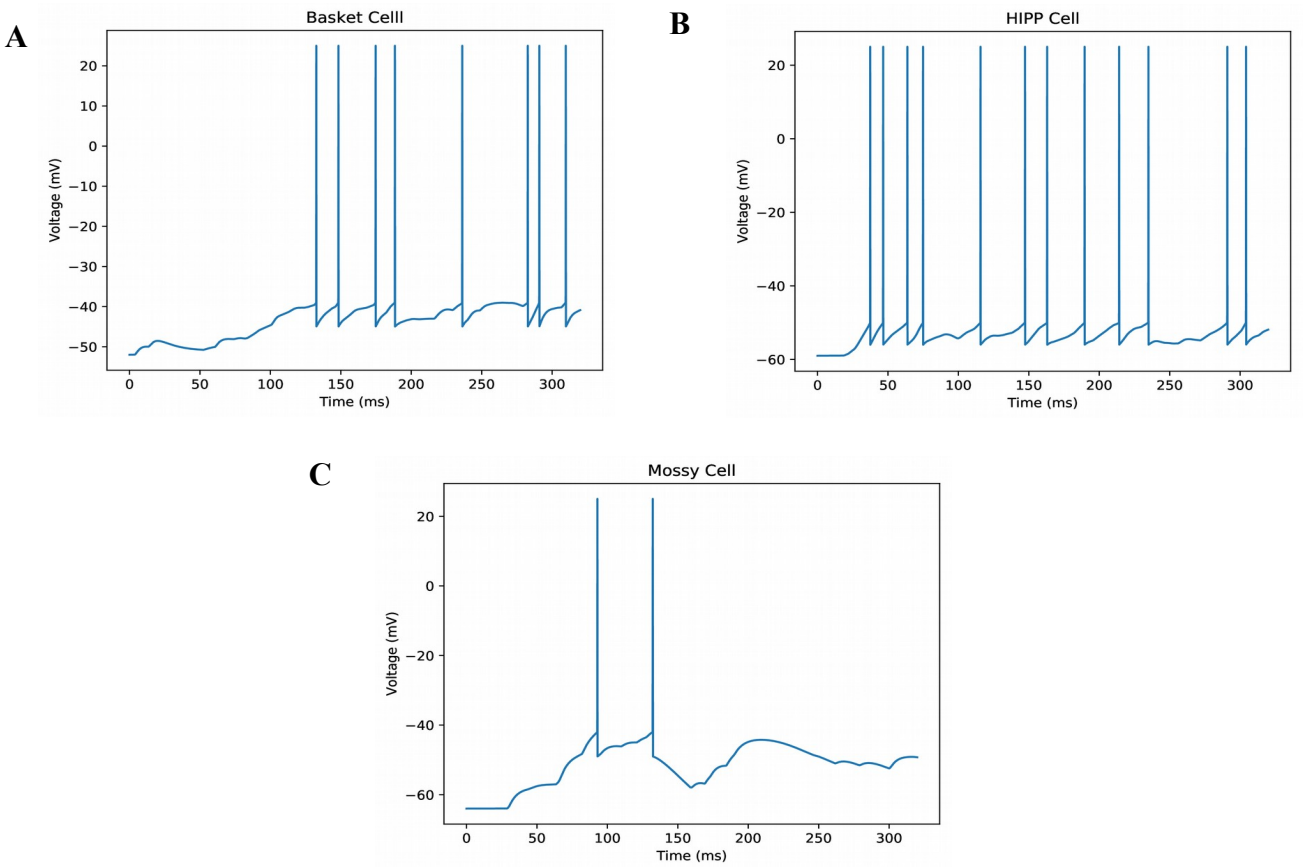

Figure 40: Firing traces of the BC, HIPP cell and MC model in response to EC inputs (300 ms). Note that APs are not explicitly modeled in I & F neurons. Due to the fast-spiking behavior we plot the voltage trace for a small time period in order to have a clear insight of emitted spikes. A) The somatic membrane voltage of the BC model in response to EC inputs. B) The somatic membrane voltage of the HIPP cell model in response to EC inputs. C) The somatic membrane voltage of the MC model in response to EC inputs.

A spike raster plot displays the spiking activity of a group of neurons over time. In a raster plot each row (y-axis) corresponds to the index of a neuron in a neuron group. The columns (x-axis) corresponds to the current time in the simulation. The presence of a dot in a given row and column, indicates that the neuron whose index corresponds to that row produced an action potential (spike) at the time corresponding to that column. For instance, if neuron 2 spikes at time 10 a dot will appear in row 2 at the column representing the 10th time index. Extending this, it can be seen that a raster plot displays the pattern of spikes across a neuron group over time. The following raster plots exhibit a spiking behavior that comes in accordance with the spiking profiles that we observe in voltage traces. Conclusively, from the adult-born granule neuronal population immature abGCs are more excitable than mature, while for the population of fast-spiking INs - BCs and HIPP - cells emit a large number of spikes. MCs exhibit in raster plot a spiking profile that comes in line with voltage traces.

A

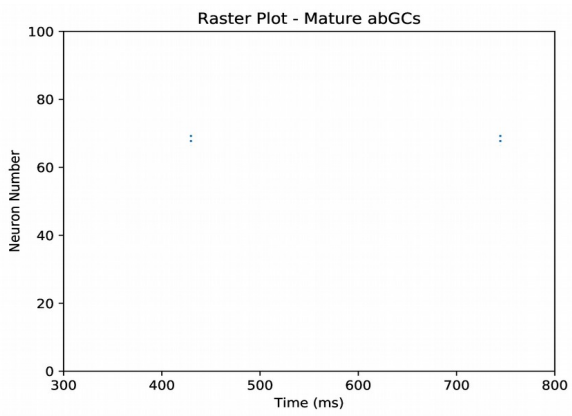

B

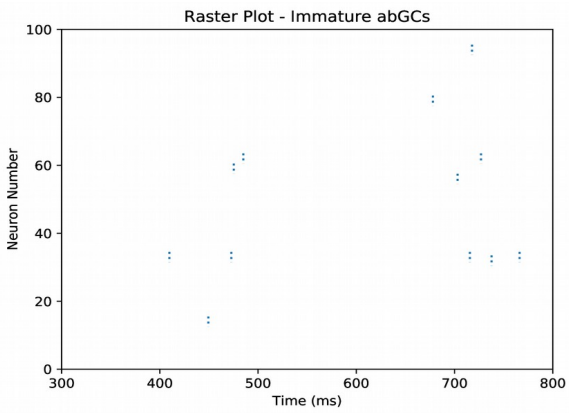

C

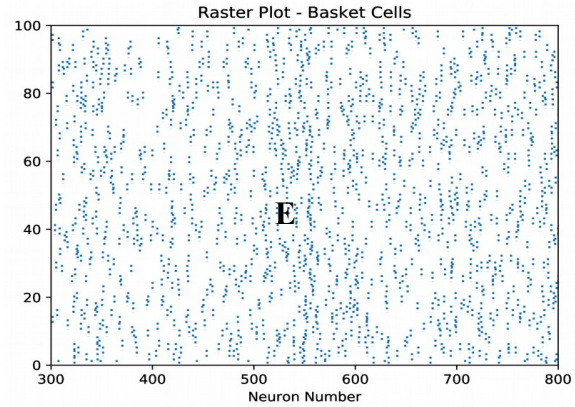

D

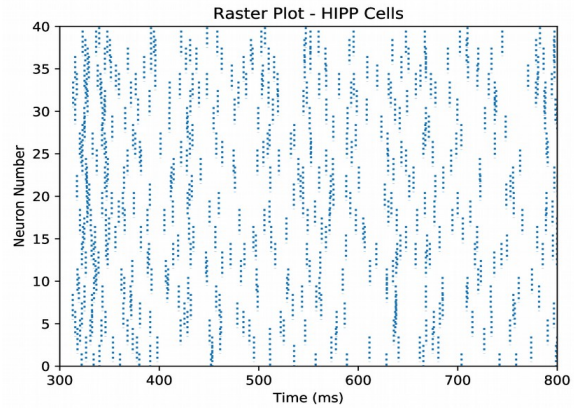

E

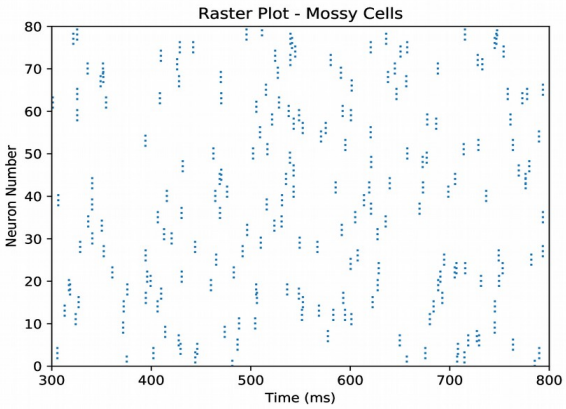

Figure 41: Raster plots of mature abGCs, immature abGCs, basket, HIPP and mossy cells. A) A spike raster plot displays the spiking activity of mature abGCs over time, B) A spike raster plot displays the spiking activity of immature abGCs over time, C) A spike raster plot displays the spiking activity of basket cells over time, D) A spike raster plot displays the spiking activity of HIPP cells over time, E) A spike raster plot displays the spiking activity of mossy cells over time

3.3 Control Networks A,B Simulations

3.3.1 GC Population

Networks A and B, are the two control DG networks that are comprised of the different developmental stages of GC populations, INs and the other excitatory population in DG network (MCs) in a scale-down approach, yet in accordance with experimental data. The composition of Network A in GCs was 1900 dbGCs, 50 mature abGCs, 50 immature abGCs (5% abGCs), while the composition of Network B was 1800 dbGCs, 100 mature abGCs and 100 immature abGCs (10% abGCs). Indeed, the GC activity in the Network A (95% dbGCs – 5% abGCs) was predicted from the model to be ~1.4% as it was calculated from experimental data for each incoming input.
In the following table are summarized some statistics (mean ± std) for activity level of each different developmental stage of GC populations in the network A as well as for the GC population in total. The statistics about activity level were calculated with formula that we described before (*see section with Materials & Methods*).

Network A	Old GCs	Mature abGCs	Immature abGCs	GCs
Activity	1.16 ± 0.37	2.76 ± 2.29	8.4 ± 4.03	1.38 ± 0.41

Table 20: Activity in the Network A. In the table are indicated the mean ± standard deviation for the activity of GC population in total as well as of each GC population at different developmental stages.

In the following bar-plots with error bars (standard deviation) we can compare more detailed the activity level of GC populations at different developmental stages and for GC population in total in control network A with 5% existence of adult neurons.

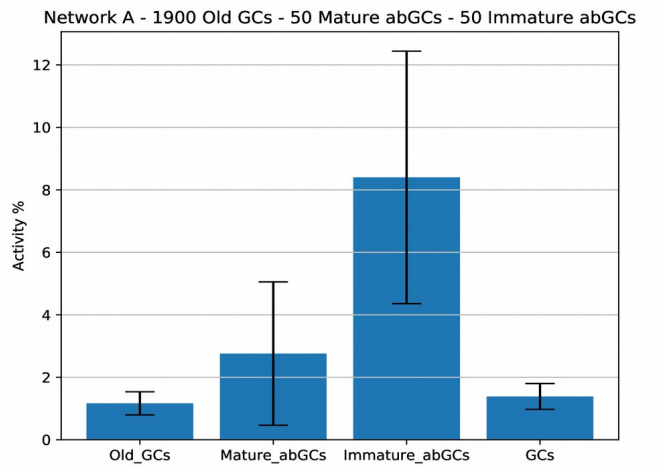

Figure 42: Bar-plots with error bars for activity of GC populations in Network A. Activity of GC populations in different developmental stages and GC population in total for the Network A.

Indeed, the activity levels are higher for the immature abGC population followed by the mature abGC population. We were expecting that taking into consideration the high excitability that abGCs indicate in the DG network. The lowest activity levels are about the dbGC population. In accordance with these observations, given that sparsity = 1 – activity, the sparsity levels for immature and mature abGC population were the lowest with higher sparsity levels in the dbGC population.

For the Network B (90% dbGCs – 10% abGCs) the activity of the GC population in the network was predicted from the model to be ~1.6% (mean ± std: 1.57 ± 0.38). This value comes in accordance with experimental findings for the activity levels of GCs in the DG network. In the following table are summarized some statistics (mean ± std) for activity level of each different developmental stage of GC populations in the network B as well as for the GC population in total. The statistics about activity level were calculated with formula that we described before (*see section with Materials & Methods*).

Network B	Old GCs	Mature abGCs	Immature abGCs	GCs
Activity	1.13 ± 0.35	2.34 ± 1.40	8.74 ± 3.18	1.57 ± 0.38

Table 21: Activity in the Network B. In the table are indicated the mean ± standard deviation for the activity of GC population as well as of each GC population at different developmental stages.

In the following bar-plots with error bars (standard deviation) we can compare more detailed the activity level of GC populations at different developmental stages and for GC population in total.

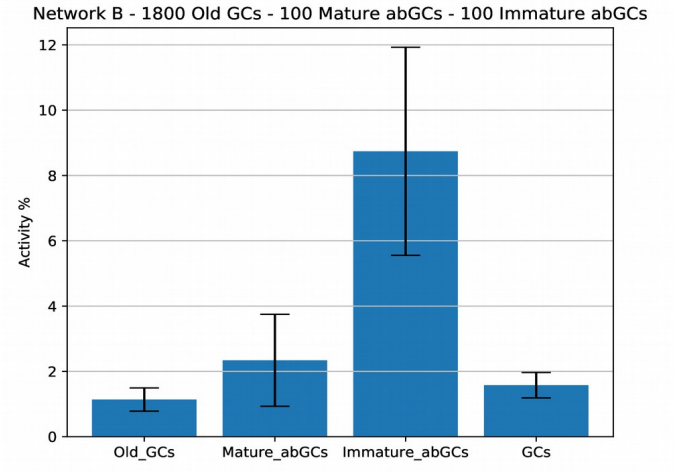

Figure 43: Bar-plots with error bars for activity of GC populations in Network B. Activity of GC populations in different developmental stages and GC population in total for the Network B.

Indeed, the activity levels are higher for the immature abGC population followed by the mature abGC population. We are expecting that taking into consideration the high excitability that abGCs indicate in the DG network. The lowest activity levels were about the dbGC (old GC) population. In accordance with these observations, given that sparsity = 1 – activity, the sparsity levels for immature and mature abGC populations were the lowest with higher sparsity levels in the dbGC

population. In the following histograms, we can conclude that indeed, in the control networks A, B the activity follows the predicted incline according to experimental data, with dbGCs being the less active followed by the more active mature and immature abGCs.

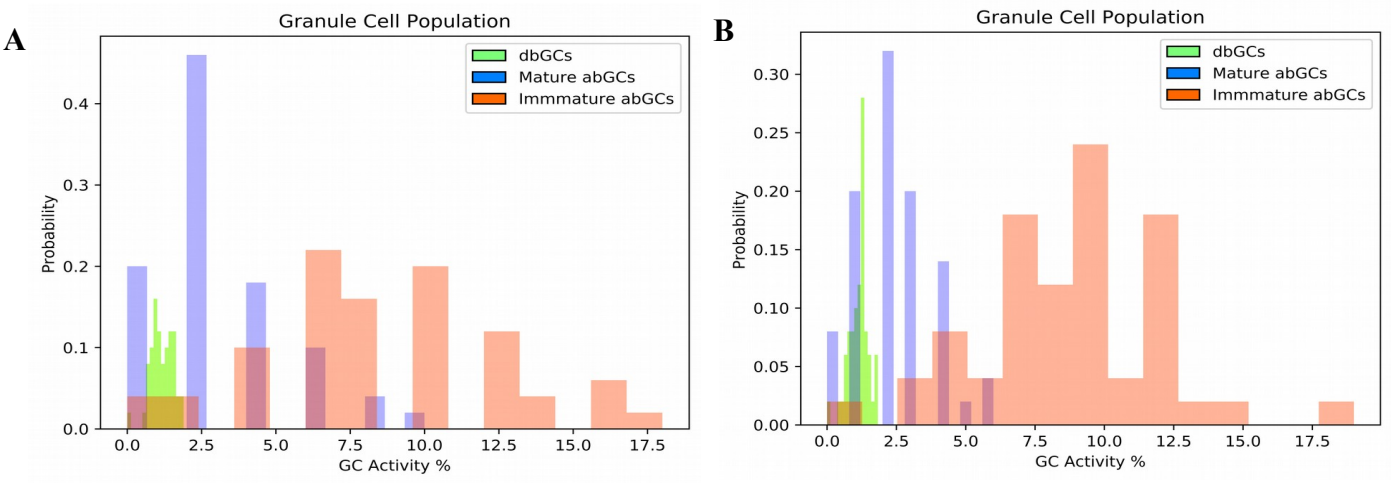

Figure 44: Common histograms for activity of GC populations in Networks A,B. A) In the same plot we can observe that the incline of activity levels of GC populations in Network A follows the pattern $activity_{dbGCs} < activity_{mature\ abGCs} < activity_{immature\ abGCs}$. B) In the same plot we can observe that the incline of activity levels of GC populations in Network B follows the pattern $activity_{dbGCs} < activity_{mature\ abGCs} < activity_{immature\ abGCs}$.

3.4 Network C Simulations

As we augmented the percentage of abGC population in the network, the activity level of the GC population was augmented too. Indeed, the Network C with the highest percentage of abGC populations (700 immature abGCs and 700 mature abGCs) exhibited higher activity in comparison with control networks A and B (mean ± std: 3.39 ± 0.67). In the following table are summarized some statistics (mean ± std) for activity of each different developmental stage of GC populations in the network C as well as for the GC population in total. The statistics about activity level were calculated with formula that we described before (*see Materials & Methods*).

Network C	Old GCs	Mature abGCs	Immature abGCs	GCs
Activity	1.13 ± 0.40	2.24 ± 0.59	6.79 ± 1.63	3.39 ± 0.67

Table 22: Activity in the Network C. In the table are indicated the mean ± standard deviation for the activity of GC population as well as of each GC population at different developmental stages.

In the following bar-plots with error bars (standard deviation) we can compare more detailed the activity level of GC populations at different developmental stages and for GC population in total.

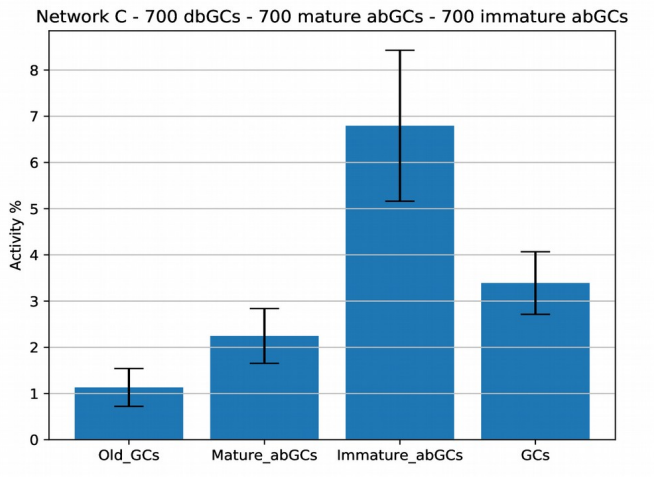

Figure 45: Bar-plots with error bars for activity of GC populations in Network C. Activity of GC populations in different developmental stages and GC population in total for the Network C.

Indeed, the activity levels are higher for the immature abGC population followed by the mature abGC population. We are expecting that, taking into consideration the high excitability that abGCs indicate in the DG network. The lowest activity levels are about the dbGC population. In accordance with these observations, given that sparsity = 1-activity, the sparsity levels for immature, mature abGC population and dbGC population exhibit the reverse relationship compared with activity levels. In the following histograms, we can conclude that indeed, in the Network C the activity follows the predicted incline according to experimental data, with dbGCs being the less active followed by the more active mature and immature abGCs.

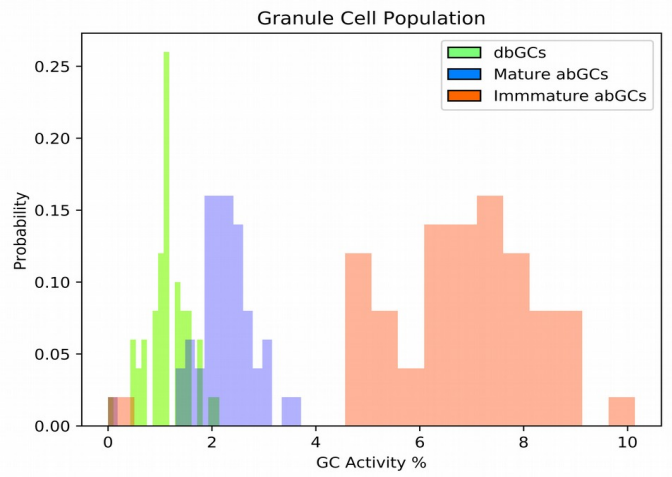

Figure 46: Common histogram for activity of GC populations in Network C. In the same plot we can observe that the incline of activity levels of GC populations in Network C follows the pattern $\text{activity}_{\text{dbGCs}} < \text{activity}_{\text{mature abGCs}} < \text{activity}_{\text{immature abGCs}}$.

3.5 Network D Simulations

The Network D, the second with the highest activity level of the GC population after the Network C, had activity approximately 3%, which is doubled compared with the control Networks A,B (mean ± std: 2.97 ± 0.61). In the Network D the composition of GCs were 50% dbGCs (1000 dbGCs) and 50% abGCs (500 immature abGCs and 500 mature abGCs). In the following table are summarized some statistics (mean ± std) for activity of each different developmental stage of GC

populations in the network D as well as for the GC population in total. The statistics about activity level were calculated with formula that we described before (*see Materials & Methods*).

Network D	Old GCs	Mature abGCs	Immature abGCs	GCs
Activity	1.044 ± 0.39	2.34 ± 0.77	7.48 ± 1.85	2.97 ± 0.61

Table 23: Activity in the Network D. In the table are indicated the mean ± standard deviation for the activity of GC population as well as of each GC population at different developmental stages.

In the following bar-plots with error bars we can compare more detailed the activity level of GC populations at different developmental stages and for GC population in total.

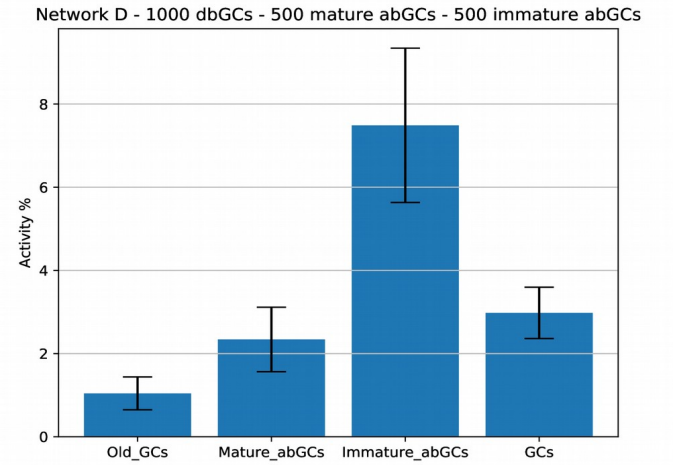

Figure 47: Bar-plots with error bars for activity of GC populations in Network D. Activity of GC populations in different developmental stages and GC population in total for Network D.

Indeed, the activity levels are higher for the immature abGC population followed by the mature abGC population. We are expecting that, taking into consideration the high excitability that abGCs indicate in the DG network. The lowest activity levels are about the dbGC population. In accordance with these observations, given that sparsity = 1-activity, the sparsity levels for immature, mature abGC population and dbGC population exhibit the reverse relationship compared with activity levels. In the following histograms, we can conclude that indeed, in the Network D the activity follows the predicted incline according to experimental data, with dbGCs being the less active followed by the more active mature and immature abGCs.

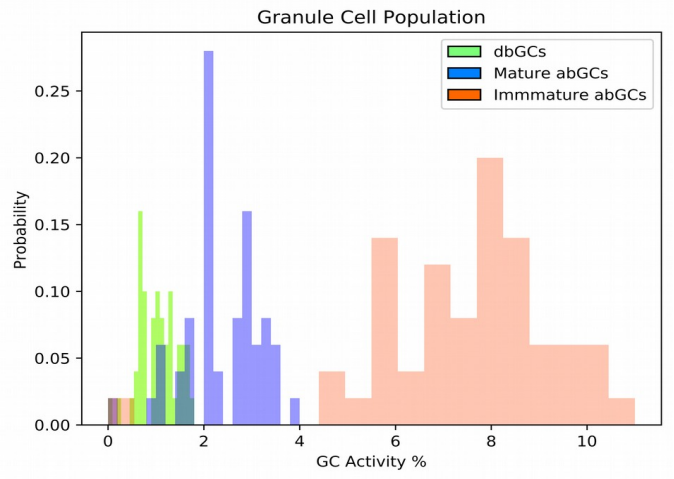

Figure 48: Common histogram for activity of GC populations in Network D. In the same plot we can observe that the incline of activity levels of GC populations in Network D follows the pattern $activity_{dbGCs} < activity_{mature\ abGCs} < activity_{immature\ abGCs}$.

3.6 Network E Simulations

In the Network E, we simulated the extreme case where adult neurogenesis is absent without abGCs in the DG Network (only 2000 dbGCs). The level of activity was the lowest in comparison with all other network simulations.

In the following table are summarized some statistics (mean ± std) for the activity of dbGC populations in the network E which – in this case – is identified with the total GC population. The statistics about activity level were calculated with formula that we described before.

Network E	Old GCs	Mature abGCs	Immature abGCs	GCs
Activity	1.19 ± 0.34	---	---	1.19 ± 0.34

Table 24: Activity of GC population in Network E. In the table are indicated the mean ± standard deviation.

Conclusively, we observe that as we augment the percentage of abGCs in the DG network while keeping the total number of GCs stable (2000 GCs), the activity level is augmented too. Hence, we observe the highest activity levels for the total GC population in the DG Network with the composition 33% dbGCs – 66% abGCs (i.e 33% immature abGCs – 33% mature abGCs) where the percentage of abGC population in the network is the highest. The second network with the highest activity was D with 50% dbGCs – 50% abGCs. The lowest activity level was pinpointed in the network E where adult neurogenesis was absent.

3.7 Network F without abGC-BC synapses

In order to unravel the effect of BC into dbGCs, abGCs and GC population in total, we performed an additional simulation in which we excluded the synapses between abGCs and BCs. This network was comprised of 1800 dbGCs (90% of the total GC population as in Network B), 100 mature abGCs and 100 immature abGCs (10% of the total GC population as in Network B).

In the following table are summarized some statistics (mean ± std) for activity of each different developmental stage of GC populations in the network F as well as for the GC population in total. The statistics about activity levels were calculated with formulas that we described before (*see section Materials & Methods*).

Network F	Old GCs	Mature abGCs	Immature abGCs	GCs
Activity	1.04 ± 0.27	16.52 ± 5.98	68.0 ± 12.78	3.10 ± 0.55

Table 25: Activity of GC population in Network F. In the table are indicated the mean ± standard deviation.

In the following bar-plots with error bars we can compare more detailed the activity levels of GC populations at different developmental stages and for GC population in total.

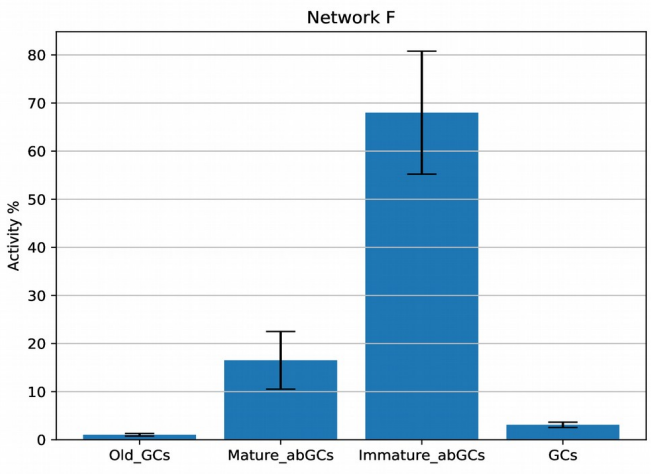

Figure 49: Bar-plots with error bars for activity of GC populations in Network F. Activity of GC populations in different developmental stages and GC population in total for the Network F.

Indeed, the activity levels are much higher for the immature abGC population followed by the mature abGC population. We are expecting that taking into consideration the high excitability that abGCs indicate in the DG network. The lowest activity levels are about the dbGC population.
In the following histogram, we can conclude that indeed, in the Network F the activity follows the predicted incline according to experimental data, with dbGCs being the less active followed by the more active mature and immature abGCs.

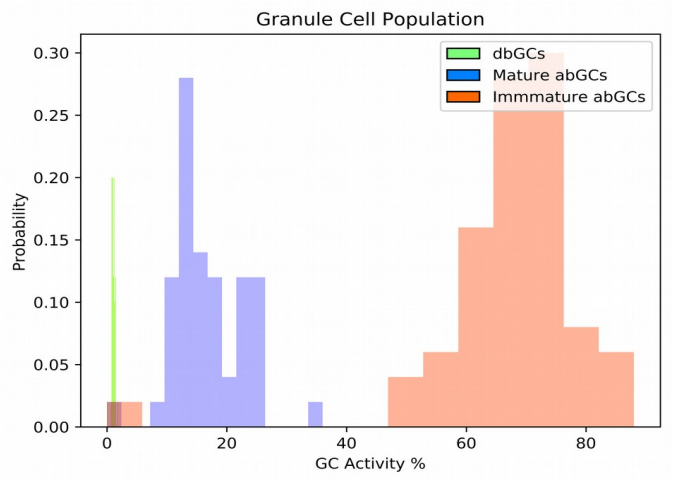

Figure 50: Common histogram for activity of GC populations in Network F. In the same plot we can observe that the incline of activity levels of GC populations in Network F follows the pattern $activity_{dbGCs} < activity_{mature\ abGCs} < activity_{immature\ abGCs}$.

3.8 Network G without abGC-MC synapses

In order to unravel the effect of MCs into abGCs, dbGCs and GC population in total, we performed an additional simulation in which we excluded the synapses between abGCs and MCs. This network was comprised of 1800 dbGCs (90% of the total GC population as in Network B), 100 mature abGCs and 100 immature abGCs (10% of the total GC population as in Network B). In the following table are summarized some statistics (mean ± std) for activity of each different developmental stage of GC populations in the network G as well as for the GC population in total. The statistics about activity levels were calculated with formulas that we described before (*see section Materials & Methods*).

Network G	Old GCs	Mature abGCs	Immature abGCs	GCs
Activity	1.15 ± 0.29	2.14 ± 1.31	7.04 ± 2.79	1.49 ± 0.33

Table 26: Activity of GC population in Network G. In the table are indicated the mean ± standard deviation.

In the following bar-plots with error bars we can compare more detailed the activity levels of GC populations at different developmental stages and for GC population in total.

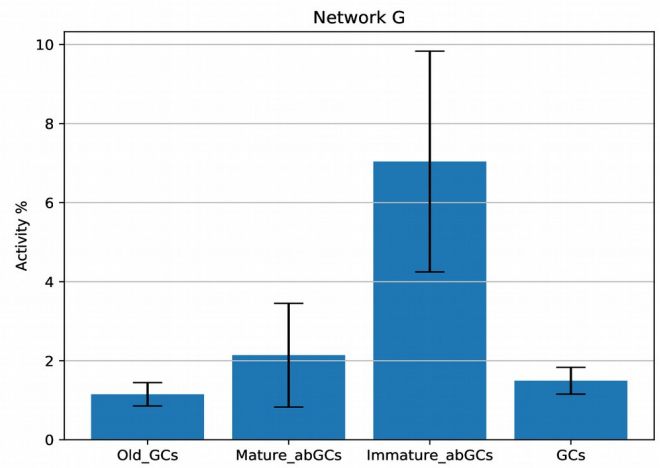

Figure 51: Bar-plots with error bars for activity of GC populations in Network G. Activity of GC populations in different developmental stages and GC population in total for the Network G without abGC-MC synapses.

Indeed, the activity levels are much higher for the immature abGC population followed by the mature abGC population. We are expecting that taking into consideration the high excitability that abGCs indicate in the DG network. The lowest activity levels are about the dbGC population. In the following histogram, we can conclude that indeed, in the Network G the activity follows the predicted incline according to experimental data, with dbGCs being the less active followed by the more active mature and immature abGCs.

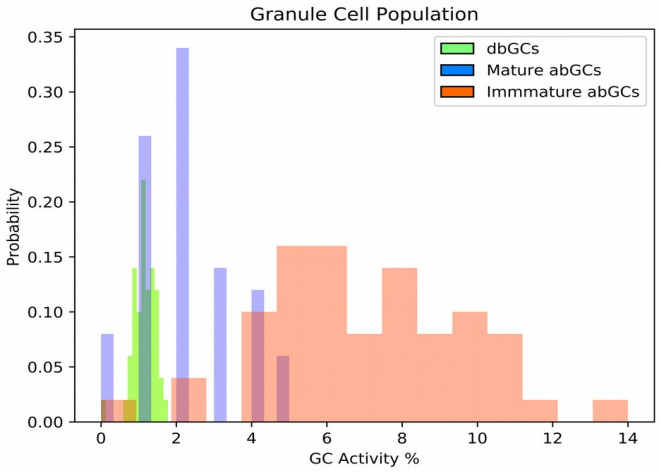

Figure 52: Common histogram for activity of GC populations in Network G. In the same plot we can observe that the incline of activity levels of GC populations in Network G follows the pattern $activity_{dbGCs} < activity_{mature\ abGCs} < activity_{immature\ abGCs}$.

3.9 Activity and sparsity of GC populations at different developmental stages for various network compositions

To put in a nutshell, we summarize the statistics (mean ± std) for activity of GC populations at three different developmental stages; as old GCs (dbGCs), mature abGCs and immature abGCs.

For dbGCs we do not observe significant differences for their activity levels for various network compositions.

dbGC	Network A	Network B	Network C	Network D	Network E	Network F	Network G
Activity	1.16 ± 0.37	1.13 ± 0.35	1.13 ± 0.40	1.044 ± 0.39	1.19 ± 0.34	1.04 ± 0.27	1.15 ± 0.29

Table 27: Activity of dbGC population for the different network compositions. In the table are indicated the mean ± standard deviation.

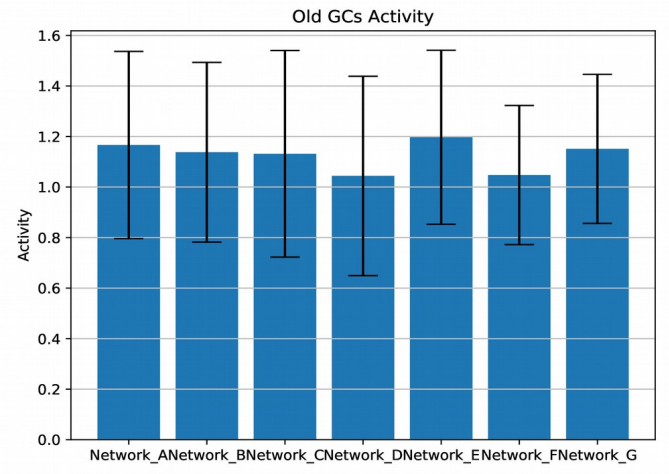

Figure 53: Bar-plots with error bars for activity of dbGC populations in different networks. Activity of dbGC population in different network simulations.

The following table summarizes the mean and standard deviation for the activity levels of mature abGCs in different DG network compositions.

Mature abGC	Network A	Network B	Network C	Network D	Network E	Network F	Network G
Activity	2.76 ± 2.29	2.34 ± 1.40	2.24 ± 0.59	2.34 ± 0.77	---	16.52 ± 5.98	2.14 ± 1.31

Table 28: Activity of mature abGC population for the different network compositions. In the table are indicated the mean ± standard deviation.

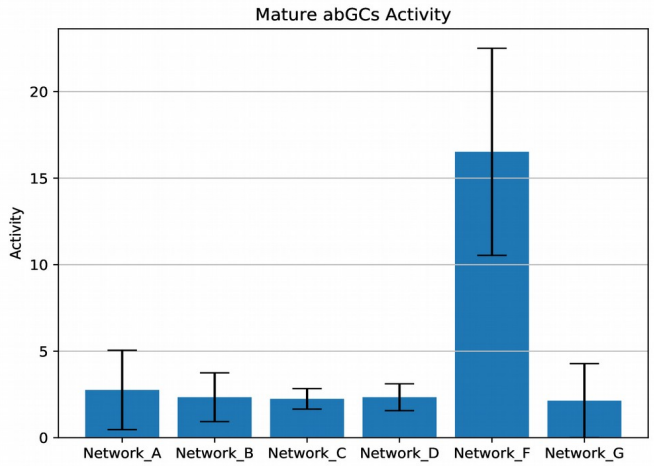

Figure 54: Bar-plots with error bars for activity of mature abGC populations in different networks. Activity of mature abGC population in different network simulations.

In the following table are summarized the mean and standard deviation for immature abGCs for different DG network compositions.

Immature abGC	Network A	Network B	Network C	Network D	Network E	Network F	Network G
Activity	8.4 ± 4.03	8.74 ± 3.18	6.79 ± 1.63	7.48 ± 1.85	---	68.0 ± 12.78	7.04 ± 2.79

Table 29: Activity of immature abGC population for the different network compositions. In the table are indicated the mean ± standard deviation.

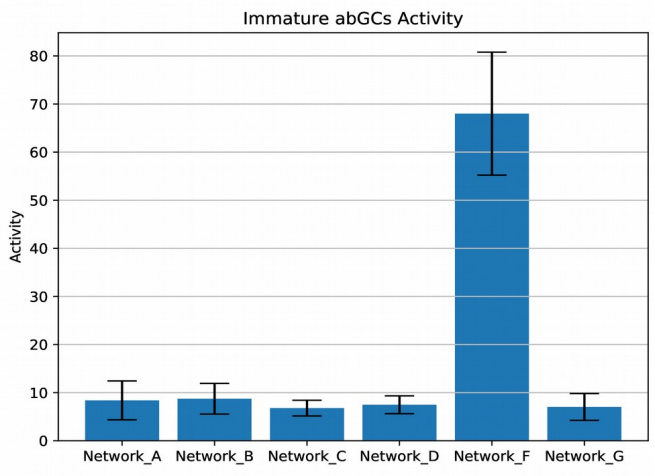

Figure 55: Bar-plots with error bars for activity of immature abGC populations in different networks. Activity of immature abGC population in different network simulations.

Conclusively, the results that we derived for activity levels of the total GC population after completing the above network simulations are summarized in the following table:

GC Population	Network A	Network B	Network C	Network D	Network E	Network F	Network G
Activity	1.38 ± 0.31	1.57 ± 0.38	3.39 ± 0.67	2.97 ± 0.61	1.19 ± 0.34	3.10 ± 0.55	1.15 ± 0.29

Table 30: Activity of GC population in different Network simulations. In the table are indicated the mean ± standard deviation.

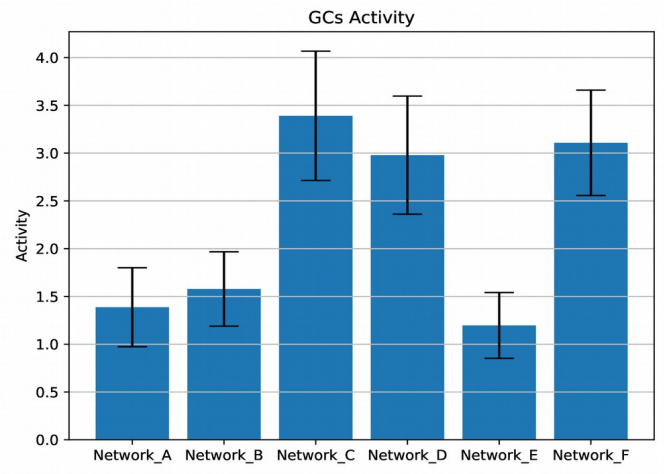

Figure 56: Bar-plots with error bars for activity of total GC population in different networks. Activity of total GC population in different network simulations.

In order to investigate if the differences in the activity of total GC population across different DG network compositions are statistically significant, we performed the Kolmogorov-Smirnov statistic test. The derived results of KS test are D-statistic and p-value. The D-statistic is the absolute maximum distance (known as supremum) between the cumulative distribution functions of the two samples, where in our case the samples are the control network (A or B) and the remaining DG networks (C, D, E, F or G). Our null hypothesis is that there is no statistically significant difference between activity levels of network A and network C. The selected level of significance is a = 0.05.

Networks A-C	GCs	dbGCs	Mature abGCs	Immature abGCs
D-statistic	0.98	0.14	0.34	0.41
p-value	1.75×10^{-22}	0.67	0.004	0.001

Table 31: Derived statistics after Kolmogorov-Smirnov test examining the activity levels between control network A and network C. We examine the statistics of KS test for the total GC population, as well as for each developmental stage of GC population separately.

As the KS statistic test proves, the difference of activity levels between control network A and network C are statistically significant for the total GC population (D-statistic = 0.98, p-value = 1.75×10^{-22}), mature abGCs (D-statistic = 0.34, p-value = 0.004) and immature abGCs (D-statistic = 0.41, p-value = 0.001). For the dbGC population the difference in activity levels are not statistically significant.

Networks B-C	GCs	dbGCs	Mature abGCs	Immature abGCs
D-statistic	0.98	0.20	0.30	0.45
p-value	1.75×10^{-22}	0.24	0.01	2.76×10^{-5}

Table 32: Derived statistics after Kolmogorov-Smirnov test examining the activity levels between control network B and network C. We examine the statistics of KS test for the total GC population, as well as for each developmental stage of GC population separately.

Considering the Network B as control, we deduce that the difference of activity levels between control network B and network C are statistically significant for the total GC population (D-statistic=0.98, p-value = 1.75×10^{-22}), mature abGCs (D-statistic = 0.34, p-value = 0.004) and immature abGCs (D-statistic = 0.36, p-value = 0.002). Again, for the dbGC population we do not

observe statistical significant difference in activity levels between control network B and network C.

Networks A-D	GCs	dbGCs	Mature abGCs	Immature abGCs
D-statistic	0.20	0.20	0.34	0.36
p-value	0.24	0.24	0.004	0.002

Table 32: Derived statistics after Kolmogorov-Smirnov test examining the activity levels between control network A and network D. We examine the statistics of KS test for the total GC population, as well as for each developmental stage of GC population separately.

Investigating the difference in activity levels between control network A and network D, we observe statistically significant difference for mature abGC population (D-statistic = 0.34, p-value = 0.004) and immature abGC population (D-statistic = 0.34, p-value = 0.002). Nevertheless, the difference in activity levels for dbGC population and the total GC population is not statistically significant.

Networks B-D	GCs	dbGCs	Mature abGCs	Immature abGCs
D-statistic	0.94	0.24	0.27	0.32
p-value	1.01×10^{-20}	0.09	0.03	0.008

Table 33: Derived statistics after Kolmogorov-Smirnov test examining the activity levels between control network B and network D. We examine the statistics of KS test for the total GC population, as well as for each developmental stage of GC population separately.

Studying the difference in activity levels between control network B and network D we observe statistically significant difference in activity levels for GC population in total (D-statistic = 0.94, p-value = 1.01×10^{-20}), mature abGCs (D-statistic = 0.27, p-value = 0.03) as well as for the immature abGC population (D-statistic = 0.32, p-value = 0.008). However, for the dbGC population we do not observe statistical significant differences in activity levels between network B and network D.

Networks A-E	GCs	dbGCs	Mature abGCs	Immature abGCs
D-statistic	0.24	0.24	---	---
p-value	0.09	0.09	---	---

Table 34: Derived statistics after Kolmogorov-Smirnov test examining the activity levels between control network A and network E. We examine the statistics of KS test for the total GC population, as well as for the dbGC population which in this case is the same as the total GC population.

Testing the difference in activity levels of GC population (here the same as dbGCs) between control network A and network E where adult neurogenesis is absent, we do not notice remarkable difference that could be characterized as statistically significant.

Network B-Network E	GCs	dbGCs	Mature abGCs	Immature abGCs
D-statistic	0.52	0.52	---	---
p-value	1.23×10^{-6}	1.23×10^{-6}	---	---

Table 35: Derived statistics after Kolmogorov-Smirnov test examining the activity levels between control network B and network E. We examine the statistics of KS test for the total GC population, as well as for the dbGC population which in this case is the same as the total GC population.

Nevertheless, for the activity levels between control network B (10% abGCs) and network E, we pinpoint statistical significant difference for the total GC population (in this case the same as dbGCs) as it is clear from the derived statistics (D-statistic = 0.52 ,p-value = 1.23×10^{-23}).

Networks A-F	GCs	dbGCs	Mature abGCs	Immature abGCs
D-statistic	0.98	0.98	0.94	0.98
p-value	1.75×10^{-22}	1.75×10^{-22}	1.01×10^{-20}	1.75×10^{-22}

Table 36: Derived statistics after Kolmogorov-Smirnov test examining the activity levels between control network A and network F. We examine the statistics of KS test for the total GC population, as well as for the dbGC population which in this case is the same as the total GC population.

From the KS-test we deduce that the difference in activity levels of all GC populations between control network A and network F are statistically significant. Thus, the absence of abGC-BC synapses has got a serious impact in activity levels of all GC populations as well as in the total GC population.

Networks B-F	GCs	dbGCs	Mature abGCs	Immature abGCs
D-statistic	0.98	0.98	0.98	0.98
p-value	1.75×10^{-22}	1.75×10^{-22}	1.75×10^{-22}	1.75×10^{-22}

Table 37: Derived statistics after Kolmogorov-Smirnov test examining the activity levels between control network B and network F. We examine the statistics of KS test for the total GC population, as well as for the dbGC population which in this case is the same as the total GC population.

Using network B as control network, we came up with the same conclusions, that activity levels of all GCs populations between control network B and network F are statistically significant.

Networks A-G	GCs	dbGCs	Mature abGCs	Immature abGCs
D-statistic	0.28	0.44	0.16	0.21
p-value	0.03	7.15×10^{-5}	0.50	0.15

Table 38: Derived statistics after Kolmogorov-Smirnov test examining the activity levels between control network A and network G. We examine the statistics of KS test for the total GC population, as well as for the dbGC population which in this case is the same as the total GC population.

The absence of abGC-MC synapses does not seem to affect the activity levels of mature and immature abGCs in a statistically significant way, as the comparison of activity levels between control network A and network G proves. Nevertheless, the activity levels of GCs in total (D-statistic = 0.28, p-value = 0.03) as well as of dbGCs (D-statistic = 0.44, p-value = 7.15×10^{-5}) are affected in a statistically significant way.

Networks B-G	GCs	dbGCs	Mature abGCs	Immature abGCS
D-statistic	0.21	0.21	0.08	0.30
p-value	0.15	0.15	0.99	0.01

Table 39: Derived statistics after Kolmogorov-Smirnov test examining the activity levels between control network B and network G. We examine the statistics of KS test for the total GC population, as well as for the dbGC population which in this case is the same as the total GC population.

Using as control network for our simulations the network B, is remarkable that only the activity levels of immature abGCs are statistically significant different compared with network B with network G (D-statistic = 0.30, p-value = 0.01). All the other GCs populations does not seem to have statistically significant different levels of activity compared with control network B.

3.10 Pattern separation in the DG Network

Having succeeding the validation of intrinsic properties for each neuronal type in the DG network, we tested the ability of the DG network to perform pattern separation, a function that is mainly attributed to the DG. In the interest of testing how the pattern separation activity of the DG network is affected by different compositions in dbGCs-abGCs – while keeping the total GC number the same (2000 GCs in total) - we presented pairs of inputs characterized by various degrees of similarity. The various degrees of similarity were modeled as overlap in the two activated EC populations. As we already mentioned, the ability of pattern separation is attributed to DG network each time that the population distance metric f_1 is substantially larger in the DG output (GC activity) compared to its input (EC cell activity). Pattern separation is estimated considering the differences in the populations of neurons that encode each input ('population distance f_1'). Thus, each trial was composed of two simulations using two input patterns within each group. The external inputs from EC Layer II cells were simulated as independent Poisson spike trains, with frequency of 40 Hz, coming in line with experimental data (***Hafting et al., 2005***). In the following table are represented the corresponding Hamming Distance (HD) and the calculated f_1 score for the different cases of external inputs from EC in the DG network.

Overlap (%)	Hamming Distance (HD)	f_1 score
90	8	0.1
80	16	0.2
70	24	0.3
60	32	0.4

Table 40: Hamming distance and f_1 score for the different cases of the pairs of external EC incoming inputs to the DG network.

With the histograms below we attempt to get insights about the activity of GC population for outputs that share different degree of similarity with the corresponding inputs from the EC Layer II.

The experimental protocol that we applied, included the presentation of control inputs to the DG Network (400 EC Layer II inputs with 10% input density) as well as a second input with a degree of similarity (60%, 70%, 80% or 90%) with the control inputs and with the same input density (40 active neurons). After running an adequate number of simulations in the DG network for each case, we derived some outputs. In order to conclude that the network performs pattern separation, it needs to be valid the following relationship:

$$\mathbf{f_{1(input)} < f_{1(output)}}$$

For all network compositions and for each case (60,70,80 or 90% overlap of incoming inputs from EC Layer II) the above relationship was valid as we can easily observe from the below diagrams.

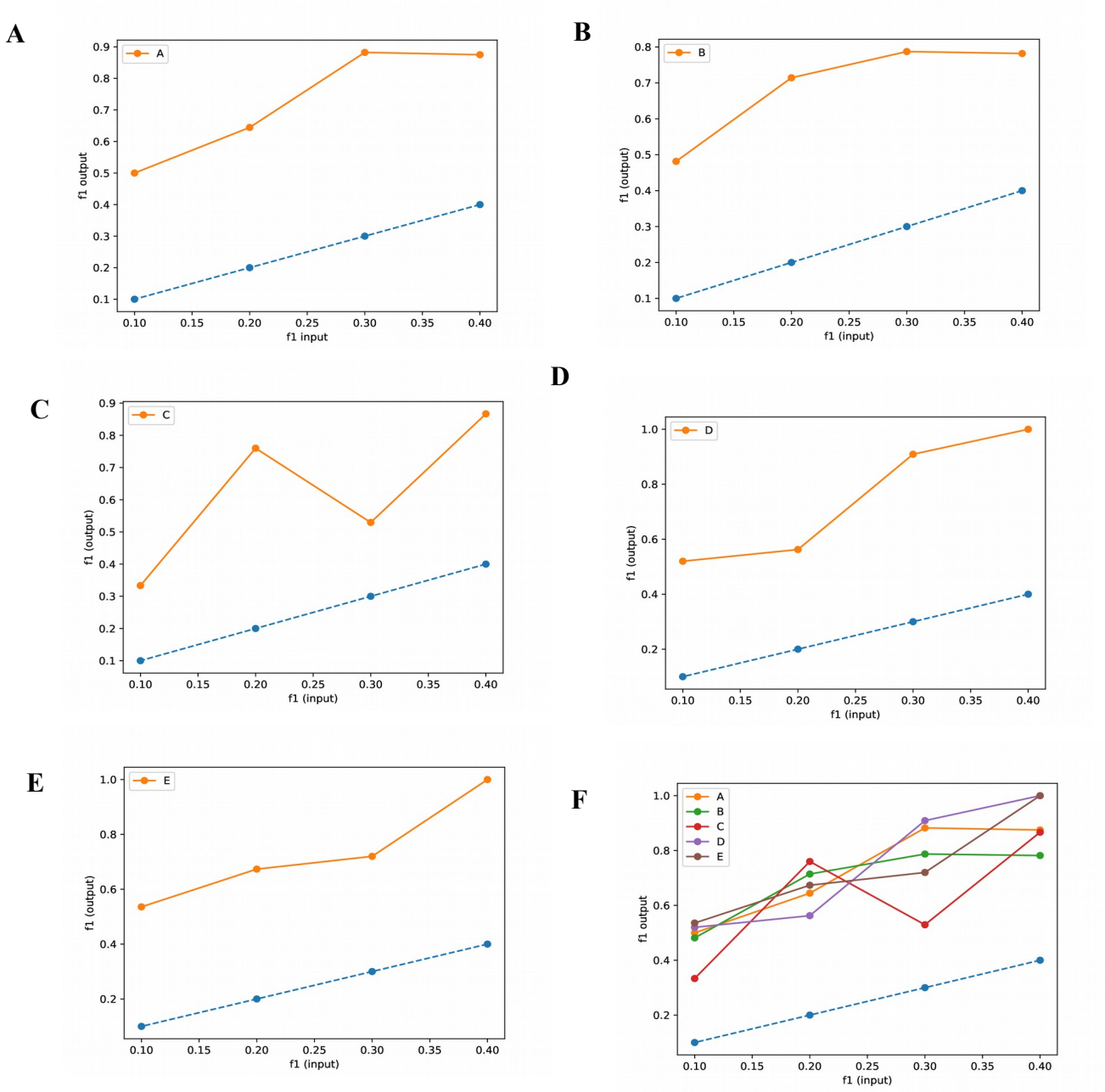

Figure 57: Input/output population distances (f_1) for different DG network compositions (Experiment 1). A) Input/output population distances (f_1) for the control network A (orange) estimated using input patterns with increased similarity. Control Network A performs pattern separation efficiency for all input patterns tested. B) Input/output population distances (f_1) for the control network B (orange) estimated using input patterns with increased similarity. Control Network B performs pattern separation efficiency for all input patterns tested. C) Input/output population distances (f_1) for network C with 700 dbGCs, 700 mature abGCs, 700 immature abGCs (orange) estimated using input patterns with increased similarity. Control Network C performs pattern separation efficiency for all input patterns tested. D) Input/output population distances (f_1) for network D with 1000 dbGCs, 500 mature abGCs and 500 immature abGCs (orange) estimated using input patterns with increased similarity. Control Network D performs pattern separation efficiency for all input patterns tested. E) Input/output population distances (f_1) for network E with 2000 dbGCs (orange) estimated using input patterns with increased similarity. Control Network E performs pattern separation efficiency for all input patterns tested. *For all diagrams the dashed line denotes the limit above which the model performs pattern separation.

In the table that is posed below, are summarized the mean and standard deviation for the f_1 scores that are derived about the output patterns of DG network after performing an adequate amount of simulations for each case (60, 70, 80 or 90% overlap of input patterns).

Network Inputs				
f_1 input	0.40	0.30	0.20	0.10
Network Outputs				
f_1 output (A)	0.80 ± 0.06	0.73 ± 0.04	0.67 ± 0.08	0.50 ± 0.06
f_1 output (B)	0.71 ± 0.05	0.67 ± 0.06	0.57 ±0.06	0.50 ± 0.06
f_1 output (C)	0.67 ±0.04	0.63 ± 0.04	0.65 ± 0.05	0.53 ± 0.05
f_1 output (D)	0.72 ± 0.06	0.63 ± 0.06	0.60 ± 0.04	0.58 ± 0.05
f_1 output (E)	0.78 ± 0.07	0.77 ± 0.06	0.65 ± 0.10	0.55 ± 0.10
f_1 output (F)	0.45± 0.04	0.39 ± 0.07	0.37 ± 0.03	0.28 ± 0.05
f_1 output (G)	0.54 ± 0.04	0.49 ± 0.04	0.39 ± 0.04	0.27 ± 0.04

Table 41: Mean and standard deviation of f1 scores for output patterns (Experiment 1). The derived statistics are about each network and for each case with 60,70,80 or 90% overlap of incoming inputs from EC Layer II.

As we can observe from the above table, for all network compositions, as the overlap in EC Layer II inputs are augmented, the f_1 score for output patterns is decreased. On the one hand, the f_1 score for output patterns is greater than the f_1 score for the input patterns, thus the pattern separation function is performed by the DG network independently from its composition in dbGCs and abGCs. Nevertheless, as the task of pattern separation becomes more demanding with higher degree of similarity for EC Layer II incoming inputs, the f_1 score decreases. However, it remains higher than the corresponding f_1 score of input patterns, which means that the pattern separation function does not seem to be disturbed.

Networks A and B are considered as control networks (1900 dbGCs – 50 mature abGCs – 50 immature abGCs for Network A and 1800 dbGCs – 100 mature abGCs – 100 immature abGCs for Network B respectively). Investigating if the ratio of dbGCs to abGCs has an impact in pattern separation function, we implemented the statistic test Kolmogorov-Smirnov (KS) having as our target to find out if the differences of f_1 scores for output patterns are statistically significant between control networks and networks with the other compositions.

In the following tables we present the derived statistics which are the D statistic and the p-value after the implementation of KS test. In the KS test, the D-statistic is the absolute maximum distance (supremum) between the cumulative distribution functions of the two samples, where the two samples in our case are:

- Network A (Control) outputs f_1 scores – Network C outputs f_1 scores
- Network B (Control) outputs f_1 scores – Network C outputs f_1 scores
- Network A (Control) outputs f_1 scores – Network D outputs f_1 scores
- Network B (Control) outputs f_1 scores – Network D outputs f_1 scores
- Network A (Control) outputs f_1 scores – Network E outputs f_1 scores
- Network B (Control) outputs f_1 scores – Network E outputs f_1 scores
- Network A (Control) outputs f_1 scores – Network F outputs f_1 scores
- Network B (Control) outputs f_1 scores – Network G outputs f_1 scores

Networks A–C f_I input	0.40	0.30	0.20	0.10
D-statistic	0.30	0.30	0.30	0.39
p-value	0.67	0.67	0.67	0.31

Table 42: D-statistic and p-value after the implementation of Kolmogorov-Smirnov test examining the f_I scores of output patterns between network A and network C (Experiment 1). The derived statistics are for each case of 60,70,80 or 90% overlap of incoming inputs from EC Layer II.

We do not observe statistically significant differences in f_I scores of output patterns between control network A and network C.

Networks B–C f_I input	0.40	0.30	0.20	0.10
D-statistic	0.20	0.40	0.40	0.50
p-value	0.97	0.31	0.31	0.11

Table 43: D-statistic and p-value after the implementation of Kolmogorov-Smirnov test examining the f_I scores of output patterns between network B and network C (Experiment 1). The derived statistics are for each case of 60,70,80 or 90% overlap of incoming inputs from EC Layer II.

We do not observe statistically significant differences in f_I scores of output patterns between control network B and network C.

Networks A–D f_I input	0.40	0.30	0.20	0.10
D-statistic	0.30	0.20	0.30	0.49
p-value	0.67	0.97	0.67	0.11

Table 44: D-statistic and p-value after the implementation of Kolmogorov-Smirnov test examining the f_I scores of output patterns between network A and network D (Experiment 1). The derived statistics are for each case of 60,70,80 or 90% overlap of incoming inputs from EC Layer II.

We do not observe statistically significant differences in f_I scores of output patterns between control network A and network D.

Networks B-D f_I input	0.40	0.30	0.20	0.10
D-statistic	0.30	0.50	0.30	0.50
p-value	0.67	0.11	0.67	0.11

Table 45: D-statistic and p-value after the implementation of Kolmogorov-Smirnov test examining the f_I scores of output patterns between network B and network D (Experiment 1). The derived statistics are for each case of 60,70,80 or 90% overlap of incoming inputs from EC Layer II.

We do not observe statistically significant differences in f_I scores of output patterns between control network B and network D.

Networks A-E f_I input	0.40	0.30	0.20	0.10
D-statistic	0.30	0.49	0.29	0.30
p-value	0.67	0.11	0.67	0.67

Table 46: D-statistic and p-value after the implementation of Kolmogorov-Smirnov test examining the f_I scores of output patterns between network A and network E (Experiment 1). The derived statistics are for each case of 60,70,80 or 90% overlap of incoming inputs from EC Layer II.

We do not observe statistically significant differences in f_1 scores of output patterns between control network A and network E.

Networks B-E f_1 input	0.40	0.30	0.20	0.10
D-statistic	0.30	0.19	0.50	0.39
p-value	0.67	0.97	0.11	0.31

Table 47: D-statistic and p-value after the implementation of Kolmogorov-Smirnov test examining the f_1 scores of output patterns between network B and network E (Experiment 1). The derived statistics are for each case of 60,70,80 or 90% overlap of incoming inputs from EC Layer II.

We do not observe statistically significant differences in f_1 scores of output patterns between control network B and network E.

Networks A-F f_1 input	0.40	0.30	0.20	0.10
D-statistic	0.80	0.80	0.80	0.80
p-value	1.40×10^{-5}	1.40×10^{-5}	1.40×10^{-5}	1.40×10^{-5}

Table 48: D-statistic and p-value after the implementation of Kolmogorov-Smirnov test examining the f_1 scores of output patterns between network A and network F (Experiment 1). The derived statistics are for each case of 60,70,80 or 90% overlap of incoming inputs from EC Layer II.

We observe statistically significant differences in f_1 scores of output patterns between control network A and network F (p-value = 1.40×10^{-5}).

Networks B-F f_1 input	0.40	0.30	0.20	0.10
D-statistic	0.80	0.80	0.80	0.80
p-value	1.40×10^{-5}	1.40×10^{-5}	1.40×10^{-5}	1.40×10^{-5}

Table 49: D-statistic and p-value after the implementation of Kolmogorov-Smirnov test examining the f_1 scores of output patterns between network B and network F (Experiment 1). The derived statistics are for each case of 60,70,80 or 90% overlap of incoming inputs from EC Layer II.

We observe statistically significant differences in f_1 scores of output patterns between control network B and network F (p-value = 1.40×10^{-5}).

Networks A-G f_1 input	0.40	0.30	0.20	0.10
D-statistic	0.80	0.80	0.80	0.80
p-value	1.40×10^{-5}	1.40×10^{-5}	1.40×10^{-5}	1.40×10^{-5}

Table 50: D-statistic and p-value after the implementation of Kolmogorov-Smirnov test examining the f_1 scores of output patterns between network A and network G (Experiment 1). The derived statistics are for each case of 60,70,80 or 90% overlap of incoming inputs from EC Layer II.

We observe statistically significant differences in f_1 scores of output patterns between control network A and network G (p-value = 1.40×10^{-5}).

Networks B-G f_1 input	0.40	0.30	0.20	0.10
D-statistic	0.80	0.80	0.80	0.80
p-value	1.40×10^{-5}	1.40×10^{-5}	1.40×10^{-5}	1.40×10^{-5}

Table 51: D-statistic and p-value after the implementation of Kolmogorov-Smirnov test examining the f_1 scores of output patterns between network B and network G (Experiment 1). The derived statistics are for each case of 60,70,80 or 90% overlap of incoming inputs from EC Layer II.

We observe statistically significant differences in f_1 scores of output patterns between control network B and network G (p-value = 1.40×10^{-5}).

In a second and third round of simulations, we created with randomization a different DG network connectivity, and we repeated the same experiment as before, implementing simulations of 10 trials for each case (60,70,80 or 90% overlap in incoming inputs of EC Layer II) and for each network. These additional experiments serve our need to validate our results which in experimental conditions is like using more animals (mice, rats) in order to collect measurements from different animals. Again, for all network compositions and for each case (60,70,80 or 90% overlap) the relationship $f_{1(input)} < f_{1(output)}$ was valid as we can easily observe from the below diagrams. The blue dashed line sets the limit above which DG networks perform pattern separation and we can easily find out that all modeled networks are able to discriminate similar incoming inputs into distinct outputs (memory representations).

A

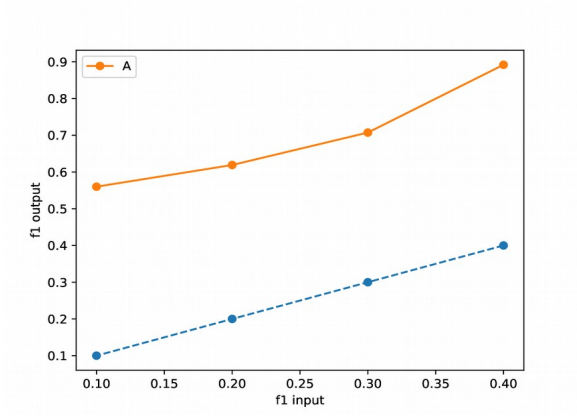

B

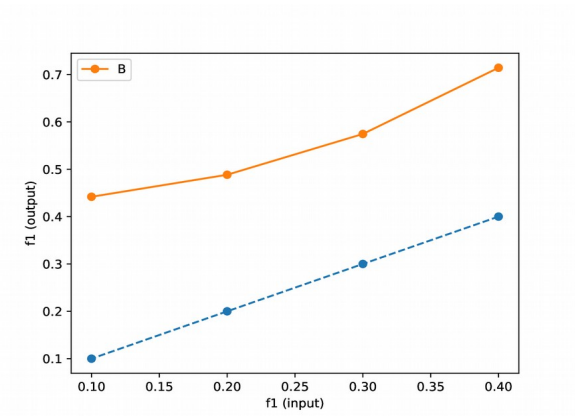

C

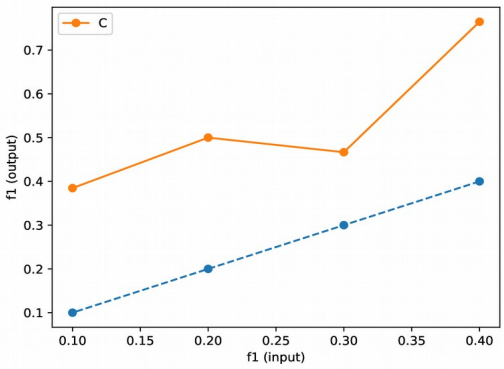

D

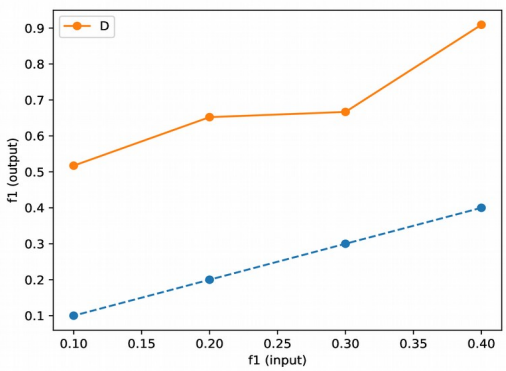

E

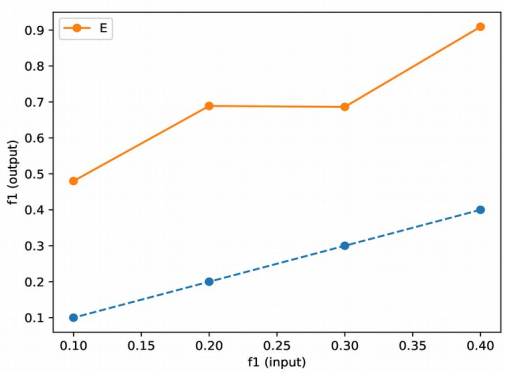

F

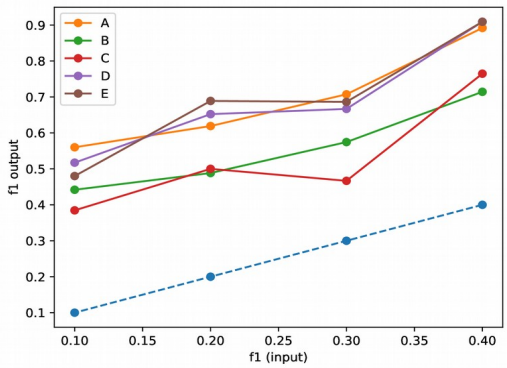

Figure 58: Input/output population distances (f_1) for different DG network compositions. A) Input/output population distances (f_1) for the control network A (orange) estimated using input patterns with increasing similarity. Control Network A performs pattern separation efficiency for all input patterns tested. B) Input/output population distances (f_1) for the control network B (orange) estimated using input patterns with increasing similarity. Control Network B performs pattern separation efficiency for all input patterns tested. C) Input/output population distances (f_1) for network C with 700 dbGCs, 700 mature abGCs, 700 immature abGCs (orange) estimated using input patterns with increasing similarity. Control Network C performs pattern separation efficiency for all input patterns tested. D) Input/output population distances (f_1) for network D with 1000 dbGCs, 500 mature abGCs and 500 immature abGCs (orange) estimated using input patterns with increasing similarity. Control Network D performs pattern separation efficiency for all input patterns tested. E) Input/output population distances (f_1) for network E with 2000 dbGCs (orange) estimated using input patterns with increasing similarity. Control Network E performs pattern separation efficiency for all input patterns tested. *For all diagrams the dashed line denotes the limit above which the model performs pattern separation.

In the plots below, we compare the pattern separation efficiency for networks C,D,E,F and G in comparison with the control network B. The dashed blue line represents the limit above which our model performs successfully pattern separation.

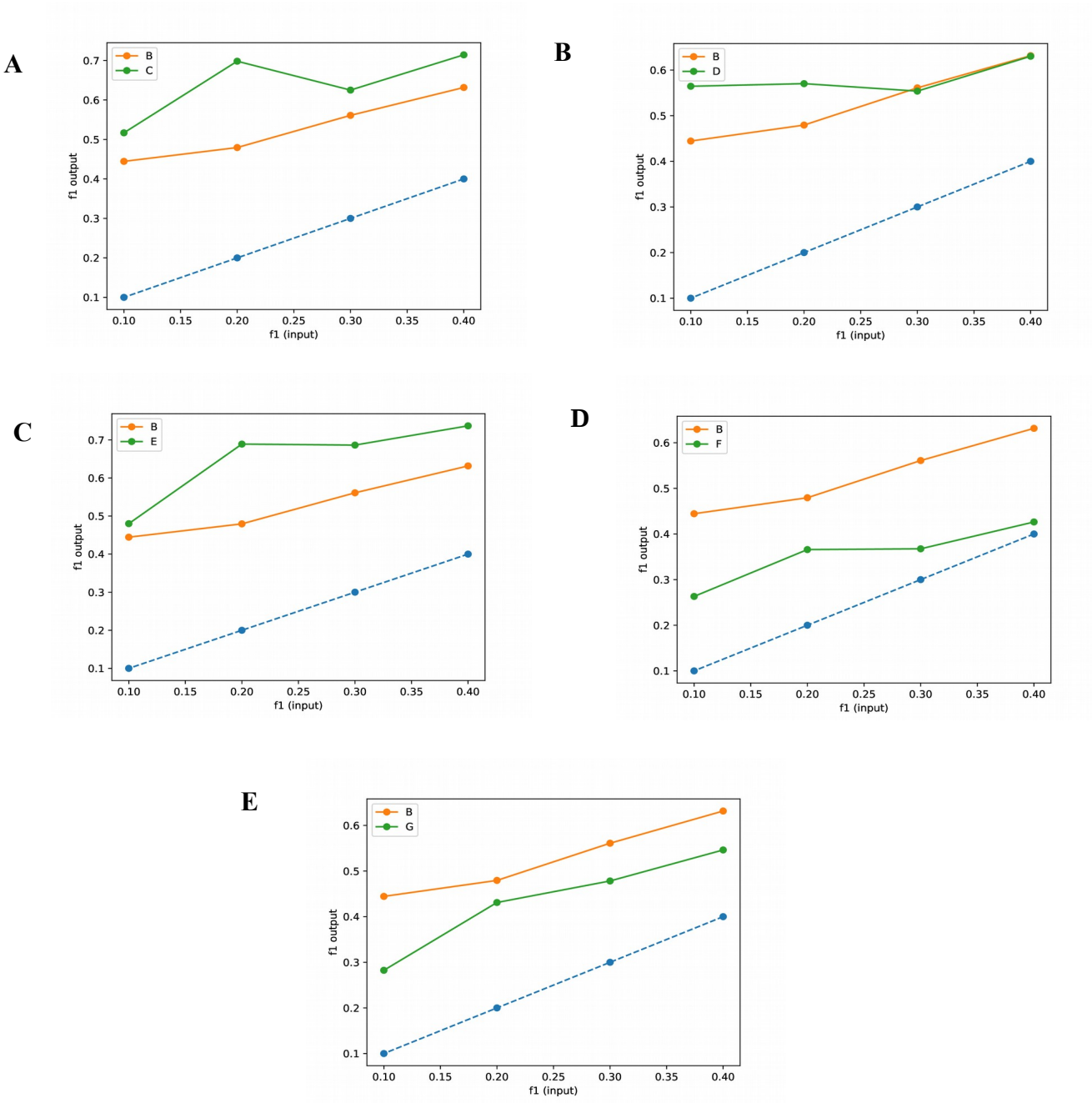

Figure 59: Input/output population distances (f_1) comparing control network B with different DG network compositions. A) Input/output population distances (f_1) for the control network B (orange) and C (green) estimated using input patterns with increasing similarity. B) Input/output population distances (f_1) for the control network B (orange) and D (green) estimated using input patterns with increasing similarity. C) Input/output population distances (f_1) for the control network B (orange) and E (green) estimated using input patterns with increasing similarity. D) Input/output population distances (f_1) for control network B (orange) and network F (green) estimated using input patterns with increasing similarity. Control Network D performs pattern separation efficiency for all input patterns tested. E) Input/output population distances (f_1) for the control network B (orange) and network G (green) estimated using input patterns with increasing similarity.*For all diagrams the dashed line denotes the limit above which the model performs pattern separation.

The main conclusion from all the previous plots is that network C, D and E succeed in pattern separation tasks better compared with the control network B. Nevertheless, we cannot contend the same for networks F and G where pattern separation ability in present but not in the same efficiency as in the control network B. Furthermore, the patterns that shared a low degree of similarity were better discriminated from networks C and D, while for inputs that shared a higher degree of similarity, the pattern separation efficiency dropped in comparable levels with control network B. However, the network E with the absence of adult neurogenesis, managed to perform better than control network B for all the cases.

4. DISCUSSION

4.1 The DG model and its target

The main target of this study was to unravel how the presence of mature and immature abGCs in the DG network affect DG network's ability to perform pattern separation. Moreover, the presence of dendritic compartments for these abGCs was taken into consideration, so we built up multicompartmental GCs with morphological features based loosely on anatomical data. In order to investigate the previous inquiries, we introduced a new computational model for DG which was inspired from a previous work of our laboratory (***Chavlis et al., 2017***). The computational model was comprised of the major excitatory neuronal population of GCs at three different developmental stages (dbGCs - > 8-weeks old, mature abGCs ~ 6-weeks old and immature abGCs ~4-weeks old). Furthermore, in the DG network was also incorporated other neuronal populations, such as the excitatory population of MCs, as well as the inhibitory interneurons BCs that target the perisomatic region of db and ab GCs as well as the HIPP interneurons that target the distal dendritic compartments of db and ab GCs. The GCs, both db and ab, were modeled as two stage integrators via the addition of dendritic branches whose properties were loosely constrained by electrophysiological and anatomical data. For the somatic compartment of GCs was used the AdEx model. For the dendritic compartments was used the simple I&F model without spike mechanism due to the experimental findings for absence of dendritic spikes in GCs. For the modeling of the rest of neuronal types in the DG network was used the AdEx model. This model could be considered as a hybrid model that stands between a simplified point neuron model (***Myers and Scharfman, 2009***) and a more detailed biophysical model (***Santhakumar et al., 2005***) for the DG network. With the model that we constructed, we were able to examine a set of different factors that may affect network's ability to perform pattern separation. We included the dendritic compartments only in the GCs (dbGCs and abGCs) in order to focus our attention in the dendritic contribution of these neuronal types, while keeping at low levels the total network complexity.

4.2 Predictions of the model

4.2.1 Insights from the activity levels

The creation of this particular DG network, gave us the opportunity to perform a number of different network simulations in which, each time -while keeping the total GC population stable (2000 GCs)- we adjusted the percentage of abGCs in the network, pursuing to find out how the ratio of db to ab GCs in the DG network may affect its ability to perform pattern separation. Moreover, we took into consideration the activity and sparsity levels of different GC populations as were indicated in the previous histograms and bar-plots (*see section Results*).

It is known that inhibition controls the activity levels of the DG network by increasing sparsity (***Jung and McNaughton 1993***) which in turn means amelioration of the pattern separation function for the DG network (***Aimone et al., 2011***). Indeed, in our network, we provided inhibition in two ways: with the inhibitory INs BCs (targeting perisomatic region of GCs) and HIPP cells (targeting

distal dendritic compartments of GCs) as well as with the MCs. At this time point we should note that the inhibition in the DG network through the MC circuitry is indirect, because the MC net effect at GCs is inhibitory according to the "dormant basket cell" hypothesis (***Jinde et al., 2012, 2013***).

During our network simulations, for the case of network F with 1800 dbGCs, 100 mature abGCs and 100 immature abGCs without synapses between abGCs and BCs, we found out that the loss of BC-abGC synapses had as a result the augmentation of the mean activity of the GC population in the DG network (mean±std: 3.10±0.55) in comparison with the control networks A,B (1.38±0.41 and 1.57±0.38 respectively). Moreover, the loss of BC-abGC synapses lead to a major increase in the activity levels of immature abGCs (68.0 ± 12.78) in comparison with control networks A,B (8.4 ± 4.03 and 8.74 ± 3.18 respectively). The same observed over-excitation is true for the mature abGC population, where the activity levels are extremely high (16.52±5.98) in comparison with control networks A,B (2.76±2.29 and 2.34±1.40 respectively). Interestingly, the difference in activity levels between control network A (or B) and network F is statistically significant different as the KS-test statistics revealed.

For the case of network G, with 1800 dbGCs, 100 mature abGCs and 100 immature abGCs without synapses between between abGCs and MCs, it was revealed that the loss of MC-abGC synapses does not seem to alter in a important way the activity levels in comparison with control networks A and B. After performing the KS-test, the comparison of activity levels between control network A and network G was characterized as statistically significant for the GC population in total (D-statistic = 0.28 , p-value = 0.03) as well as for the dbGC population (D-statistic = 0.44, p-value = 7.15×10^{-5}). When we utilize as control the network B, the difference in activity levels between control network B and network G was statistically significant only for the immature abGC population (D-statistic = 0.30, p-value = 0.01). Moreover, the absence of abGC-MC synapses does not lead to an over-excitation of the abGC population.

Another pattern that we observe as far as the activity levels are concerned, is the fact that as we augment the percentage of abGCs in the DG network while keeping the total number of DG population stable (2000 GCs), we observe an augmentation in the activity levels of the total GC population. Indeed, in Network C (33% dbGCs – 66% abGCs), where we have got the highest percentage of abGCs in the DG network, we have the highest activity level for GC population in total (3.39±0.67) and follows the Network D (50% dbGCs-50% abGCs) with the second higher activity level for the GC population in total (2.97±0.61). The lowest activity level of GC population is present in the Network E (2000 dbGCs) where adult neurogenesis is absent (1.19±0.34). Interestingly, the KS-test proves that the difference in activity levels of mature and immature abGCs was statistically significant augmented for networks C and D in comparison with the respective activity levels in control networks A or B.

Our model, shows that as we augment the presence of abGCs in the DG network, the activity levels of the GC population is augmented too, while the implementation of KS statistical analysis highlights the statistical significance of the previous ascertainment. This observation is true due to the higher intrinsic excitability of abGC population that seems to contribute in the total GC population as our simulations prove.

4.2.2 Insights from pattern separation efficiency

Having articulated the definition of pattern separation and having defined the formula about the calculation of the population-distance metric f_1 score, we managed to test the pattern separation efficiency of the DG network. In order to accomplish this, we constructed pair of inputs from the EC Layer II. These pairs of inputs shared a degree of similarity. More specifically, the one input has got input density 10% (400 EC inputs → 40 EC inputs active), while the second input was constructed with the exact same way and the same input density, sharing 60%, 70%, 80% or 90% similarity with the previous input.

Interestingly, we observe that the DG network is able to perform pattern separation while its composition in GCs may be adjusted. This conclusion could be derived by the diagrams of f_1 scores for inputs and outputs where we highlight the relationship $f_{1(input)} < f_{1(output)}$ which is valid for cases in which pattern separation happens.

The results that we collected after performing the aforementioned simulations showed us that for easier tasks of pattern separation (60%, 70% similarity between inputs with $f_{1(input)}$ scores 0.4 and 0.3 respectively), the presence of more abGCs in the DG network does not seem to augments network's capacity to perform pattern separation. While elevating the difficulty of the pattern separation task, (80%, 90% similarity between incoming input patterns from EC Layer II with $f_{1(input)}$ scores 0.2 and 0.1 respectively), we pinpoint that the $f_{1(output)}$ scores are decreased compared with the $f_{1(output)}$ scores for the cases where the inputs patterns to EC Layer II share a smaller degree of similarity.

To put it concisely, we infer that the presence of abGCs does not seem to have a major impact in pattern separation task. For the cases of more complex tasks, like the introduction of inputs patterns from EC Layer II that share a high degree of similarity (80%, 90%) into the DG network, does not seem to contribute significant in the pattern separation function of the DG network. This finding comes in accordance with a previous computational model of our laboratory (***Chavlis et al., 2017***) which supports that the number of GC dendrites correlates positively with pattern separation efficiency due to the higher sparsity levels provided by having multiple dendrites. In this model, higher sparsity arises from the requirement of having at least two dendrites simultaneously active in order to fire a GC model neuron. As a result, abGCs with shorter or fewer dendrites do not contribute to sparsity – and consequently to pattern separation-as much as the dbGC population.

Performing comparisons for pattern separation efficiency between control network B and networks C,D,E,F or G, we deduce that network C, D and E perform more efficiently pattern separation in comparison with control network B. Interestingly, the networks C and D with 66% and 50% abGCs respectively, manage to accomplish the pattern separation task in a more efficient way for more easily tasks ($f_{1(input)}$ = 0.4, 0.3) compared with control network B. For more challenging tasks ($f_{1(input)}$ = 0.2, 0.1), the pattern separation efficiency for networks C, D remains but drops in levels comparable with control network B.

For the extreme case where adult neurogenesis is absent, we deduce that network E performs better the pattern separation tasks for all cases if we make the comparison with control network B. This conclusion is true not only for the easy tasks, but also for the more difficult trials, where incoming inputs had a greater degree of similarity.

Notably, for the case of network F, where the inhibitory synapses between abGCs and BCs where absent, the pattern separation ability remains, however it is visibly better performed by the control

network B. Hence, we can contend that the absence of abGC-BC synapses affect negatively but do not abolish pattern separation efficiency of this DG network.
After establishing the control networks A,B ability to perform pattern separation, we tested its validity against experimental data taking into consideration the role of inhibition in this phenomenon. The control DG network models A,B reproduced successfully the experimental findings (***Engin et al., 2015***) whereby inhibition exerted by BCs was critical for the sparse firing of GCs. Interestingly, the removal of abGC-BC synapses resulted in an over-excitation of the GC and especially abGC population, which impaired the pattern separation ability of network F. These findings also come in line with the previously referred experimental conclusions that pinpoint increased memory interference under conditions of reduced BC activity (***Engin et al., 2015***).
What is more, the MCs are thought to control the excitability of GCs in the DG network (***Jinde et al., 2013***), so we constructed also the network G in which we abolished the synapses between abGC and MCs. This handling resulted in a deterioration of the DG network to perform pattern separation in comparison with control network B. However, we did not observe an over-excitation in GC activity, something that is consistent with experimental data (***Ratzliff et al,, 2004***).

To put it more concisely, the simulations tend to articulate that the elevated presence of abGCs in network C,D aids the pattern separation function for easier tasks but does not seem to affect it better than the control network B for more challenging cases. The extreme case of network E without adult neurogenesis seems to ameliorate pattern separation compared with control network B for all tasks; for easier to more difficult. Last but not least, the absence of BCs or MCs synapses with abGC population lead to DG networks that perform pattern separation but not better than control network B, highlighting the importance of inhibition in the proper function of discrimination of similar incoming inputs into less similar outputs.

5. BIBLIOGRAPHY

Abrous, D. N., Koehl, M., & Le Moal, M. (2005). Adult neurogenesis: From precursors to network and physiology. *Physiological Reviews*, *85*(2), 523–569. https://doi.org/10.1152/physrev.00055.2003

Adlaf, E. W., Vaden, R. J., Niver, A. J., Manuel, A. F., Onyilo, V. C., Araujo, M. T., … Overstreet-Wadiche, L. (2017). Adult-born neurons modify excitatory synaptic transmission to existing neurons. *ELife*, *6*, 1–25. https://doi.org/10.7554/eLife.19886

Aimone, J. B., Deng, W., & Gage, F. H. (2010). Adult neurogenesis: Integrating theories and separating functions. *Trends in Cognitive Sciences*, *14*(7), 325–337. https://doi.org/10.1016/j.tics.2010.04.003

Aimone, J. B., Deng, W., & Gage, F. H. (2011a). Resolving New Memories: A Critical Look at the Dentate Gyrus, Adult Neurogenesis, and Pattern Separation. *Neuron*, *70*(4), 589–596. https://doi.org/10.1016/j.neuron.2011.05.010

Aimone, J. B., Deng, W., & Gage, F. H. (2011b). Resolving New Memories: A Critical Look at the Dentate Gyrus, Adult Neurogenesis, and Pattern Separation. *Neuron*, *70*(4), 589–596. https://doi.org/10.1016/j.neuron.2011.05.010

Aimone, J. B., Wiles, J., & Gage, F. H. (2006). Potential role for adult neurogenesis in the encoding of time in new memories. *Nature Neuroscience*, *9*(6), 723–727. https://doi.org/10.1038/nn1707

Aimone, J. B., Wiles, J., & Gage, F. H. (2009). Computational Influence of Adult Neurogenesis on Memory Encoding. *Neuron*, *61*(2), 187–202. https://doi.org/10.1016/j.neuron.2008.11.026

Altman, J., & Bayer, S. A. (1990). Migration and distribution of two populations of hippocampal granule cell precursors during the perinatal and postnatal periods. *Journal of Comparative Neurology*, *301*(3), 365–381. https://doi.org/10.1002/cne.903010304

Amaral, D. G. (1978). A golgi study of cell types in the hilar region of the hippocampus in the rat. *Journal of Comparative Neurology*, *182*(5), 851–914. https://doi.org/10.1002/cne.901820508

Amaral, D. G., Ishizuka, N., & Claiborne, B. (1990). Chapter Neurons, numbers and the hippocampal network. *Progress in Brain Research*, *83*(C), 1–11. https://doi.org/10.1016/S0079-6123(08)61237-6

Amaral, D. G., Scharfman, H. E., & Lavenex, P. (2007). The dentate gyrus: fundamental neuroanatomical organization (dentate gyrus for dummies). *Progress in Brain Research*, *163*. https://doi.org/10.1016/S0079-6123(07)63001-5

Ambrogini, P., Lattanzi, D., Ciuffoli, S., Agostini, D., Bertini, L., Stocchi, V., … Cuppini, R. (2004). Morpho-functional characterization of neuronal cells at different stages of maturation in granule cell layer of adult rat dentate gyrus. *Brain Research*, *1017*(1–2), 21–31. https://doi.org/10.1016/j.brainres.2004.05.039

Anacker, C., & Hen, R. (2017). Adult hippocampal neurogenesis and cognitive flexibility-linking memory and mood. *Nature Reviews Neuroscience*, *18*(6), 335–346. https://doi.org/10.1038/nrn.2017.45

Anacker, C., Luna, V. M., Stevens, G. S., Millette, A., Shores, R., Jimenez, J. C., … Hen, R. (2018). Hippocampal neurogenesis confers stress resilience by inhibiting the ventral dentate gyrus. *Nature*, *559*(7712), 98–102. https://doi.org/10.1038/s41586-018-0262-4

Andersen, P., Bliss, T. V. P., & Skrede, K. K. (1971). Lamellar organization of hippocampal excitatory pathways. *Experimental Brain Research*, *13*(2), 222–238. https://doi.org/10.1007/BF00234087

Anderson, M. L., Sisti, H. M., Curlik, D. M., & Shors, T. J. (2011). Associative learning increases adult neurogenesis during a critical period. *European Journal of Neuroscience*, *33*(1), 175–181. https://doi.org/10.1111/j.1460-9568.2010.07486.x

Apple, D. M., Solano-Fonseca, R., & Kokovay, E. (2017). Neurogenesis in the aging brain. *Biochemical Pharmacology*, *141*(4), 77–85. https://doi.org/10.1016/j.bcp.2017.06.116

Appleby, P. A., Kempermann, G., & Wiskott, L. (2011). The role of additive neurogenesis and synaptic plasticity in a hippocampal memory model with grid-cell like input. *PLoS Computational Biology*, *7*(1). https://doi.org/10.1371/journal.pcbi.1001063

Appleby, P. A., & Wiskott, L. (2009). Additive neurogenesis as a strategy for avoiding interference in a sparsely-coding dentate gyrus. *Network: Computation in Neural Systems*, *20*(3), 137–161. https://doi.org/10.1080/09548980902993156

Aradi, I., & Holmes, W. R. (1999). Active dendrites regulate spatio-temporal synaptic integration in hippocampal dentate granule cells. *Neurocomputing*, *26–27*, 45–51. https://doi.org/10.1016/S0925-2312(99)00087-9

Bakker, A., Kirwan, C. B., Miller, M., & Stark, C. E. L. (2008). Pattern separation in the human hippocampal CA3 and dentate gyrus. *Science*, *319*(5870), 1640–1642. https://doi.org/10.1126/science.1152882

Barnea, A., & Nottebohm, F. (1994). Seasonal recruitment of hippocampal neurons in adult free-ranging black- capped chickadees. *Proceedings of the National Academy of Sciences of the United States of America*, *91*(23), 11217–11221. https://doi.org/10.1073/pnas.91.23.11217

Bartos, M., Vida, I., Frotscher, M., Geiger, J. R., & Jonas, P. (2001). Rapid signaling at inhibitory synapses in a dentate gyrus interneuron network. *The Journal of Neuroscience : The Official Journal of the Society for Neuroscience*, *21*(8), 2687–2698. https://doi.org/21/8/2687 [pii]

Bartos, M., Vida, I., & Jonas, P. (2007). Synaptic mechanisms of synchronized gamma oscillations in inhibitory interneuron networks. *Nature Reviews Neuroscience*, *8*(1), 45–56. https://doi.org/10.1038/nrn2044

Ben-Ari, Y. (2002). Excitatory actions of GABA during development: The nature of the nurture. *Nature Reviews Neuroscience*, *3*(9), 728–739. https://doi.org/10.1038/nrn920

Bergmann, O., Spalding, K. L., & Frisén, J. (2015a). Adult neurogenesis in humans. *Cold Spring Harbor Perspectives in Medicine*, *5*(8), 1–13. https://doi.org/10.1101/cshperspect.a018994

Bergmann, O., Spalding, K. L., & Frisén, J. (2015b). Adult neurogenesis in humans. *Cold Spring Harbor Perspectives in Medicine*, *5*(7). https://doi.org/10.1101/cshperspect.a018994

Beth, T. (1988). Efficient zero-knowledge identification scheme for smart cards. *Lecture Notes in Computer Science (Including Subseries Lecture Notes in Artificial Intelligence and Lecture Notes in Bioinformatics)*, *330 LNCS*(6), 77–84. https://doi.org/10.1007/3-540-45961-8_7

Biebl, M., Cooper, C. M., Winkler, J., & Kuhn, H. G. (2000). Analysis of neurogenesis and programmed cell death reveals a self- renewing capacity in the adult rat brain. *Neuroscience Letters*, *291*(1), 17–20. https://doi.org/10.1016/S0304-3940(00)01368-9

Bischofberger, J., & Schinder, A. F. (2008). Maturation and Functional Integration of New Granule Cells into the Adult Hippocampus. *Cold Spring Harbor Monograph Archive*, *52*, 299–319. https://doi.org/10.1101/087969784.52.299

Blackstad, J. S., Osen, K. K., Scharfman, H. E., Storm-Mathisen, J., Blackstad, T. W., & Leergaard, T. B. (2016). Observations on hippocampal mossy cells in mink (Neovison vison) with special reference to dendrites ascending to the granular and molecular layers. *Hippocampus*, *26*(2), 229–245. https://doi.org/10.1002/hipo.22518

Bliss, T. V. P., & Collingridge, G. L. (1993). A synaptic model of memory: Long-term potentiation in the hippocampus. *Nature*, *361*(6407), 31–39. https://doi.org/10.1038/361031a0

Boldrini, M., Fulmore, C. A., Tartt, A. N., Simeon, L. R., Pavlova, I., Poposka, V., … Mann, J. J. (2018). Human Hippocampal Neurogenesis Persists throughout Aging. *Cell Stem Cell*, *22*(4), 589-599.e5. https://doi.org/10.1016/j.stem.2018.03.015

Boldrini, M., Santiago, A. N., Hen, R., Dwork, A. J., Rosoklija, G. B., Tamir, H., … John Mann, J. (2013). Hippocampal granule neuron number and dentate gyrus volume in antidepressant-treated and untreated major depression. *Neuropsychopharmacology*, *38*(6), 1068–1077. https://doi.org/10.1038/npp.2013.5

Bostock, E., Muller, R. U., & Kubie, J. L. (1991). Experience□dependent modifications of hippocampal place cell firing. *Hippocampus*, *1*(2), 193–205. https://doi.org/10.1002/hipo.450010207

Braak, H., Thal, D. R., Ghebremedhin, E., & Del Tredici, K. (2011). Stages of the pathologic process in alzheimer disease: Age categories from 1 to 100 years. *Journal of Neuropathology and Experimental Neurology*, *70*(11), 960–969. https://doi.org/10.1097/NEN.0b013e318232a379

Brette, R., & Gerstner, W. (2005). Adaptive exponential integrate-and-fire model as an effective description of neuronal activity. *Journal of Neurophysiology*, *94*(5), 3637–3642. https://doi.org/10.1152/jn.00686.2005

Brette, R., & Goodman, D. F. M. (2011). Vectorized algorithms for spiking neural network simulation. *Neural Computation*, *23*(6), 1503–1535. https://doi.org/10.1162/NECO_a_00123

Bruel-Jungerman, E., Laroche, S., & Rampon, C. (2005). New neurons in the dentate gyrus are involved in the expression of enhanced long-term memory following environmental enrichment. *European Journal of Neuroscience*, *21*(2), 513–521. https://doi.org/10.1111/j.1460-9568.2005.03875.x

Buckmaster, P. S., & Jongen-Rêlo, A. L. (1999). Highly specific neuron loss preserves lateral inhibitory circuits in the dentate gyrus of kainate-induced epileptic rats. *Journal of Neuroscience*, *19*(21), 9519–9529. https://doi.org/10.1523/jneurosci.19-21-09519.1999

Buckmaster, P. S., Wenzel, H. J., Kunkel, D. D., & Schwartzkroin, P. A. (1996). Axon arbors and synaptic connections of hippocampal mossy cells in the rat in vivo. *Journal of Comparative Neurology*, *366*(2), 270–292. https://doi.org/10.1002/(SICI)1096-9861(19960304)366:2<270::AID-CNE7>3.0.CO;2-2

Burgess, N., Maguire, E. A., & O'Keefe, J. (2002). The human hippocampus and spatial and episodic memory. *Neuron*, *35*(4), 625–641. https://doi.org/10.1016/S0896-6273(02)00830-9

Burkitt, A. N. (2006). A review of the integrate-and-fire neuron model: II. Inhomogeneous synaptic input and network properties. *Biological Cybernetics*, *95*(2), 97–112. https://doi.org/10.1007/s00422-006-0082-8

Cameron, D. B., Mishra, A., & Brown, A. N. (2016). The growth of impact evaluation for international development: how much have we learned? *Journal of Development Effectiveness*, *8*(1), 1–21. https://doi.org/10.1080/19439342.2015.1034156

Cameron, H. A., Woolley, C. S., McEwen, B. S., & Gould, E. (1993). Differentiation of newly born neurons and glia in the dentate gyrus of the adult rat. *Neuroscience*, *56*(2), 337–344. https://doi.org/10.1016/0306-4522(93)90335-D

Cameron, Heather A., & Dayer, A. G. (2008). New Interneurons in the Adult Neocortex: Small, Sparse, but Significant? *Biological Psychiatry*, *63*(7), 650–655. https://doi.org/10.1016/j.biopsych.2007.09.023

Carleton, A., Petreanu, L. T., Lansford, R., Alvarez-Buylla, A., & Lledo, P. M. (2003). Becoming a new neuron in the adult olfactory bulb. *Nature Neuroscience*, *6*(5), 507–518. https://doi.org/10.1038/nn1048

Cayre, M., Malaterre, J., Scotto-Lomassese, S., Strambi, C., & Strambi, A. (2002). The common properties of neurogenesis in the adult brain: From invertebrates to vertebrates. *Comparative Biochemistry and Physiology - B Biochemistry and Molecular Biology*, *132*(1), 1–15. https://doi.org/10.1016/S1096-4959(01)00525-5

Chancey, J. H., Adlaf, E. W., Sapp, M. C., Pugh, P. C., Wadiche, J. I., & Overstreet-Wadiche, L. S. (2013). GABA Depolarization Is Required for Experience-Dependent Synapse Unsilencing in Adult-Born Neurons. *Journal of Neuroscience*, *33*(15), 6614–6622. https://doi.org/10.1523/JNEUROSCI.0781-13.2013

Chavlis, S., Petrantonakis, P. C., & Poirazi, P. (2017). Dendrites of dentate gyrus granule cells contribute to pattern separation by controlling sparsity. *Hippocampus*, *27*(1), 89–110. https://doi.org/10.1002/hipo.22675

Chawla, M. K., Guzowski, J. F., Ramirez-Amaya, V., Lipa, P., Hoffman, K. L., Marriott, L. K., … Barnes, C. A. (2005). Sparse, environmentally selective expression of Arc RNA in the upper blade of the rodent fascia dentata by brief spatial experience. *Hippocampus*, *15*(5), 579–586. https://doi.org/10.1002/hipo.20091

Chiang, P.-H., Wu, P.-Y., Kuo, T.-W., Liu, Y.-C., Chan, C.-F., Chien, T.-C., … Lien, C.-C. (2012). GABA Is Depolarizing in Hippocampal Dentate Granule Cells of the Adolescent and Adult Rats. *Journal of Neuroscience*, *32*(1), 62–67. https://doi.org/10.1523/JNEUROSCI.3393-11.2012

Chirumamilla, S., Sun, D., Bullock, M. R., & Colello, R. J. (2002). Traumatic brain injury induced cell proliferation in the adult mammalian central nervous system. *Journal of Neurotrauma*, *19*(6), 693–703. https://doi.org/10.1089/08977150260139084

Chiu, I. M., Morimoto, E. T. A., Goodarzi, H., Liao, J. T., O'Keeffe, S., Phatnani, H. P., … Maniatis, T. (2013). A neurodegeneration-specific gene-expression signature of acutely isolated microglia from an amyotrophic lateral sclerosis mouse model. *Cell Reports*, *4*(2), 385–401. https://doi.org/10.1016/j.celrep.2013.06.018

Cho, K. O., Lybrand, Z. R., Ito, N., Brulet, R., Tafacory, F., Zhang, L., … Hsieh, J. (2015). Aberrant hippocampal neurogenesis contributes to epilepsy and associated cognitive decline. *Nature Communications*, *6*. https://doi.org/10.1038/ncomms7606

Claiborne, B. J., Amaral, D. G., & Cowan, W. M. (1990). Quantitative, three□dimensional analysis of granule cell dendrites in the rat dentate gyrus. *Journal of Comparative Neurology*, *302*(2), 206–219. https://doi.org/10.1002/cne.903020203

Clelland, C. D., Choi, M., Romberg, C., Clemenson, G. D., Fragniere, A., Tyers, P., … Bussey, T. J. (2009). A functional role for adult hippocampal neurogenesis in spatial pattern separation. *Science*, *325*(5937), 210–213. https://doi.org/10.1007/978-3-7091-1292-2_2

Cobb, S. (1995). *Synchronization of neuronal*.

Cope, E. C., & Gould, E. (2019). Adult Neurogenesis, Glia, and the Extracellular Matrix. *Cell Stem Cell*, *24*(5), 690–705. https://doi.org/10.1016/j.stem.2019.03.023

Coras, R., Pauli, E., Li, J., Schwarz, M., Rössler, K., Buchfelder, M., … Blumcke, I. (2014). Differential influence of hippocampal subfields to memory formation: Insights from patients with temporal lobe epilepsy. *Brain*, *137*(7), 1945–1957. https://doi.org/10.1093/brain/awu100

Couillard-Despres, S., Winner, B., Karl, C., Lindemann, G., Schmid, P., Aigner, R., … Aigner, L. (2006). Targeted transgene expression in neuronal precursors: Watching young neurons in the old brain. *European Journal of Neuroscience*, *24*(6), 1535–1545. https://doi.org/10.1111/j.1460-9568.2006.05039.x

Coultrip, R., Granger, R., & Lynch, G. (1992). A cortical model of winner-take-all competition via lateral inhibition. *Neural Networks*, *5*(1), 47–54. https://doi.org/10.1016/S0893-6080(05)80006-1

Crain, B., Cotman, C., Taylor, D., & Lynch, G. (1973). A quantitative electron microscopic study of synaptogenesis in the dentate gyrus of the rat. *Brain Research*, *63*(C), 195–204. https://doi.org/10.1016/0006-8993(73)90088-7

Creer, D. J., Romberg, C., Saksida, L. M., van Praag, H., & Bussey, T. J. (2010). Running enhances spatial pattern separation in mice. *Proceedings of the National Academy of Sciences*, *107*(5), 2367–2372. https://doi.org/10.1073/pnas.0911725107

Danielson, N. B. B., Kaifosh, P., Zaremba, J. D. D., Lovett-Barron, M., Tsai, J., Denny, C. A. A., … Kheirbek, M. A. A. (2016a). Distinct Contribution of Adult-Born Hippocampal Granule Cells to Context Encoding. *Neuron*, *90*(1), 101–112. https://doi.org/10.1016/j.neuron.2016.02.019

Danielson, N. B. B., Kaifosh, P., Zaremba, J. D. D., Lovett-Barron, M., Tsai, J., Denny, C. A. A., … Kheirbek, M. A. A. (2016b). Distinct Contribution of Adult-Born Hippocampal Granule Cells to Context Encoding. *Neuron*. https://doi.org/10.1016/j.neuron.2016.02.019

Danzer, S. C. (2012). Depression, stress, epilepsy and adult neurogenesis. *Experimental Neurology*, *233*(1), 22–32. https://doi.org/10.1016/j.expneurol.2011.05.023

Danzer, S. C. (2019). Adult Neurogenesis in the Development of Epilepsy. *Epilepsy Currents*, *19*(5), 316–320. https://doi.org/10.1177/1535759719868186

Das, G. D. (n.d.). *Altman1965*.

Dash, P. K., Mach, S. A., & Moore, A. N. (2001). Enhanced neurogenesis in the rodent following traumatic brain injury. *Journal of Neuroscience Research*, *63*(4), 313–319. https://doi.org/10.1002/1097-4547(20010215)63:4<313::AID-JNR1025>3.0.CO;2-4

David, D. J., Samuels, B. A., Rainer, Q., Wang, J. W., Marsteller, D., Mendez, I., … Hen, R. (2009). Neurogenesis-Dependent and -Independent Effects of Fluoxetine in an Animal Model of Anxiety/Depression. *Neuron*, *62*(4), 479–493. https://doi.org/10.1016/j.neuron.2009.04.017

Dayer, A. G., Ford, A. A., Cleaver, K. M., Yassaee, M., & Cameron, H. A. (2003). Short-term and long-term survival of new neurons in the rat dentate gyrus. *Journal of Comparative Neurology*, *460*(4), 563–572. https://doi.org/10.1002/cne.10675

Deisseroth, K., Singla, S., Toda, H., Monje, M., Palmer, T. D., & Malenka, R. C. (2004). Excitation-neurogenesis coupling in adult neural stem/progenitor cells. *Neuron*, *42*(4), 535–552. https://doi.org/10.1016/S0896-6273(04)00266-1

Delpire, E. (2000). Cation-chloride cotransporters in neuronal communication. *News in Physiological Sciences*, *15*(6), 309–312. https://doi.org/10.1152/physiologyonline.2000.15.6.309

Deng, W., Aimone, J. B., & Gage, F. H. (2010). New neurons and new memories: How does adult hippocampal neurogenesis affect learning and memory? *Nature Reviews Neuroscience*, *11*(5), 339–350. https://doi.org/10.1038/nrn2822

Deng, W., Saxe, M. D., Gallina, I. S., & Gage, F. H. (2009). Adult-born hippocampal dentate granule cells undergoing maturation modulate learning and memory in the brain. *Journal of Neuroscience*, *29*(43), 13532–13542. https://doi.org/10.1523/JNEUROSCI.3362-09.2009

Denny, B. T., Kober, H., Wager, T. D., & Ochsner, K. N. (2012). A meta-analysis of functional neuroimaging studies of self- and other judgments reveals a spatial gradient for mentalizing in medial prefrontal cortex. *Journal of Cognitive Neuroscience*, *24*(8), 1742–1752. https://doi.org/10.1162/jocn_a_00233

Desmond, N. L., & Levy, W. B. (1985). Granule cell dendritic spine density in the rat hippocampus varies with spine shape and location. *Neuroscience Letters*, *54*(2–3), 219–224. https://doi.org/10.1016/S0304-3940(85)80082-3

Diamantaki, M., Frey, M., Berens, P., Preston-Ferrer, P., & Burgalossi, A. (2016). Sparse activity of identified dentate granule cells during spatial exploration. *ELife*, *5*(OCTOBER2016), 1–17. https://doi.org/10.7554/eLife.20252.001

Dieni, C. V., Nietz, A. K., Panichi, R., Wadiche, J. I., & Overstreet-Wadiche, L. (2013). Distinct Determinants of Sparse Activation during Granule Cell Maturation. *Journal of Neuroscience*, *33*(49), 19131–19142. https://doi.org/10.1523/JNEUROSCI.2289-13.2013

Dieni, Cristina V., Panichi, R., Aimone, J. B., Kuo, C. T., Wadiche, J. I., & Overstreet-Wadiche, L. (2016). Low excitatory innervation balances high intrinsic excitability of immature dentate neurons. *Nature Communications*, *7*, 1–13. https://doi.org/10.1038/ncomms11313

Döbrössy, M. D., Drapeau, E., Aurousseau, C., Le Moal, M., Piazza, P. V., & Abrous, D. N. (2003). Differential effects of learning on neurogenesis: Learning increases or decreases the number of newly born cells depending on their birth date. *Molecular Psychiatry*, *8*(12), 974–982. https://doi.org/10.1038/sj.mp.4001419

Doetsch, F. (2003). The glial identity of neural stem cells. *Nature Neuroscience*, *6*(11), 1127–1134. https://doi.org/10.1038/nn1144

Doetsch, F., & Hen, R. (2005). Young and excitable: The function of new neurons in the adult mammalian brain. *Current Opinion in Neurobiology*, *15*(1), 121–128. https://doi.org/10.1016/j.conb.2005.01.018

Drapeau, E., Mayo, W., Aurousseau, C., Le Moal, M., Piazza, P. V., & Abrous, D. N. (2003). Spatial memory performances of aged rats in the water maze predict levels of hippocampal neurogenesis. *Proceedings of the National Academy of Sciences of the United States of America*, *100*(SUPPL. 2), 14385–14390. https://doi.org/10.1073/pnas.2334169100

Dupret, D., Fabre, A., Döbrössy, M. D., Panatier, A., Rodríguez, J. J., Lamarque, S., … Abrous, D. N. (2007). Spatial learning depends on both the addition and removal of new hippocampal neurons. *PLoS Biology*, *5*(8), 1683–1694. https://doi.org/10.1371/journal.pbio.0050214

Dupret, D., Revest, J. M., Koehl, M., Ichas, F., De Giorgi, F., Costet, P., … Piazza, P. V. (2008). Spatial relational memory requires hippocampal adult neurogenesis. *PLoS ONE*, *3*(4). https://doi.org/10.1371/journal.pone.0001959

Ehninger, D., & Kempermann, G. (2008). Neurogenesis in the adult hippocampus. *Cell and Tissue Research*, *331*(1), 243–250. https://doi.org/10.1007/s00441-007-0478-3

Eichenbaum, H. (2000). *Eichenbaum.NRN.00.pdf*. *1*(October), 1–10. https://doi.org/10.1038/35036213

Engin, E., Zarnowska, E. D., Benke, D., Tsvetkov, E., Sigal, M., Keist, R., … Rudolph, U. (2015). Tonic Inhibitory Control of Dentate Gyrus Granule Cells by α5-Containing GABA $_A$ Receptors Reduces Memory Interference. *The Journal of Neuroscience*, *35*(40), 13698–13712. https://doi.org/10.1523/JNEUROSCI.1370-15.2015

Epp, J. R., Spritzer, M. D., & Galea, L. A. M. (2007). Hippocampus-dependent learning promotes survival of new neurons in the dentate gyrus at a specific time during cell maturation. *Neuroscience*, *149*(2), 273–285. https://doi.org/10.1016/j.neuroscience.2007.07.046

Eriksson, P. S., Perfilieva, E., Björk-Eriksson, T., Alborn, A. M., Nordborg, C., Peterson, D. A., & Gage, F. H. (1998). Neurogenesis in the adult human hippocampus. *Nature Medicine*, *4*(11), 1313–1317. https://doi.org/10.1038/3305

Esposito, M. S. (2005). Neuronal Differentiation in the Adult Hippocampus Recapitulates Embryonic Development. *Journal of Neuroscience*, *25*(44), 10074–10086. https://doi.org/10.1523/JNEUROSCI.3114-05.2005

F E E D - F O R W a R D Inhibition in the. (1984). *Progress in Neurobiology*, *22*, 131–153.

Faghihi, F., & Moustafa, A. A. (2015). A computational model of pattern separation efficiency in the dentate gyrus with implications in schizophrenia. *Frontiers in Systems Neuroscience*, *9*(MAR), 1–12. https://doi.org/10.3389/fnsys.2015.00042

Fanselow, M. S., & Dong, H. W. (2010). Are the Dorsal and Ventral Hippocampus Functionally Distinct Structures? *Neuron*, *65*(1), 7–19. https://doi.org/10.1016/j.neuron.2009.11.031

Felix-Ortiz, A. C., & Tye, K. M. (2014). Amygdala inputs to the ventral hippocampus bidirectionally modulate social behavior. *Journal of Neuroscience*, *34*(2), 586–595. https://doi.org/10.1523/JNEUROSCI.4257-13.2014

Flood, D. G., Buell, S. J., Defiore, C. H., Horwitz, G. J., & Coleman, P. D. (1985). Age-related dendritic growth in dentate gyrus of human brain is followed by regression in the “oldest old.” *Brain Research*, *345*(2), 366–368. https://doi.org/10.1016/0006-8993(85)91018-2

Flood, D. G., Buell, S. J., Horwitz, G. J., & Coleman, P. D. (1987). Dendritic extent in human dentate gyrus granule cells in normal aging and senile dementia. *Brain Research*, *402*(2), 205–216. https://doi.org/10.1016/0006-8993(87)90027-8

Fourcaud-trocme, N., Hansel, D., Vreeswijk, C. Van, & Brunel, N. (2003). *<Spike Mechanisms Determine Response To Fluctuating Inputs.Pdf>*. *23*(37), 11628–11640.

Frankland, P. W., Filipkowski, R. K., Cestari, V., McDonald, R. J., & Silva, A. J. (1998). The dorsal hippocampus is essential for context discrimination but not for contextual conditioning. *Behavioral Neuroscience*, *112*(4), 863–874. https://doi.org/10.1037/0735-7044.112.4.863

Freundl, T. F., & Buzsi5ki2, G. (1996). Interneurons of the Hippocampus. *Hippogimpus*, *6*, 347–470.

Friedman, W. J. (2001). *Comment on ‘“ Potential Role for Adult Neurogenesis in the Encoding of Time in New Memories .”’ 504*(2007), 503–504. https://doi.org/10.1002/hipo

Frotscher, M., Seress, L., Schwerdtfeger, W. K., & Buhl, E. (1991). The mossy cells of the fascia dentata: A comparative study of their fine structure and synaptic connections in rodents and primates. *Journal of Comparative Neurology*, *312*(1), 145–163. https://doi.org/10.1002/cne.903120111

Fuchs, E., & Gould, E. (2000). In vivo neurogenesis in the adult brain: Regulation and functional implications. *European Journal of Neuroscience*, *12*(7), 2211–2214. https://doi.org/10.1046/j.1460-9568.2000.00130.x

G.F.S. (1923). The Bell system technical journal. *Journal of the Franklin Institute*, *196*(4), 519–520. https://doi.org/10.1016/s0016-0032(23)90506-5

Gage, F. H. (2000). Mammalian neural stem cells. *Science*, *287*(5457), 1433–1438. https://doi.org/10.1126/science.287.5457.1433

Ge, S., Goh, E. L. K., Sailor, K. A., Kitabatake, Y., Ming, G. L., & Song, H. (2006). GABA regulates synaptic integration of newly generated neurons in the adult brain. *Nature*, *439*(7076), 589–593. https://doi.org/10.1038/nature04404

Ge, S., Yang, C. hao, Hsu, K. sen, Ming, G. li, & Song, H. (2007). A Critical Period for Enhanced Synaptic Plasticity in Newly Generated Neurons of the Adult Brain. *Neuron*, *54*(4), 559–566. https://doi.org/10.1016/j.neuron.2007.05.002

Gilbert, P. E., Kesner, R. P., & Lee, I. (2001). Dissociating hippocampal subregions: A double dissociation between dentate gyrus and CA1. *Hippocampus*, *11*(6), 626–636. https://doi.org/10.1002/hipo.1077

Goodman, D. F. M., & Brette, R. (2009). The brian simulator. *Frontiers in Neuroscience*, *3*(SEP), 192–197. https://doi.org/10.3389/neuro.01.026.2009

Gould, E. (2007). How widespread is adult neurogenesis in mammals? *Nature Reviews Neuroscience*, *8*(6), 481–488. https://doi.org/10.1038/nrn2147

Gould, E., Beylin, A., Tanapat, P., Reeves, A., & Shors, T. J. (1999). Learning enhances adult neurogenesis in the hippocampal formation. *Nature Neuroscience*, *2*(3), 260–265. https://doi.org/10.1038/6365

Gould, E., Tanapat, P., Mcewen, B. S., Flügge, G., & Fuchs, E. (1998). Proliferation of granule cell precursors in the dentate gyrus of adult monkeys is diminished by stress. *Proceedings of the National Academy of Sciences of the United States of America*, *95*(6), 3168–3171. https://doi.org/10.1073/pnas.95.6.3168

Gross, C. G. (2000). Neurogenesis in the adult brain: Death of a dogma. *Nature Reviews Neuroscience*, *1*(1), 67–73. https://doi.org/10.1038/35036235

Gu, Y., Arruda-Carvalho, M., Wang, J., Janoschka, S. R., Josselyn, S. A., Frankland, P. W., & Ge, S. (2012). Optical controlling reveals time-dependent roles for adult-born dentate granule cells. *Nature Neuroscience*, *15*(12), 1700–1706. https://doi.org/10.1038/nn.3260

Hafting, T., Fyhn, M., Molden, S., Moser, M. B., & Moser, E. I. (2005). Microstructure of a spatial map in the entorhinal cortex. *Nature*, *436*(7052), 801–806. https://doi.org/10.1038/nature03721

Halasy, K., & Somogyl, P. (1993). *Distribution of GABAergic Synapses and Their Targets in the Dentate Gyrus of Rat : a Quantitative Immunoelectron Microscopic Analysis dentate gyrus , are innervated by entorhinal , associa- to be inhibitory and use GABA as neurotransmitter . tion is the s*. *34*, 299–308.

Han, Z., Buhl, E. H., Lorinczıln, Z., & Somogyi, P. (1992). A High Degree of Spatial Selectivity in the Axonal and Dendritic Domains of Physiologically Identified Local-circuit Neurons in the Dentate Gyms of the Rat Hippocampus - Han - 2006 - European Journal of Neuroscience - Wiley Online Library. *Onlinelibrary.Wiley.Com*, *5*, 395–410. Retrieved from http://onlinelibrary.wiley.com/doi/10.1111/j.1460-9568.1993.tb00507.x/pdf %5Cnpapers3://publication/uuid/72E9D592-CC0E-4ACB-95FF-F3C286C61114

Harrison, P. J. (2004). The hippocampus in schizophrenia: A review of the neuropathological evidence and its pathophysiological implications. *Psychopharmacology*, *174*(1), 151–162. https://doi.org/10.1007/s00213-003-1761-y

Hasselmo, M. E., Schnell, E., & Barkai, E. (1995). Dynamics of learning and recall at excitatory recurrent synapses and cholinergic modulation in rat hippocampal region CA3. *Journal of Neuroscience*, *15*(7 II), 5249–5262. https://doi.org/10.1523/jneurosci.15-07-05249.1995

Henke, P. G. (1990). Hippocampal pathway to the amygdala and stress ulcer development. *Brain Research Bulletin*, *25*(5), 691–695. https://doi.org/10.1016/0361-9230(90)90044-Z

Henze, D. A., & Buzsáki, G. (2007). Hilar mossy cells: functional identification and activity in vivo. *Progress in Brain Research*, *163*(973). https://doi.org/10.1016/S0079-6123(07)63012-X

Herschel, W. (1800). Philosophical Transactions of the Royal Society of London. *Philosophical Transactions of the Royal Society of London*, *90*(1800), 284–292. https://doi.org/10.1098/rstb.2010.0374

Hillman, C. H., Erickson, K. I., & Kramer, A. F. (2008). Be smart, exercise your heart: Exercise effects on brain and cognition. *Nature Reviews Neuroscience*, *9*(1), 58–65. https://doi.org/10.1038/nrn2298

Hollands, C., Bartolotti, N., & Lazarov, O. (2016). Alzheimer's Disease and Hippocampal Adult Neurogenesis; Exploring Shared Mechanisms. *Frontiers in Neuroscience*, *10*(May), 1–8. https://doi.org/10.3389/fnins.2016.00178

Hughes, K. R. (1965). *Dorsal and Ventral Hippocampus Lesions and*. *19*(4), 325–332.

Hunsaker, M. R., & Kesner, R. P. (2008). Evaluating the differential roles of the dorsal dentate gyrus, dorsal CA3, and dorsal CA1 during a temporal ordering for spatial locations task. *Hippocampus*, *18*(9), 955–964. https://doi.org/10.1002/hipo.20455

Hvoslef-Eide, M., & Oomen, C. A. (2016). Adult neurogenesis and pattern separation in rodents: A critical evaluation of data, tasks and interpretation. *Frontiers in Biology*, *11*(3), 168–181. https://doi.org/10.1007/s11515-016-1406-2

Ide, Y., Fujiyama, F., Okamoto-Furuta, K., Tamamaki, N., Kaneko, T., & Hisatsune, T. (2008). Rapid integration of young newborn dentate gyrus granule cells in the adult hippocampal circuitry. *European Journal of Neuroscience*, *28*(12), 2381–2392. https://doi.org/10.1111/j.1460-9568.2008.06548.x

Ikrar, T., Guo, N., He, K., Besnard, A., Levinson, S., Hill, A., … Sahay, A. (2013). Adult neurogenesis modifies excitability of the dentate gyrus. *Frontiers in Neural Circuits*, *7*(DEC), 1–15. https://doi.org/10.3389/fncir.2013.00204

Imayoshi, I., Sakamoto, M., Ohtsuka, T., Takao, K., Miyakawa, T., Yamaguchi, M., … Kageyama, R. (2008). Roles of continuous neurogenesis in the structural and functional integrity of the adult forebrain. *Nature Neuroscience*, *11*(10), 1153–1161. https://doi.org/10.1038/nn.2185

Jack, C. R., Petersen, R. C., Xu, Y., O'Brien, P. C., Smith, G. E., Ivnik, R. J., … Kokmen, E. (2000). Rates of hippocampal atrophy correlate with change in clinical status in aging and AD. *Neurology*, *55*(4), 484–489. https://doi.org/10.1212/wnl.55.4.484

Jahr, C. E., & Stevens, C. F. (1990). Voltage Dependence of NMDA-Activated Predicted by Single-Channel Kinetics. *Journal of Neuroscience*, *10*(9), 3178–3182.

Jessberger, S., & Gage, F. H. (2014). Adult neurogenesis: Bridging the gap between mice and humans. *Trends in Cell Biology*, *24*(10), 558–563. https://doi.org/10.1016/j.tcb.2014.07.003

Jessberger, S., & Kempermann, G. (2003). Adult-born hippocampal neurons mature into activity-dependent responsiveness. *European Journal of Neuroscience*, *18*(10), 2707–2712. https://doi.org/10.1111/j.1460-9568.2003.02986.x

Jessberger, S., & Parent, J. M. (2015). Epilepsy and adult neurogenesis. *Cold Spring Harbor Perspectives in Biology*, *7*(12). https://doi.org/10.1101/cshperspect.a020677

Jin, K., Minami, M., Lan, J. Q., Mao, X. O., Batteur, S., Simon, R. P., & Greenberg, D. A. (2001). Neurogenesis in dentate subgranular zone and rostral subventricular zone after focal cerebral ischemia in the rat. *Proceedings of the National Academy of Sciences of the United States of America*, *98*(8), 4710–4715. https://doi.org/10.1073/pnas.081011098

Jinde, S., Zsiros, V., Jiang, Z., Nakao, K., Pickel, J., Kohno, K., … Nakazawa, K. (2012). Hilar Mossy Cell Degeneration Causes Transient Dentate Granule Cell Hyperexcitability and Impaired Pattern Separation. *Neuron*, *76*(6), 1189–1200. https://doi.org/10.1016/j.neuron.2012.10.036

Jinde, S., Zsiros, V., & Nakazawa, K. (2013). Hilar mossy cell circuitry controlling dentate granule cell excitability. *Frontiers in Neural Circuits*, *7*(JAN), 1–10. https://doi.org/10.3389/fncir.2013.00014

Jung, M. W., & McNaughton, B. L. (1993). Spatial selectivity of unit activity in the hippocampal granular layer. *Hippocampus*, *3*(2), 165–182. https://doi.org/10.1002/hipo.450030209

Kaplan, M. S. (2001). Environment complexity stimulates visual cortex neurogenesis: Death of a dogma and a research career. *Trends in Neurosciences*, *24*(10), 617–620. https://doi.org/10.1016/S0166-2236(00)01967-6

Kaplan, M. S., & Hinds, J. W. (1977). Neurogenesis in the adult rat: Electron microscopic analysis of light radioautographs. *Science*, *197*(4308), 1092–1094. https://doi.org/10.1126/science.887941

Katsimpardi, L., & Lledo, P. M. (2018). Regulation of neurogenesis in the adult and aging brain. *Current Opinion in Neurobiology*, *53*, 131–138. https://doi.org/10.1016/j.conb.2018.07.006

Kee, N., Teixeira, C. M., Wang, A. H., & Frankland, P. W. (2007). Preferential incorporation of adult-generated granule cells into spatial memory networks in the dentate gyrus. *Nature Neuroscience*, *10*(3), 355–362. https://doi.org/10.1038/nn1847

Kempermann, G., & Gage, F. H. (1999). Experience-dependent regulation of adult hippocampal neurogenesis: Effects of long-term stimulation and stimulus withdrawal. *Hippocampus*, *9*(3), 321–332. https://doi.org/10.1002/(SICI)1098-1063(1999)9:3<321::AID-HIPO11>3.0.CO;2-C

Kempermann, G., Jessberger, S., Steiner, B., & Kronenberg, G. (2004). Milestones of neuronal development in the adult hippocampus. *Trends in Neurosciences*, *27*(8), 447–452. https://doi.org/10.1016/j.tins.2004.05.013

Kempermann, G., Kuhn, H. G., & Gage, F. H. (1996). *in an Enriched Environment*. *7079*(1995), 432–434.

Kempermann, G., Kuhn, H. G., & Gage, F. H. (1998). Experience-induced neurogenesis in the senescent dentate gyrus. *Journal of Neuroscience*, *18*(9), 3206–3212. https://doi.org/10.1523/jneurosci.18-09-03206.1998

Kesner, R. P., & Rolls, E. T. (2015). A computational theory of hippocampal function, and tests of the theory: New developments. *Neuroscience and Biobehavioral Reviews*, *48*, 92–147. https://doi.org/10.1016/j.neubiorev.2014.11.009

Kheirbek, M. A., Drew, L. J., Burghardt, N. S., Costantini, D. O., Tannenholz, L., Ahmari, S. E., … Henl, R. (2013). Differential control of learning and anxiety along the dorsoventral axis of the dentate gyrus. *Neuron*, *77*(5), 955–968. https://doi.org/10.1016/j.neuron.2012.12.038

Kim, S., Kim, Y., Lee, S. H., & Ho, W. K. (2018). Dendritic spikes in hippocampal granule cells are necessary for long-term potentiation at the perforant path synapse. *ELife*, *7*(1973), 1–21. https://doi.org/10.7554/eLife.35269

Kim, S. M., & Frank, L. M. (2009). Hippocampal lesions impair rapid learning of a continuous spatial alternation task. *PLoS ONE*, *4*(5). https://doi.org/10.1371/journal.pone.0005494

Kirby, E. D., Friedman, A. R., Covarrubias, D., Ying, C., Sun, W. G., Goosens, K. A., … Kaufer, D. (2012). Basolateral amygdala regulation of adult hippocampal neurogenesis and fear-related activation of newborn neurons. *Molecular Psychiatry*, *17*(5), 527–536. https://doi.org/10.1038/mp.2011.71

Kitabatake, Y., Sailor, K. A., Ming, G. li, & Song, H. (2007). Adult Neurogenesis and Hippocampal Memory Function: New Cells, More Plasticity, New Memories? *Neurosurgery Clinics of North America*, *18*(1), 105–113. https://doi.org/10.1016/j.nec.2006.10.008

Kitamura, T., Saitoh, Y., Murayama, A., Sugiyama, H., & Inokuchi, K. (2010). LTP induction within a narrow critical period of immature stages enhances the survival of newly generated neurons in the adult rat dentate gyrus. *Molecular Brain*, *3*(1), 1–8. https://doi.org/10.1186/1756-6606-3-13

Kjelstrup, K. B., Solstad, T., Brun, V. H., Hafting, T., Leutgeb, S., Witter, M. P., … Moser, M. B. (2008). Finite scale of spatial representation in the hippocampus. *Science*, *321*(5885), 140–143. https://doi.org/10.1126/science.1157086

Klausberger, T., & Somogyi, P. (2008). Neuronal diversity and temporal dynamics: The unity of hippocampal circuit operations. *Science*, *321*(5885), 53–57. https://doi.org/10.1126/science.1149381

Kneisler, T. B., & Dingledine, R. (1995). Synaptic input from CA3 pyramidal cells to dentate basket cells in rat hippocampus. *The Journal of Physiology*, *487*(1), 125–146. https://doi.org/10.1113/jphysiol.1995.sp020866

Kokoeva, M. V., Yin, H., & Flier, J. S. (2005). Neurogenesis in the hypothalamus of adult mice: Potential role in energy balance. *Science*, *310*(5748), 679–683. https://doi.org/10.1126/science.1115360

Kornack, D. R., & Rakic, P. (1999). Continuation of neurogenesis in the hippocampus of the adult macaque monkey. *Proceedings of the National Academy of Sciences of the United States of America*, *96*(10), 5768–5773. https://doi.org/10.1073/pnas.96.10.5768

Kraushaar, U., Jonas, P., Misgeld, U., & Yuste, R. (2000). Efficacy and stability of quantal GABA release at a hippocampal interneuron-principal neuron synapse. *The Journal of Neuroscience : The Official Journal of the Society for Neuroscience*, *20*(15), 5594–5607. https://doi.org/10.1523/jneurosci.2787-06.2006

Krueppel, R., Remy, S., & Beck, H. (2011). Dendritic integration in hippocampal dentate granule cells. *Neuron*, *71*(3), 512–528. https://doi.org/10.1016/j.neuron.2011.05.043

Kuhn, H. G., Dickinson-Anson, H., & Gage, F. H. (1996). Neurogenesis in the dentate gyrus of the adult rat: Age-related decrease of neuronal progenitor proliferation. *Journal of Neuroscience*, *16*(6), 2027–2033. https://doi.org/10.1523/jneurosci.16-06-02027.1996

Larimer, P., & Strowbridge, B. W. (2010). Representing information in cell assemblies: Persistent activity mediated by semilunar granule cells. *Nature Neuroscience*, *13*(2), 213–222. https://doi.org/10.1038/nn.2458

Lazarov, O., & Marr, R. A. (2010). Neurogenesis and Alzheimer's disease: At the crossroads. *Experimental Neurology*, *223*(2), 267–281. https://doi.org/10.1016/j.expneurol.2009.08.009

Leão, R. N., Mikulovic, S., Leão, K. E., Munguba, H., Gezelius, H., Enjin, A., … Kullander, K. (2012). OLM interneurons differentially modulate CA3 and entorhinal inputs to hippocampal CA1 neurons. *Nature Neuroscience*, *15*(11), 1524–1530. https://doi.org/10.1038/nn.3235

Lee, I., & Kesner, R. P. (2004). Encoding versus retrieval of spatial memory: Double dissociation between the dentate gyrus and the perforant path inputs into CA3 in the dorsal hippocampus. *Hippocampus*, *14*(1), 66–76. https://doi.org/10.1002/hipo.10167

Lefebvre, J., Hutt, A., Knebel, J. F., Whittingstall, K., & Murray, M. M. (2015). Stimulus statistics shape oscillations in nonlinear recurrent neural networks. *Journal of Neuroscience*, *35*(7), 2895–2903. https://doi.org/10.1523/JNEUROSCI.3609-14.2015

Leinekugel, X., Medina, I., Khalilov, I., Ben-Ari, Y., & Khazipov, R. (1997). Ca2+ oscillations mediated by the synergistic excitatory actions of GABA(A) and NMDA receptors in the neonatal hippocampus. *Neuron*, *18*(2), 243–255. https://doi.org/10.1016/S0896-6273(00)80265-2

Lemaire, V., Tronel, S., Montaron, M. F., Fabre, A., Dugast, E., & Abrous, D. N. (2012). Long-lasting plasticity of hippocampal adult-born neurons. *Journal of Neuroscience*, *32*(9), 3101–3108. https://doi.org/10.1523/JNEUROSCI.4731-11.2012

Leuner, Bendetta, Mendolia-Loffredo, S., Kozorovitskiy, Y., Samburg, D., Gould, E., & Shors, T. J. (2004). Learning enhances the survival of new neurons beyond the time when the hippocampus is required for memory. *Journal of Neuroscience*, *24*(34), 7477–7481. https://doi.org/10.1523/JNEUROSCI.0204-04.2004

Leuner, Benedetta, Gould, E., & Shors, T. J. (2006). Is there a link between adult neurogenesis and learning? *Hippocampus*, *16*(3), 216–224. https://doi.org/10.1002/hipo.20153

Leutgeb, J. K., Leutgeb, S., Moser, M. B., & Moser, E. I. (2007). Pattern separation in the dentate gyrus and CA3 of the hippocampus. *Science*, *315*(5814), 961–966. https://doi.org/10.1126/science.1135801

Levone, B. R., Cryan, J. F., & O'Leary, O. F. (2015). Role of adult hippocampal neurogenesis in stress resilience. *Neurobiology of Stress*, *1*(1), 147–155. https://doi.org/10.1016/j.ynstr.2014.11.003

Libersat, F., & Duch, C. (2004). Mechanisms of dendritic maturation. *Molecular Neurobiology*, *29*(3), 303–320. https://doi.org/10.1385/MN:29:3:303

Liu, J., Solway, K., Messing, R. O., & Sharp, F. R. (1998). Increased neurogenesis in the dentate gyrus after transient global ischemia in gerbils. *Journal of Neuroscience*, *18*(19), 7768–7778. https://doi.org/10.1523/jneurosci.18-19-07768.1998

Lledo, P. M., Alonso, M., & Grubb, M. S. (2006). Adult neurogenesis and functional plasticity in neuronal circuits. *Nature Reviews Neuroscience*, *7*(3), 179–193. https://doi.org/10.1038/nrn1867

Llorens-Martín, M., Jurado-Arjona, J., Avila, J., & Hernández, F. (2015). Novel connection between newborn granule neurons and the hippocampal CA2 field. *Experimental Neurology*, *263*, 285–292. https://doi.org/10.1016/j.expneurol.2014.10.021

London, M., & Häusser, M. (2005). Dendritic Computation. *Annual Review of Neuroscience*, *28*(1), 503–532. https://doi.org/10.1146/annurev.neuro.28.061604.135703

Lübke, J., Frotscher, M., & Spruston, N. (1998a). Specialized electrophysiological properties of anatomically identified neurons in the hilar region of the rat fascia dentata. *Journal of Neurophysiology*, *79*(3), 1518–1534. https://doi.org/10.1152/jn.1998.79.3.1518

Lübke, J., Frotscher, M., & Spruston, N. (1998b). Specialized Electrophysiological Properties of Anatomically Identified Neurons in the Hilar Region of the Rat Fascia Dentata. *Journal of Neurophysiology*, *79*(3), 1518–1534. https://doi.org/10.1152/jn.1998.79.3.1518

Luna, V. M., Anacker, C., Burghardt, N. S., Khandaker, H., Andreu, V., Millette, A., … Hen, R. (2019). Adult-born hippocampal neurons bidirectionally modulate entorhinal inputs into the dentate gyrus. *Science*, *364*(6440), 578–583. https://doi.org/10.1126/science.aat8789

Luzzati, F., Fasolo, A., & Peretto, P. (2011). Combining confocal laser scanning microscopy with serial section reconstruction in the study of adult neurogenesis. *Frontiers in Neuroscience*, *5*(MAY), 1–14. https://doi.org/10.3389/fnins.2011.00070

Lynch, M., Sayin, Ü., Bownds, J., Janumpalli, S., & Sutula, T. (2000). Long-term consequences of early postnatal seizures on hippocampal learning and plasticity. *European Journal of Neuroscience*, *12*(7), 2252–2264. https://doi.org/10.1046/j.1460-9568.2000.00117.x

Maguire, E. A., Gadian, D. G., Johnsrude, I. S., Good, C. D., Ashburner, J., Frackowiak, R. S. J., & Frith, C. D. (2000). Navigation-related structural change in the hippocampi of taxi drivers. *Proceedings of the National Academy of Sciences of the United States of America*, *97*(8), 4398–4403. https://doi.org/10.1073/pnas.070039597

Mandyam, C. D., & Koob, G. F. (2012). The addicted brain craves new neurons: Putative role for adult-born progenitors in promoting recovery. *Trends in Neurosciences*, *35*(4), 250–260. https://doi.org/10.1016/j.tins.2011.12.005

Marín-Burgin, A., Mongiat, L. A., Pardi, M. B., & Schinder, A. F. (2012a). Unique processing during a period of high excitation/inhibition balance in adult-born neurons. *Science*, *335*(6073), 1238–1242. https://doi.org/10.1126/science.1214956

Marín-Burgin, A., Mongiat, L. A., Pardi, M. B., & Schinder, A. F. (2012b). Unique processing during a period of high excitation/inhibition balance in adult-born neurons. *Science*, *335*(6073), 1238–1242. https://doi.org/10.1126/science.1214956

Markus, E. J., Qin, Y. L., Leonard, B., Skaggs, W. E., McNaughton, B. L., & Barnes, C. A. (1995). Interactions between location and task affect the spatial and directional firing of hippocampal neurons. *Journal of Neuroscience*, *15*(11), 7079–7094. https://doi.org/10.1523/jneurosci.15-11-07079.1995

Markwardt, S. J., Wadiche, J. I., & Overstreet-Wadiche, L. S. (2009). Input-Specific GABAergic Signaling to Newborn Neurons in Adult Dentate Gyrus. *Journal of Neuroscience*, *29*(48), 15063–15072. https://doi.org/10.1523/JNEUROSCI.2727-09.2009

Marrone, D. F., Adams, A. A., & Satvat, E. (2011). Increased pattern separation in the aged fascia dentata. *Neurobiology of Aging*, *32*(12), 2317.e23-2317.e32. https://doi.org/10.1016/j.neurobiolaging.2010.03.021

Martina, M., Yao, G. L., & Bean, B. P. (2003). Properties and functional role of voltage-dependent potassium channels in dendrites of rat cerebellar Purkinje neurons. *Journal of Neuroscience*, *23*(13), 5698–5707. https://doi.org/10.1523/jneurosci.23-13-05698.2003

Mathews, E. A., Morgenstern, N. A., Piatti, V. C., Zhao, C., Jessberger, S., Schinder, A. F., & Gage, F. H. (2010). A distinctive layering pattern of mouse dentate granule cells is generated by developmental and adult neurogenesis. *Journal of Comparative Neurology*, *518*(22), 4479–4490. https://doi.org/10.1002/cne.22489

McBain, C. J. (2001). Interneurons unbound. *Nature Reviews Neuroscience*, *2*(1), 11–23. https://doi.org/10.1038/35049047

Mcclelland, J. L., Mcnaughton, B. L., & Reilly, R. C. O. (1995). *Schwertmann&Cornell2000ptBook.pdf*. *102*(3), 419–457. https://doi.org/10.1037/0033-295X.102.3.419

McHugh, T. J., Jones, M. W., Quinn, J. J., Balthasar, N., Coppari, R., Elmquist, J. K., … Tonegawa, S. (2007). Dentate gyrus NMDA receptors mediate rapid pattern separation in the hippocampal network. *Science*, *317*(5834), 94–99. https://doi.org/10.1126/science.1140263

McKinnon, M. C., Yucel, K., Nazarov, A., & MacQueen, G. M. (2009). A meta-analysis examining clinical predictors of hippocampal volume in patients with major depressive disorder. *Journal of Psychiatry and Neuroscience*, *34*(1), 41–54.

McNaughton, B. L., & Morris, R. G. M. (1987). Hippocampal synaptic enhancement and information storage within a distributed memory system. *Trends in Neurosciences*, *10*(10), 408–415. https://doi.org/10.1016/0166-2236(87)90011-7

Mcnaughton, L., Chen, L. L., & Markus, J. (n.d.). *1991, McNaughton- landmarks and direction.PDF*. *3*(2).

Miller-Delaney, S. F. C., Bryan, K., Das, S., McKiernan, R. C., Bray, I. M., Reynolds, J. P., … Henshall, D. C. (2015). Differential DNA methylation profiles of coding and non-coding genes define hippocampal sclerosis in human temporal lobe epilepsy. *Brain*, *138*(3), 616–631. https://doi.org/10.1093/brain/awu373

Ming, Guo-li, & Song, H. (2005). Adult Neurogenesis in the Mammalian Central Nervous System. *Annual Review of Neuroscience*, *28*(1), 223–250. https://doi.org/10.1146/annurev.neuro.28.051804.101459

Ming, Guo li, & Song, H. (2011). Adult Neurogenesis in the Mammalian Brain: Significant Answers and Significant Questions. *Neuron*, *70*(4), 687–702. https://doi.org/10.1016/j.neuron.2011.05.001

Mirescu, C., & Gould, E. (2006). Stress and adult neurogenesis. *Hippocampus*, *16*(3), 233–238. https://doi.org/10.1002/hipo.20155

Moreno-Jiménez, E. P., Flor-García, M., Terreros-Roncal, J., Rábano, A., Cafini, F., Pallas-Bazarra, N., … Llorens-Martín, M. (2019). Adult hippocampal neurogenesis is abundant in neurologically healthy subjects and drops sharply in patients with Alzheimer's disease. *Nature Medicine*, *25*(4), 554–560. https://doi.org/10.1038/s41591-019-0375-9

Moser, E., Moser, M. B., & Andersen, P. (1993). Spatial learning impairment parallels the magnitude of dorsal hippocampal lesions, but is hardly present following ventral lesions. *Journal of Neuroscience*, *13*(9), 3916–3925. https://doi.org/10.1523/jneurosci.13-09-03916.1993

Muller, R. U., & Kubie, J. L. (1987). The effects of changes in the environment on the spatial firing of hippocampal complex-spike cells. *Journal of Neuroscience*, *7*(7), 1951–1968. https://doi.org/10.1523/jneurosci.07-07-01951.1987

Myers, C. E., & Scharfman, H. E. (2009). A Role for hilar cells in pattern separation in the dentate gyrus: A computational approach. *Hippocampus*, *19*(4), 321–337. https://doi.org/10.1002/hipo.20516

Myers, C. E., & Scharfman, H. E. (2011). Pattern separation in the dentate gyrus: A role for the CA3 backprojection. *Hippocampus*, *21*(11), 1190–1215. https://doi.org/10.1002/hipo.20828

Nakashiba, T., Cushman, J. D., Pelkey, K. A., Renaudineau, S., Buhl, D. L., McHugh, T. J., … Tonegawa, S. (2012). Young dentate granule cells mediate pattern separation, whereas old granule cells facilitate pattern completion. *Cell*, *149*(1), 188–201. https://doi.org/10.1016/j.cell.2012.01.046

Nakashiba, T., Young, J. Z., McHugh, T. J., Buhl, D. L., & Tonegawa, S. (2008). Transgenic inhibition of synaptic transmission reveals role of CA3 output in hippocampal learning. *Science*, *319*(5867), 1260–1264. https://doi.org/10.1126/science.1151120

nature02553. (n.d.).

Neylan, T. C., Editor, S., & Scoville, W. B. (2000). NEUROPSYCHIATRY CLASSICS Memory and the Medial Temporal Lobe : Patient H . M . Loss of Recent Memory After Bilateral Hippocampal Lesions. *Journal Of Neuropsychiatry*, *253*(5026), 1380–1386.

Nicoll, A., & Blakemore, C. (1993). Patterns of Local Connectivity in the Neocortex. *Neural Computation*, *5*(5), 665–680. https://doi.org/10.1162/neco.1993.5.5.665

Nitz, D., & McNaughton, B. (2004). Differential Modulation of CA1 and Dentate Gyrus Interneurons during Exploration of Novel Environments. *Journal of Neurophysiology*, *91*(2), 863–872. https://doi.org/10.1152/jn.00614.2003

Nottebohm, F. (2002). Neuronal replacement in adult brain. *Brain Research Bulletin*, *57*(6), 737–749. https://doi.org/10.1016/S0361-9230(02)00750-5

O'Keefe, J., Dostrovsky, J., & J. O'Keefe, J. D. (1971). Short Communications The hippocampus as a spatial map . Preliminary evidence from unit activity in the freely-moving rat. *Brain Research*, *34*(1), 171–175. Retrieved from http://www.ncbi.nlm.nih.gov/pubmed/5124915

O'Mara, S. (2005). The subiculum: what it does, what it might do, and what we don't yet know. *Acta Neurobiologiae Experimentalis*, *65*(5), 271–282.

O'Reilly, R. C., & McClelland, J. L. (1994). Hippocampal conjunctive encoding, storage, and recall: Avoiding a trade□ off. *Hippocampus*, *4*(6), 661–682. https://doi.org/10.1002/hipo.450040605

Olshausen, B. A., & Field, D. J. (2004). Sparse coding of sensory inputs. *Current Opinion in Neurobiology*, *14*(4), 481–487. https://doi.org/10.1016/j.conb.2004.07.007

Opendak, M., Offit, L., Monari, P., Schoenfeld, T. J., Sonti, A. N., Cameron, H. A., & Gould, E. (2016). Lasting adaptations in social behavior produced by social disruption and inhibition of adult neurogenesis. *Journal of Neuroscience*, *36*(26), 7027–7038. https://doi.org/10.1523/JNEUROSCI.4435-15.2016

Overstreet-Wadiche, L. S., Bromberg, D. A., Bensen, A. L., & Westbrook, G. L. (2006). Seizures accelerate functional integration of adult-generated granule cells. *Journal of Neuroscience*, *26*(15), 4095–4103. https://doi.org/10.1523/JNEUROSCI.5508-05.2006

Owens, D. F., & Kriegstein, A. R. (2002). Is there more to GABA than synaptic inhibition? *Nature Reviews Neuroscience*, *3*(9), 715–727. https://doi.org/10.1038/nrn919

Parent, J. M., Yu, T. W., Leibowitz, R. T., Geschwind, D. H., Sloviter, R. S., & Lowenstein, D. H. (1997). Dentate granule cell neurogenesis is increased by seizures and contributes to aberrant network reorganization in the adult rat hippocampus. *Journal of Neuroscience*, *17*(10), 3727–3738. https://doi.org/10.1523/jneurosci.17-10-03727.1997

Payne, J. A., Rivera, C., Voipio, J., & Kaila, K. (2003). Cation-chloride co-transporters in neuronal communication, development and trauma. *Trends in Neurosciences*, *26*(4), 199–206. https://doi.org/10.1016/S0166-2236(03)00068-7

Pelkey, K. A., Chittajallu, R., Craig, M. T., Tricoire, L., Wester, J. C., & McBain, C. J. (2017). Hippocampal gabaergic inhibitory interneurons. *Physiological Reviews*, *97*(4), 1619–1747. https://doi.org/10.1152/physrev.00007.2017

Petrantonakis, P. C., & Poirazi, P. (2014). A compressed sensing perspective of hippocampal function. *Frontiers in Systems Neuroscience*, *8*(AUG), 1–13. https://doi.org/10.3389/fnsys.2014.00141

Petrantonakis, P. C., & Poirazi, P. (2015). Dentate Gyrus circuitry features improve performance of sparse approximation algorithms. *PLoS ONE*, *10*(1), 1–17. https://doi.org/10.1371/journal.pone.0117023

Piatti, V. C., Espósito, M. S., & Schinder, A. F. (2006). The timing of neuronal development in adult hippocampal neurogenesis. *Neuroscientist*, *12*(6), 463–468. https://doi.org/10.1177/1073858406293538

Pinar, C., Fontaine, C. J., Triviño-Paredes, J., Lottenberg, C. P., Gil-Mohapel, J., & Christie, B. R. (2017). Revisiting the flip side: Long-term depression of synaptic efficacy in the hippocampus. *Neuroscience and Biobehavioral Reviews*, *80*, 394–413. https://doi.org/10.1016/j.neubiorev.2017.06.001

Pouille, F., & Scanziani, M. (2004). Routing of spike series by dynamic circuits in the hippocampus. *Nature*, *429*(6993), 717–723. https://doi.org/10.1038/nature02615

Pouille, F., Scanziani, M., Pouille, F., & Scanziani, M. (2001). Enforcement of Temporal Fidelity in Pyramidal Cells by Somatic Feed-Forward Inhibition Linked references are available on JSTOR for this article : Enforcement of Temporal Fidelity in Pyramidal Cells by Somatic Feed-Forward Inhibition. *Science*, *293*(5532), 1159–1163. Retrieved from http://www.ncbi.nlm.nih.gov/pubmed/15170216

Praag, H. Van, Kempermann, G., & Gage, F. H. (1999). *Stochastic Model.Pdf*. *2*(3). https://doi.org/10.1038/6368

Praag, H. Van, Schinder, A. F., Christie, B. R., Toni, N., Palmer, T. D., Gage, F. H., … Fernandes, K. J. L. (2010). Widespread deficits in adult neurogenesis precede plaque and tangle formation in the 3xTg mouse model of Alzheimer's disease. *European Journal of Neuroscience*, *32*(6), 905–920. https://doi.org/10.1111/j.1460-9568.2010.07379.x

Rakic, P., & Nowakowski, R. S. (1981). The time of origin of neurons in the hippocampal region of the rhesus monkey. *Journal of Comparative Neurology*, *196*(1), 99–128. https://doi.org/10.1002/cne.901960109

Rakic, Pasko. (2002). Progress: Neurogenesis in adult primate neocortex: An evaluation of the evidence. *Nature Reviews Neuroscience*, *3*(1), 65–71. https://doi.org/10.1038/nrn700

Ramirez-Amaya, V. (2005). Spatial Exploration-Induced Arc mRNA and Protein Expression: Evidence for Selective, Network-Specific Reactivation. *Journal of Neuroscience*, *25*(7), 1761–1768. https://doi.org/10.1523/JNEUROSCI.4342-04.2005

Ramirez-Amaya, V., Marrone, D. F., Gage, F. H., Worley, P. F., & Barnes, C. A. (2006). Integration of New Neurons into Functional Neural Networks. *Journal of Neuroscience*, *26*(47), 12237–12241. https://doi.org/10.1523/JNEUROSCI.2195-06.2006

Rangel, L. M., Alexander, A. S., Aimone, J. B., Wiles, J., Gage, F. H., Chiba, A. A., & Quinn, L. K. (2014). Temporally selective contextual encoding in the dentate gyrus of the hippocampus. *Nature Communications*, *5*, 1–9. https://doi.org/10.1038/ncomms4181

Ratzliff, A. D. H., Howard, A. L., Santhakumar, V., Osapay, I., & Soltesz, I. (2004). Rapid Deletion of Mossy Cells Does Not Result in a Hyperexcitable Dentate Gyrus: Implications for Epileptogenesis. *Journal of Neuroscience*, *24*(9), 2259–2269. https://doi.org/10.1523/JNEUROSCI.5191-03.2004

Represa, A., & Ben-Ari, Y. (2005). Trophic actions of GABA on neuronal development. *Trends in Neurosciences*, *28*(6 SPEC. ISS.), 278–283. https://doi.org/10.1016/j.tins.2005.03.010

Revest, J. M., Dupret, D., Koehl, M., Funk-Reiter, C., Grosjean, N., Piazza, P. V., & Abrous, D. N. (2009). Adult hippocampal neurogenesis is involved in anxiety-related behaviors. *Molecular Psychiatry*, *14*(10), 959–967. https://doi.org/10.1038/mp.2009.15

Ribak, C. E., Seress, L., & Amaral, D. G. (1985). The development, ultrastructure and synaptic connections of the mossy cells of the dentate gyrus. *Journal of Neurocytology*, *14*(5), 835–857. https://doi.org/10.1007/BF01170832

Rodríguez, J. J., & Verkhratsky, A. (2011). Neurogenesis in Alzheimer's disease. *Journal of Anatomy*, *219*(1), 78–89. https://doi.org/10.1111/j.1469-7580.2011.01343.x

Rotheneichner, P., Marschallinger, J., Couillard-Despres, S., & Aigner, L. (2013). Neurogenesis and neuronal regeneration in status epilepticus. *Epilepsia*, *54*(SUPPL. 6), 40–42. https://doi.org/10.1111/epi.12274

Rubin, R. D., Watson, P. D., Duff, M. C., & Cohen, N. J. (2014). The role of the hippocampus in flexible cognition and social behavior. *Frontiers in Human Neuroscience*, *8*(SEP), 1–15. https://doi.org/10.3389/fnhum.2014.00742

Sahay, A., & Hen, R. (2007). Adult hippocampal neurogenesis in depression. *Nature Neuroscience*, *10*(9), 1110–1115. https://doi.org/10.1038/nn1969

Sahay, A., Scobie, K. N., Hill, A. S., O'Carroll, C. M., Kheirbek, M. A., Burghardt, N. S., … Hen, R. (2011). Increasing adult hippocampal neurogenesis is sufficient to improve pattern separation. *Nature*, *472*(7344), 466–470. https://doi.org/10.1038/nature09817

Sahay, A., Wilson, D. A., & Hen, R. (2011). Pattern Separation: A Common Function for New Neurons in Hippocampus and Olfactory Bulb. *Neuron*, *70*(4), 582–588. https://doi.org/10.1016/j.neuron.2011.05.012

Santhakumar, V., Aradi, I., & Soltesz, I. (2005). Role of mossy fiber sprouting and mossy cell loss in hyperexcitability: A network model of the dentate gyrus incorporating cell types and axonal topography. *Journal of Neurophysiology*, *93*(1), 437–453. https://doi.org/10.1152/jn.00777.2004

Santoro, A. (2013). Reassessing pattern separation in the dentate gyrus. *Frontiers in Behavioral Neuroscience*, *7*(JUL), 1–4. https://doi.org/10.3389/fnbeh.2013.00096

Satvat, E., Schmidt, B., Argraves, M., Marrone, D. F., & Markus, E. J. (2011). Changes in task demands alter the pattern of zif268 expression in the dentate gyrus. *Journal of Neuroscience*, *31*(19), 7163–7167. https://doi.org/10.1523/JNEUROSCI.0094-11.2011

Scharfman, H. E. (1991). Dentate hilar cells with dendrites in the molecular layer have lower tresholds for synaptic activation by perforant path than granule cells. *Journal of Neuroscience*, *11*(6), 1660–1673. https://doi.org/10.1523/jneurosci.11-06-01660.1991

Scharfman, Helen E. (2007). The CA3 "backprojection" to the dentate gyrus. *Progress in Brain Research*, *163*(07), 627–637. https://doi.org/10.1016/S0079-6123(07)63034-9

Scharfman, Helen E. (2016). The enigmatic mossy cell of the dentate gyrus. *Nature Reviews Neuroscience*, *17*(9), 562–575. https://doi.org/10.1038/nrn.2016.87

Scharfman, Helen E., Goodman, J. H., & Sollas, A. L. (2000). Granule-like neurons at the hilar/CA3 border after status epilepticus and their synchrony with area CA3 pyramidal cells: Functional implications of seizure-induced neurogenesis. *Journal of Neuroscience*, *20*(16), 6144–6158. https://doi.org/10.1523/jneurosci.20-16-06144.2000

Scharfman, Helen E., & Myers, C. E. (2013). Hilar mossy cells of the dentate gyrus: A historical perspective. *Frontiers in Neural Circuits*, *6*(JAN), 1–17. https://doi.org/10.3389/fncir.2012.00106

Schlessinger, A. R., Cowan, W. M., & Gottlieb, D. I. (1975). An autoradiographic study of the time of origin and the pattern of granule cell migration in the dentate gyrus of the rat. *Journal of Comparative Neurology*, *159*(2), 149–175. https://doi.org/10.1002/cne.901590202

Schmidt-Salzmann, C., Li, L., & Bischofberger, J. (2014). Functional properties of extrasynaptic AMPA and NMDA receptors during postnatal hippocampal neurogenesis. *Journal of Physiology*, *592*(1), 125–140. https://doi.org/10.1113/jphysiol.2013.267203

Schoenfeld, T. J., & Gould, E. (2012). Stress, stress hormones, and adult neurogenesis. *Experimental Neurology*, *233*(1), 12–21. https://doi.org/10.1016/j.expneurol.2011.01.008

Schoenfeld, T. J., Rada, P., Pieruzzini, P. R., Hsueh, B., & Gould, E. (2013). Physical exercise prevents stress-induced activation of granule neurons and enhances local inhibitory mechanisms in the dentate gyrus. *Journal of Neuroscience*, *33*(18), 7770–7777. https://doi.org/10.1523/JNEUROSCI.5352-12.2013

Schwarzer, C., & Sperk, G. (1995). Hippocampal granule cells express glutamic acid decarboxylase-67 after limbic seizures in the rat. *Neuroscience*, *69*(3), 705–709. https://doi.org/10.1016/0306-4522(95)00348-M

Scobie, K. N., Hall, B. J., Wilke, S. A., Klemenhagen, K. C., Fujii-Kuriyama, Y., Ghosh, A., … Sahay, A. (2009). Krüppel-like factor 9 is necessary for late-phase neuronal maturation in the developing dentate gyrus and during adult hippocampal neurogenesis. *Journal of Neuroscience*, *29*(31), 9875–9887. https://doi.org/10.1523/JNEUROSCI.2260-09.2009

Scopa, C., Marrocco, F., Latina, V., Ruggeri, F., Corvaglia, V., La Regina, F., … Cattaneo, A. (2019). Impaired adult neurogenesis is an early event in Alzheimer's disease neurodegeneration, mediated by intracellular Aβ oligomers. *Cell Death & Differentiation*. https://doi.org/10.1038/s41418-019-0409-3

Scott, A. C. (1973). Information processing in Dendritic Trees. *Mathematical Biosciences*, *18*(1–2), 153–160. https://doi.org/10.1016/0025-5564(73)90026-6

Seidenfaden, R., Desoeuvre, A., Bosio, A., Virard, I., & Cremer, H. (2006). Glial conversion of SVZ-derived committed neuronal precursors after ectopic grafting into the adult brain. *Molecular and Cellular Neuroscience*, *32*(1–2), 187–198. https://doi.org/10.1016/j.mcn.2006.04.003

Seress, L., & Mrzljak, L. (1987). Basal dendrites of granule cells are normal features of the fetal and adult dentate gyrus of both monkey and human hippocampal formations. *Brain Research*, *405*(1), 169–174. https://doi.org/10.1016/0006-8993(87)91003-1

Shihabuddin, L. S., Horner, P. J., Ray, J., & Gage, F. H. (2000). Adult spinal cord stem cells generate neurons after transplantation in the adult dentate gyrus. *Journal of Neuroscience*, *20*(23), 8727–8735. https://doi.org/10.1523/jneurosci.20-23-08727.2000

Shors, T. J., Miesegaes, G., Beylin, A., Zhao, M., Rydel, T., & Gould, E. (2001). Neurogenesis in the adult is involved in the formation of trace memories. *Nature*, *410*(6826), 372–376. https://doi.org/10.1038/35066584

Shors, T. J., Townsend, D. A., Zhao, M., Kozorovitskiy, Y., & Gould, E. (2002). Neurogenesis may relate to some but not all types of hippocampal-dependent learning. *Hippocampus*, *12*(5), 578–584. https://doi.org/10.1002/hipo.10103

Sierra, A., Encinas, J. M., Deudero, J. J. P., Chancey, J. H., Enikolopov, G., Overstreet-Wadiche, L. S., … Maletic-Savatic, M. (2010). Microglia shape adult hippocampal neurogenesis through apoptosis-coupled phagocytosis. *Cell Stem Cell*, *7*(4), 483–495. https://doi.org/10.1016/j.stem.2010.08.014

Sloviter, R. S. (1987). Decreased hippocampal inhibition and a selective loss of interneurons in experimental epilepsy. *Science*, *235*(4784), 73–76. https://doi.org/10.1126/science.2879352

Sloviter, R. S. (1989). Calcium□binding protein (calbindin□D28k) and parvalbumin immunocytochemistry: Localization in the rat hippocampus with specific reference to the selective vulnerability of hippocampal neurons to seizure activity. *Journal of Comparative Neurology*, *280*(2), 183–196. https://doi.org/10.1002/cne.902800203

Sloviter, R. S., & Lømo, T. (2012). Updating the lamellar hypothesis of hippocampal organization. *Frontiers in Neural Circuits*, *6*(DEC), 1–16. https://doi.org/10.3389/fncir.2012.00102

Snyder, E. M., Philpot, B. D., Huber, K. M., Dong, X., Fallon, J. R., & Bear, M. F. (2001). Internalization of ionotropic glutamate receptors in response to mGluR activation. *Nature Neuroscience*, *4*(11), 1079–1085. https://doi.org/10.1038/nn746

Snyder, J. S., Hong, N. S., McDonald, R. J., & Wojtowicz, J. M. (2005). A role for adult neurogenesis in spatial long-term memory. *Neuroscience*, *130*(4), 843–852. https://doi.org/10.1016/j.neuroscience.2004.10.009

Snyder, Jason S. (2019). Recalibrating the Relevance of Adult Neurogenesis. *Trends in Neurosciences*, *42*(3), 164–178. https://doi.org/10.1016/j.tins.2018.12.001

Snyder, Jason S., Choe, J. S., Clifford, M. A., Jeurling, S. I., Hurley, P., Brown, A., … Cameron, H. A. (2009). Adult-born hippocampal neurons are more numerous, faster maturing, and more involved in behavior in rats than in mice. *Journal of Neuroscience*, *29*(46), 14484–14495. https://doi.org/10.1523/JNEUROSCI.1768-09.2009

Song, H., Kempermann, G., Wadiche, L. O., Zhao, C., Schinder, A. F., & Bischofberger, J. (2005). New neurons in the adult mammalian brain: Synaptogenesis and functional integration. *Journal of Neuroscience*, *25*(45), 10366–10368. https://doi.org/10.1523/JNEUROSCI.3452-05.2005

Song, H., Stevens, C. F., & Gage, F. H. (2002). Astroglia induce neurogenesis from adult neural stem cells. *Nature*, *417*(6884), 39–44. https://doi.org/10.1038/417039a

Sorrells, S. F., Paredes, M. F., Cebrian-Silla, A., Sandoval, K., Qi, D., Kelley, K. W., … Alvarez-Buylla, A. (2018). Human hippocampal neurogenesis drops sharply in children to undetectable levels in adults. *Nature*, *555*(7696), 377–381. https://doi.org/10.1038/nature25975

Spalding, K. L., Bergmann, O., Alkass, K., Bernard, S., Salehpour, M., Huttner, H. B., … Frisén, J. (2013). XDynamics of hippocampal neurogenesis in adult humans. *Cell*, *153*(6), 1219. https://doi.org/10.1016/j.cell.2013.05.002

Squire, L. R. (1992). Memory and the Hippocampuss: A Synthesis From Findings With Rats, Monkeys, and Humans. *Psychological Review*, *99*(2), 195–231. https://doi.org/10.1037/0033-295X.99.2.195

Squire, L. R., Stark, C. E. L., & Clark, R. E. (2004). the Medial Temporal Lobe. *Annual Review of Neuroscience*, *27*(1), 279–306. https://doi.org/10.1146/annurev.neuro.27.070203.144130

Stevens, R., & Cowey, A. (1973). Effects of dorsal and ventral hippocampal lesions on spontaneous alternation, learned alternation and probability learning in rats. *Brain Research*, *52*(C), 203–224. https://doi.org/10.1016/0006-8993(73)90659-8

Steward, O., White, W. F., Cotman, C. W., & Lynch, G. (1976). Potentiation of excitatory synaptic transmission in the normal and in the reinnervated dentate gyrus of the rat. *Experimental Brain Research*, *26*(4), 423–441. https://doi.org/10.1007/BF00234223

Stone, S. S. D., Teixeira, C. M., DeVito, L. M., Zaslavsky, K., Josselyn, S. A., Lozano, A. M., & Frankland, P. W. (2011). Stimulation of Entorhinal Cortex Promotes Adult Neurogenesis and Facilitates Spatial Memory. *Journal of Neuroscience*, *31*(38), 13469–13484. https://doi.org/10.1523/JNEUROSCI.3100-11.2011

Strange, B. A., Witter, M. P., Lein, E. S., & Moser, E. I. (2014). Functional organization of the hippocampal longitudinal axis. *Nature Reviews Neuroscience*, *15*(10), 655–669. https://doi.org/10.1038/nrn3785

Street, C. (1979). *(Received 6*. 375–388.

Suciu, C. S., Mæland, D., Hoffmann, A. C., Vik, A., & Wærnhus, I. (2015). The use of nanoparticles for solid oxide fuel cell components. *AES-ATEMA International Conference Series - Advances and Trends in Engineering Materials and Their Applications*, *10-14-Octo*, 81–85.

Sun, B., Halabisky, B., Zhou, Y., Palop, J. J., Yu, G., Mucke, L., & Gan, L. (2009). Imbalance between GABAergic and Glutamatergic Transmission Impairs Adult Neurogenesis in an Animal Model of Alzheimer's Disease. *Cell Stem Cell*, *5*(6), 624–633. https://doi.org/10.1016/j.stem.2009.10.003

Sun, W., Winseck, A., Vinsant, S., Park, O. H., Kim, H., & Oppenheim, R. W. (2004). Programmed cell death of adult-generated hippocampal neurons is mediated by the proapoptotic gene bax. *Journal of Neuroscience*, *24*(49), 11205–11213. https://doi.org/10.1523/JNEUROSCI.1436-04.2004

Tannenholz, L., Hen, R., & Kheirbek, M. A. (2016). GluN2B-containg NMDA receptors on adult-born granule cells contribute to the antidepressant action of fluoxetine. *Frontiers in Neuroscience*, *10*(MAY), 1–14. https://doi.org/10.3389/fnins.2016.00242

Tashiro, A., Sandler, V. M., Toni, N., Zhao, C., & Gage, F. H. (2006a). NMDA-receptor-mediated, cell-specific integration of new neurons in adult dentate gyrus. *Nature*, *442*(7105), 929–933. https://doi.org/10.1038/nature05028

Tashiro, A., Sandler, V. M., Toni, N., Zhao, C., & Gage, F. H. (2006b). NMDA-receptor-mediated, cell-specific integration of new neurons in adult dentate gyrus. *Nature*, *442*(7105), 929–933. https://doi.org/10.1038/nature05028

Tashiro, A., Zhao, C., & Gage, F. H. (2007). Retrovirus-mediated single-cell gene knockout technique in adult newborn neurons in vivo. *Nature Protocols*, *1*(6), 3049–3055. https://doi.org/10.1038/nprot.2006.473

Taupin, P. (2006). Adult neurogenesis in mammals. *Current Opinion in Molecular Therapeutics*, *8*(4), 345–351. https://doi.org/10.1126/science.aav6885

Temple, S., & Alvarez-Buylla, A. (1999). Stem cells in the adult mammalian central nervous system. *Current Opinion in Neurobiology*, *9*(1), 135–141. https://doi.org/10.1016/S0959-4388(99)80017-8

Thompson, D. K., Wood, S. J., Doyle, L. W., Warfield, S. K., Lodygensky, G. A., Anderson, P. J., … Inder, T. E. (2008). Neonate hippocampal volumes: Prematurity, perinatal predictors, and 2-year outcome. *Annals of Neurology*, *63*(5), 642–651. https://doi.org/10.1002/ana.21367

Toda, T., Parylak, S. L., Linker, S. B., & Gage, F. H. (2019). The role of adult hippocampal neurogenesis in brain health and disease. *Molecular Psychiatry*, *24*(1), 67–87. https://doi.org/10.1038/s41380-018-0036-2

Toni, N., Laplagne, D. A., Zhao, C., Lombardi, G., Ribak, C. E., Gage, F. H., & Schinder, A. F. (2008). Neurons born in the adult dentate gyrus form functional synapses with target cells. *Nature Neuroscience*, *11*(8), 901–907. https://doi.org/10.1038/nn.2156

Toni, N., Teng, E. M., Bushong, E. A., Aimone, J. B., Zhao, C., Consiglio, A., … Gage, F. H. (2007). Synapse formation on neurons born in the adult hippocampus. *Nature Neuroscience*, *10*(6), 727–734. https://doi.org/10.1038/nn1908

Tozuka, Y., Fukuda, S., Namba, T., Seki, T., & Hisatsune, T. (2005). GABAergic excitation promotes neuronal differentiation in adult hippocampal progenitor cells. *Neuron*, *47*(6), 803–815. https://doi.org/10.1016/j.neuron.2005.08.023

Treves, A., Tashiro, A., Witter, M. E., & Moser, E. I. (2008a). What is the mammalian dentate gyrus good for? *Neuroscience*, *154*(4), 1155–1172. https://doi.org/10.1016/j.neuroscience.2008.04.073

Treves, A., Tashiro, A., Witter, M. E., & Moser, E. I. (2008b). What is the mammalian dentate gyrus good for? *Neuroscience*, *154*(4), 1155–1172. https://doi.org/10.1016/j.neuroscience.2008.04.073

Treves, Alessandro, & Rolls, E. T. (1994). Computational analysis of the role of the hippocampus in memory. *Hippocampus*. https://doi.org/10.1002/hipo.450040319

Trinchero, M. F., Buttner, K. A., Sulkes Cuevas, J. N., Temprana, S. G., Fontanet, P. A., Monzón-Salinas, M. C., … Schinder, A. F. (2017). High Plasticity of New Granule Cells in the Aging Hippocampus. *Cell Reports*, *21*(5), 1129–1139. https://doi.org/10.1016/j.celrep.2017.09.064

Tronel, S., Belnoue, L., Grosjean, N., Revest, J. M., Piazza, P. V., Koehl, M., & Abrous, D. N. (2012). Adult-born neurons are necessary for extended contextual discrimination. *Hippocampus*, *22*(2), 292–298. https://doi.org/10.1002/hipo.20895

Tronel, S., Fabre, A., Charrier, V., Oliet, S. H. R., Gage, F. H., & Abrous, D. N. (2010). Spatial learning sculpts the dendritic arbor of adult-born hippocampal neurons. *Proceedings of the National Academy of Sciences of the United States of America*, *107*(17), 7963–7968. https://doi.org/10.1073/pnas.0914613107

van Praag, H. (2009). Exercise and the brain: something to chew on. *Trends in Neurosciences*, *32*(5), 283–290. https://doi.org/10.1016/j.tins.2008.12.007

Van Praag, H., Shubert, T., Zhao, C., & Gage, F. H. (2005). Exercise enhances learning and hippocampal neurogenesis in aged mice. *Journal of Neuroscience*, *25*(38), 8680–8685. https://doi.org/10.1523/JNEUROSCI.1731-05.2005

Varela-Nallar, L., & Inestrosa, N. C. (2013). Wnt signaling in the regulation of adult hippocampal neurogenesis. *Frontiers in Cellular Neuroscience*, *7*(JUNE), 1–11. https://doi.org/10.3389/fncel.2013.00100

Villasana, L. E., Westbrook, G. L., & Schnell, E. (2014). Neurologic impairment following closed head injury predicts post-traumatic neurogenesis. *Experimental Neurology*, *261*, 156–162. https://doi.org/10.1016/j.expneurol.2014.05.016

Villasana, Laura E., Kim, K. N., Westbrook, G. L., & Schnell, E. (2015). Functional integration of adult-born hippocampal neurons after traumatic brain injury. *ENeuro*, *2*(5). https://doi.org/10.1523/ENEURO.0056-15.2015

Vivar, C., Potter, M. C., Choi, J., Lee, J. Y., Stringer, T. P., Callaway, E. M., … Van Praag, H. (2012). Monosynaptic inputs to new neurons in the dentate gyrus. *Nature Communications*, *3*(May), 1107–1111. https://doi.org/10.1038/ncomms2101

Wadiche, L. O., Bromberg, D. A., Bensen, A. L., & Westbrook, G. L. (2005). GABAergic signaling to newborn neurons in dentate gyrus. *Journal of Neurophysiology*, *94*(6), 4528–4532. https://doi.org/10.1152/jn.00633.2005

Wang, D. D., & Kriegstein, A. R. (2008). GABA regulates excitatory synapse formation in the neocortex via NMDA receptor activation. *Journal of Neuroscience*, *28*(21), 5547–5558. https://doi.org/10.1523/JNEUROSCI.5599-07.2008

Wang, L., Swank, J. S., Glick, I. E., Gado, M. H., Miller, M. I., Morris, J. C., & Csernansky, J. G. (2003). Changes in hippocampal volume and shape across time distinguish dementia of the Alzheimer type from healthy aging. *NeuroImage*, *20*(2), 667–682. https://doi.org/10.1016/S1053-8119(03)00361-6

Wang, S., & Wojtowicz, J. M. (1997). Effect of GABA(B) receptors on synaptic interactions in dentate gyrus granule neurons of the rat. *Neuroscience*, *79*(1), 117–127. https://doi.org/10.1016/S0306-4522(96)00638-0

Wang, Sihyung, Lee, J. S., Hyun, J., Kim, J., Kim, S. U., Cha, H. J., & Jung, Y. (2015). Tumor necrosis factor-inducible gene 6 promotes liver regeneration in mice with acute liver injury. *Stem Cell Research and Therapy*, *6*(1), 1–12. https://doi.org/10.7554/eLife.03104

Weisz, V. I., & Argibay, P. F. (2009). A putative role for neurogenesis in neurocomputational terms: Inferences from a hippocampal model. *Cognition*, *112*(2), 229–240. https://doi.org/10.1016/j.cognition.2009.05.001

Weisz, V. I., & Argibay, P. F. (2012). Neurogenesis interferes with the retrieval of remote memories: Forgetting in neurocomputational terms. *Cognition*, *125*(1), 13–25. https://doi.org/10.1016/j.cognition.2012.07.002

West, M. J., Slomianka, L., & Gundersen, H. J. G. (1991). Unbiased stereological estimation of the total number of neurons in the subdivisions of the rat hippocampus using the optical fractionator. *The Anatomical Record*, *231*(4), 482–497. https://doi.org/10.1002/ar.1092310411

Williams, J. M. G., Barnhofer, T., Crane, C., Herman, D., Raes, F., Watkins, E., & Dalgleish, T. (2007). Autobiographical memory specificity and emotional disorder. *Psychological Bulletin*, *133*(1), 122–148. https://doi.org/10.1037/0033-2909.133.1.122

Winocur, G., Wojtowicz, J. M., Sekeres, M., Snyder, J. S., & Wang, S. (2006). Inhibition of neurogenesis interferes with hippocampus-dependent memory function. *Hippocampus*, *16*(3), 296–304. https://doi.org/10.1002/hipo.20163

Wiskott, L., Rasch, M. J., & Kempermann, G. (2006). A functional hypothesis for adult hippocampal neurogenesis: Avoidance of catastrophic interference in the dentate gyrus. *Hippocampus*, *16*(3), 329–343. https://doi.org/10.1002/hipo.20167

Witter, M. P. (2007). The perforant path: projections from the entorhinal cortex to the dentate gyrus. *Progress in Brain Research*, *163*, 43–61. https://doi.org/10.1016/S0079-6123(07)63003-9

Wurmser, A. E., Palmer, T. D., & Gage, F. H. (2004). Cellular interactions in the stem cell niche. *Science*, *304*(5675), 1253–1255. https://doi.org/10.1126/science.1099344

Yassa, M. A., & Stark, C. E. L. (2011). Pattern separation in the hippocampus. *Trends in Neurosciences*, *34*(10), 515–525. https://doi.org/10.1016/j.tins.2011.06.006

Yassa, M. A., Stark, S. M., Bakker, A., Albert, M. S., Gallagher, M., & Stark, C. E. L. (2010). High-resolution structural and functional MRI of hippocampal CA3 and dentate gyrus in patients with amnestic Mild Cognitive Impairment. *NeuroImage*, *51*(3), 1242–1252. https://doi.org/10.1016/j.neuroimage.2010.03.040

Yim, M. Y., Hanuschkin, A., & Wolfart, J. (2015). Intrinsic rescaling of granule cells restores pattern separation ability of a dentate gyrus network model during epileptic hyperexcitability. *Hippocampus*, *25*(3), 297–308. https://doi.org/10.1002/hipo.22373

Yun, S., Reynolds, R. P., Masiulis, I., & Eisch, A. J. (2016). Re-evaluating the link between neuropsychiatric disorders and dysregulated adult neurogenesis. *Nature Medicine*, *22*(11), 1239–1247. https://doi.org/10.1038/nm.4218

Zhang, W. J., Tan, Y. F., Yue, J. T. Y., Vranic, M., & Wojtowicz, J. M. (2008). Impairment of hippocampal neurogenesis in streptozotocin-treated diabetic rats. *Acta Neurologica Scandinavica*, *117*(3), 205–210. https://doi.org/10.1111/j.1600-0404.2007.00928.x

Zhao, C. (2006). Distinct Morphological Stages of Dentate Granule Neuron Maturation in the Adult Mouse Hippocampus. *Journal of Neuroscience*, *26*(1), 3–11. https://doi.org/10.1523/JNEUROSCI.3648-05.2006

Zhao, Chunmei, Deng, W., & Gage, F. H. (2008). Mechanisms and Functional Implications of Adult Neurogenesis. *Cell*, *132*(4), 645–660. https://doi.org/10.1016/j.cell.2008.01.033

Zhao, Y., Jaber, V., & Lukiw, W. J. (2016). Over-expressed pathogenic mirnas in Alzheimer's disease (AD) and prion disease (PrD) drive deficits in TREM2-mediated Aβ42 peptide clearance. *Frontiers in Aging Neuroscience*, *8*(JUN), 1–5. https://doi.org/10.3389/fnagi.2016.00140

Zhu, L. L., Zhao, T., Li, H. S., Zhao, H., Wu, L. Y., Ding, A. S., … Fan, M. (2005). Neurogenesis in the adult rat brain after intermittent hypoxia. *Brain Research*, *1055*(1–2), 1–6. https://doi.org/10.1016/j.brainres.2005.04.075

Zupanc, G. K. H., & Sîrbulescu, R. F. (2011). Adult neurogenesis and neuronal regeneration in the central nervous system of teleost fish. *European Journal of Neuroscience*, *34*(6), 917–929. https://doi.org/10.1111/j.1460-9568.2011.07854.x